USP22 controls tumorigenicity by regulating interferon responses and the stability of the tumor suppressor PML

Dissertation

zur Erlangung des Doktorgrades der Naturwissenschaften

vorgelegt beim Fachbereich 14 Biochemie, Chemie und Pharmazie

der Johann Wolfgang Goethe-Universität

in Frankfurt am Main

von

Lisa Kowald

aus Eberswalde

Frankfurt am Main, 2022

(D30)

Vom Fachbereich 14 der Johann Wolfgang Goethe-Universität als Dissertation angenommen.

Dekan: Prof. Dr. Clemens Glaubitz, FB14
Gutachter 1: Prof. Dr. Volker Dötsch, FB14
Gutachter 2: Dr. rer. nat. habil. Sjoerd J.L. van Wijk, FB16

Datum der Disputation: 17.04.2023

Table of contents

List of figures

List of tables

List of abbreviations

aa	Amino acid
AML	Acute myelocytic leukemia
AMP	Adenosine monophosphate
APC/C	Anaphase promoting complex/cyclosome
APL	Acute promyelocytic leukemia
APS	Ammonium persulfate
ATG	Autophagy-related protein
ATO	Arsenic trioxide, As_2O_3
ATP	Adenosine triphosphate
ATRA	All-*trans* retinoic acid
ATXN	Ataxin
bcr	Break point cluster
BMI-1	B-cell specific murine leukemia virus integration site-1
BRCA	Breast cancer associated gene
BRISC	BDCC36 isopeptidase complex
BSA	Bovine serum albumin fraction V
C/EBP	CCAAT/enhancer-binding protein
cAMP	3'-5'-Cyclic AMP
CD	Cluster of differentiation
CDK	Cyclin-dependent kinase
cDNA	Copy DNA
Chk2	Checkpoint kinase 2
CHX	Cycloheximide
cIAP	Cellular inhibitor of apoptosis
CK2	Casein kinase 2
CPB	CREB binding protein
CREB	cAMP response element-binding protein
CRISPR	Clustered regularly interspaced short palindromic repeats
C-terminus	Carboxyl terminus
CXCR	C-X-C motif chemokine receptor
D	Aspartic Acid
DAPI	4',6-Diamidino-2-phenylindol
DNA	Desoxyribonucleic acid
DR	Direct repeat motif
DTT	Dithiothreitol
DUB	Deubiquitylase
DUSP	Domain in the USP domain

E. coli	Escherichia coli bacterium
E6AP	E6-associated protein
ECL	Enhanced chemoluminescence
EDTA	Ethylenediaminetetraacetic acid
eGFP	Enhanced green fluorescent protein
ENY2	Enhancer of yellow 2 homologue
ERK2	Extracellular signal-regulated kinase 2
ESC	Embryonic stem cell
ESCRT	Endosomal sorting complex required for transport
EV	Empty vector
FACS	Fluorescence activated cell sorting
FAT	Human leucocyte antigen F-adjacent transcript
FBP	Far upstream binding protein
FCS	Fetal calf serum
FITC	Fluorescein-5-isothiocyanate
FLT3-ITD	FLT3 internal tandem duplication
GOI	Gene of interest
GST	Glutathion S-transferase
h	Hours
H2Bub1	Mono-ubiquitylated histone H2B
HA	Human influenza Hemagglutinin tag
HACE	HECT domain and ankyrin repeat containing E3 ligase
HDAC	Histone deacetylase
HECT	Homologous to E6AP C-terminus
HEK	Human embryonic kidney cells
Hes1	Hairy and enhancer of split 1
hIECs	Human intestinal epithelial cells
HIF1α	Hypoxia inducible factor 1 α
HIPK	Homeodomain-interacting protein kinase
HPV	Human papilloma virus
HSPC	Hematopoietic stem and progenitor cell
HSV-1	Herpes simplex virus type 1
IF	Immunofluorescence
IFN	Interferon
In vitro	In test tube
In vivo	In living organism
IP	Immunoprecipitation
IRF	Interferon-regulatory transcription factor
ISG	Interferon-stimulated gene
ISRE	Interferon-stimulated responsive element
IκBα	Inhibitor of NF-κB alpha

JAK	Janus kinase
JAMM	JAB1/MPN/MOV34 metalloprotease
K	Lysine
kDa	Kilo Dalton
KLHL	Kelch like family member
KO	Knock out
KRAS	Kirsten rat sarcoma viral oncogene
LIC	Leukemia initiating cell
LUBAC	Linear ubiquitin chain assembly complex
M	Methionine
mA, mg, mL, mM	Milliampère, -gram, -liter, -molar
µg, µL, µM	Microgram, -liter, -molar
MDM2	Mouse double minute 2 homologue
MFI	Mean fluorescence intensity
min	Minutes
MINDY	Motif interacting with ubiquitin-containing novel DUB family
mRNA	Messenger RNA
MS	Mass spectrometry
mTOR	Mammalian target of Rapamycin
n.h.t.	Non-human target
NB	Nuclear body
NEDD	Neural precursor cell expressed developmentally down-regulated protein
NEM	N-ethylmaleimide
NES	Nuclear export signal
NF-κB	Nuclear factor kappa B
Ni^{2+}-NTA	Nickel-Nitrilotriacetic acid
NLS	Nuclear localization sequence
N-terminus	Amino terminus
OAS	2'-5'-oligoadenylate synthetase
ORF	Open reading frame
OTU	Ovarian tumor protease
PBS	Phosphate buffered saline
PcG	Polycomb Group
PCNA	Proliferating cell nuclear antigen
PD-1	Programmed death receptor-1
PD-L1	Programmed death receptor ligand-1
PE	Phosphatidylethanolamine
PFA	Paraformaldehyde
PIAS	Protein inhibitor of activated STAT
PIC	Protease inhibitor cocktail
PKA	Protein kinase A

PML	Promyelocytic leukemia protein
PRR	Pattern recognition receptor
PTM	Post-translational modifications
qRT-PCR	Quantitative real time-polymerase chain reaction
R	Arginine
RanBP	Ran binding protein
RARE	RAR-responsive element
RARα	Retinoic acid receptor alpha
RBCC	RING-B-Box-Coiled-Coil motif
RBR	RING-in-between-RING
RFP	Red fluorescent protein
RING	Really interesting new gene
RIPK	Receptor interacting kinase
RNA	Ribonucleic acid
RNF	RING-finger protein
ROS	Reactive oxygen species
RXR	Retinoid X receptor
S	Serine
SAE	SUMO-activating enzyme
SAGA	Spt-Ada-Gcn5 acetyltransferase
SCF	Skp1-Cul1-F-box protein
SDS-PAGE	Sodium dodecyl sulfate-polyacrylamide gel electrophoresis
sec	Seconds
SEM	Standard error of means
SENP	Sentrin-specific protease
SeV	Sendai Virus
sgRNA	Single guide RNA
SIAH	Seven in absentia homologue
SILAC	Stable isotope labeling of amino acids in cell culture
SIM	SUMO-interacting motif
SIRT	Sirtuin
SMRT	Silencing mediator of retinoid and thyroid receptors
SOX2	Sex-determining region Y-box 2
STAT	Signal transducer and activator
STING	Stimulator of interferon genes
STUB1	STIP1 homology and U-box containing protein 1
STUbL	SUMO-targeted ubiquitin ligase
SUMO	Small ubiquitin-like modifier
TAD	Transactivation domain
TEMED	Tetramethylethylenediamine
TGFß	Transforming growth factor ß

TNFα	Tumor necrosis factor alpha
TRAF	TNF receptor associated factor
TRF	Telomeric repeat binding factor
TRIM	Tripartite motif
TRITC	Tetramethyl-rhodamine isothiocyanate
TSA	Trichostatin A
TUBE	Tandem ubiquitin binding entity
U	Enzymatic unit
UBD	Ubiquitin-binding domain
UBE	Ubiquitin-conjugation enzyme
UBE1L	Ubiquitin-activating enzyme E1-like
UbL	Ubiquitin-like modifiers
UCH	Ubiquitin C-terminal hydrolase
UHRF1	Ubiquitin-like with PHD and RING finger domain 1
ULP	Ubiquitin-like protease
USP	Ubiquitin-specific protease
VSV	Vesicular stomatitis virus
WBC	White blood cell count
ZnF	Zinc finger domain
ZUFSP	Zinc finger with UFM1-specific peptidase domain protein
zVAD.fmk	Z-Val-Ala-DL-Asp-fluoromethylketone

1 Abstract

Post-translational modifications (PTMs) of cell fate regulating proteins determine their stability, localization and function and control the activation of cell protective signaling pathways. Particularly in aberrantly dividing cancer cells the surveillance of cell cycle progression is essential to control tumorigenicity. In a variety of carcinomas, lymphomas and leukemias, the tumor-suppressive functions of the apoptosis- and senescence-regulating promyelocytic leukemia protein (PML) is controlled by numerous PTMs. PML poly-ubiquitylation and polySUMOylation at several lysine (K) residues induce PML degradation that is correlated to a progressive and invasive cancer phenotype. Besides several known E3 ubiquitin protein ligases that are involved in PML degradation, less is known about PML-specific deubiquitylases (DUBs), the respective DUB-controlled ubiquitin conjugation sites and the functional consequences of PML (de)ubiquitylation. Here, we show that the pro-tumorigenic DUB USP22 critically regulates PML protein stability by modifying PML residue K394 in advanced colon carcinoma cells *in vitro* and that this modification also impacts the homeostasis and function of the leukemia-associated mutant variant PML-RARα. We found that ablation of USP22 decreases PML mono-ubiquitylation and correlates with a prolonged protein half-live in colon carcinoma and acute promyelocytic leukemia (APL) cell lines. Additionally, silencing of USP22 enhances interferon and interferon-stimulated gene (ISG) expression in APL cells *in vitro*, which together with prolonged PML-RARα stability increases the APL cell sensitivity towards differentiation treatment. In accordance with the novel roles of USP22 as suppressor of the interferon response in human intestinal epithelial cells (hIECs), our findings imply USP22-dependent surveillance of PML-RARα stability and interferon signaling in human leukemia cells, revealing USP22 as central regulator of leukemia pathogenesis.

2 Introduction

2.1 Ubiquitylation

The translation of the genetic code of eukaryotes into functional proteins is regulated in a complex multi-step manner. For instance, variations in chromatin topology determine the transcriptional accessibility of DNA, while alternative splicing of transcribed messenger RNA (mRNA) introduces another level of diversification. The next level of complexity is than achieved by post-translational modifications (PTMs) of translated proteins, generating a proteome that is three orders of magnitude greater than the actual number of genes encoded in our DNA [1]. PTMs are highly dynamic covalent attachments between specific chemical moieties or polypeptides and protein backbones and sidechains. Well known protein modifications include phosphorylation, acetylation, methylation and glycosylation as well as ubiquitylation and SUMOylation. The PTM code is generated by ‘writers’, ‘readers’ and ‘erasers’ that reflect PTM-conjugating enzymes, PTM-binding domain comprising molecules and PTM-cleaving enzymes, respectively [2]. PTM writers are for example kinases, acetyltransferases or ubiquitin ligases, whereas phosphatases, deacetylases and deubiquitylases (DUBs) regulate the removal of conjugated groups. This adaptability of protein modifications influences protein conformation, stability, localization or activity, which allows the cell to quickly react to physiological changes [1].

Ubiquitylation is one type of PTMs that allows distinct protein fate modulations, dependent on the composition of the attached ubiquitin chains. Ubiquitin is an evolutionary highly conserved small protein of 76 amino acids, weighing about 8.5 kDa. It has a globular 3D structure, consisting of a flexible C-terminus, a short 3(10)-helix, one α-helix and one β-sheet that together form a hydrophobic core which is referred to as ‘ß-grasp fold’ (Figure 1A) [3]. The flexible C-terminus is the anchor for covalent attachment of ubiquitin to lysin residues of target proteins or other ubiquitin moieties, a process termed ‘ubiquitylation’ (or equally ‘ubiquitination’ or ‘ubiquitinylation’). Ubiquitin moieties are assembled at a target protein by the enzymatic ubiquitin conjugation cascade, composed of E1 ubiquitin-activating enzymes, E2 ubiquitin-conjugating enzymes and E3 ubiquitin protein ligases [4]. Ubiquitin activation by E1 enzymes occurs under adenosine triphosphate (ATP) consumption by the generation of an adenylated C-terminus, followed by AMP release due to the thioester formation between the catalytic core of the E1 enzyme and the ubiquitin monomer. In a next step, the ubiquitin moiety is transferred to the thiol group of the catalytic cysteine of an E2 ubiquitin-conjugating enzyme in a transthiolation reaction. Finally, E3 protein ligases catalyze the covalent isopeptide-bond formation of ubiquitin molecules with an exposed amino group of a target protein by either bringing the target residue in close proximity to the ubiquitin-conjugated E2 enzyme, as in the

case of really interesting new gene (RING)-type E3 ligases, or the E3 ligase exerts a sequential ubiquitin transfer with an intermediate thioester formation to an own catalytic cysteine, as done by homologous to the E6-associated protein (E6AP) C-terminus (HECT)-type and RING-in-between-RING (RBR)-type E3 ligases [5]. The whole process is reversed by DUBs that hydrolyze the isopeptide bond and re-expose the C-terminal glycine residue of a ubiquitin monomer for repeated target conjugation. Overall, more than 600 human E3 ligases, 40 E2 ubiquitin-conjugating enzymes and about 100 DUBs provide a huge pool of enzyme combinations [6], resulting in a vast variety of ubiquitin chain-types, each determining a distinct fate of the ubiquitylated protein (Figure 1B+C).

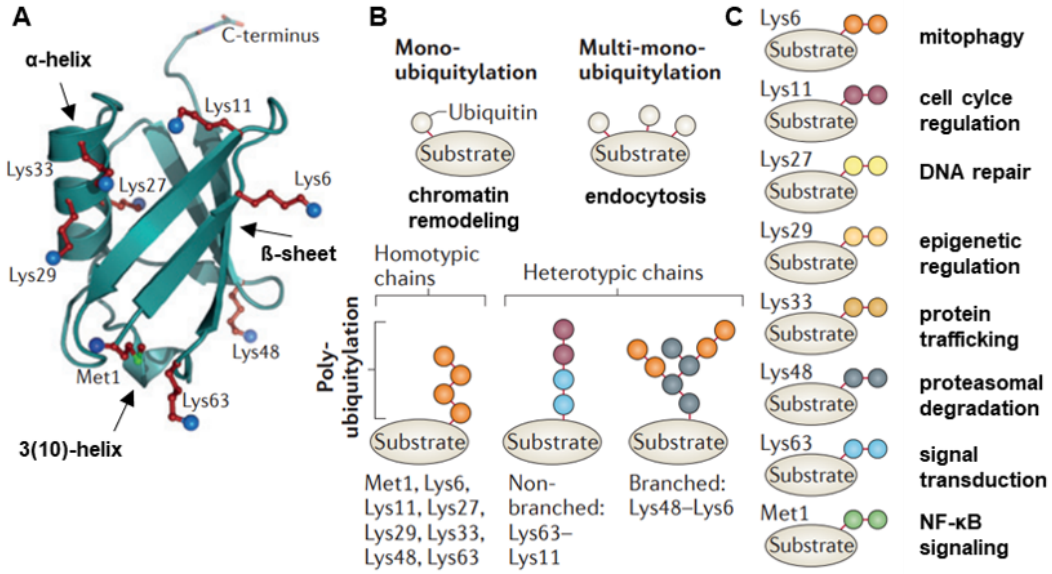

Figure 1: Ubiquitin and variations of the ubiquitin code. A: 3D-cartoon of ubiquitin (PDB: 1UBQ) with prominent secondary structure features: 3.5-turn α-helix, 5-strand ß-sheet and short 3(10)-helix. Seven lysine residues (Lys) and the initial methionine (Met) are represented as red sticks with blue spherical amino-groups. B: Different ubiquitin chain topologies with indicated lysine residues that adopt certain chain types. Homotypic poly-ubiquitin chains comprise identically linked ubiquitin moieties, while heterotypic chains are composed of mixed inter-ubiquitin linkages. The color code is depicted in C. C: Possible lysine linkages of intra-ubiquitin bonds with exemplary biological processes for each linkage type. Figure adapted from [7]

2.1.1 Poly-ubiquitin linkage types

Once a protein is marked with a single ubiquitin moiety, termed ‘mono-ubiquitylated’, the ligation cascade either terminates, as in the case of mono-ubiquitylated histone H2B [8], or the mono-ubiquitin is elongated to a poly-ubiquitin chain. Here, additional ubiquitin monomers are ligated to one of seven available lysine (Lys, K) residues or the N-terminal methionine (Met, M) residue, exposed by the initial ubiquitin (Figure 1A) [9]. Homotypic chains of one of the internal ubiquitin residues K6, K11, K27, K29, K33, K48 or K63 or M1 result in a variety of cellular signaling events, including protein degradation, protein compartmentalization or downstream signaling cascade activation [9]. While some physiological processes can be tightly attributed to a certain linkage type with the corresponding ubiquitin-conjugating

enzymes, many other pathways are regulated by ubiquitylation marks of mixed linkage chains with individual effects on the substrate proteins.

Poly-ubiquitin-dependent protein degradation correlates with homotypic K48-linked poly-ubiquitin chains, which were firstly discovered to govern homeostatic protein turnover in yeast [10]. This discovery was honored with the Nobel Prize in chemistry in 2004, awarded to Aaron Ciechanover, Avram Hershko and Irwin Rose [11, 12]. K48 linkage-specificity is directed by specific E2- and E3-enzymes, such as the ubiquitin-conjugating enzyme E2 R1 (UBE2R1) and the cullin-RING E3 ligase complex Skp1-Cul1-F-box protein (SCF) [13]. Also, the human HECT E3 ligase E6AP (also known as UBE3A) is highly specific for K48-linked ubiquitylation [14]. Poly-ubiquitin chains consisting of K63-linked ubiquitin moieties are for example involved in DNA repair and immunological cytokine signaling [15]. E2 and E3 enzymes with K63-linkage specificity are for example UBE2N and HECT E3 ligase neural precursor cell expressed developmentally down-regulated protein 4 (NEDD4) [14, 16]. Together with K63-linkages, M1-assembled chains form linear poly-ubiquitin chains that predominantly regulate innate immunity and NF-κB signaling [17]. The specialized E3 ligase complex involved in this chain type is the linear ubiquitin chain assembly complex (LUBAC) that is tightly associated with tumor necrosis factor (TNF)-signaling that regulates cell survival [18]. Furthermore, K11-linked homotypic poly-ubiquitin chains are assembled by the linkage-specific E2 enzyme UBE2S and the multi-subunit RING E3 ligase anaphase promoting complex/cyclosome (APC/C) in the context of cell cycle regulation. Here, UBE2S adds K11-linked ubiquitin moieties onto existing K48-linked ubiquitin polymers, resulting in branched heterotypic chains that promote protein degradation [19]. While K11 is closely related to proteolytic signaling, K27-linked ubiquitylation is clearly associated with non-degradative functions. Among a great number of identified substrates, K27-linkages are detected on numerous proteins involved in innate immune response, e.g. stimulator of interferon genes (STING), as consequence of viral infection, interferon-signaling and cytosolic DNA sensing, as recently reviewed [6]. E3 ligases involved in these processes are NEDD4, Tripartite motif family member 23 (TRIM23) and HECT domain and ankyrin repeat containing E3 ligase 1 (HACE1).

Further non-degradative chains are composed of K33 linkages that are ligated by the Cullin 3-kelch like family member 20 (KLHL20)-E3 complex and have been associated with proteins targeted for trafficking to the Golgi membrane network [20]. Apart from the Golgi network, mitochondria are also closely associated with poly-ubiquitin chain type-specificity. Proteins embedded in the outer mitochondrial membrane of damaged mitochondria are decorated with K6-linked poly-ubiquitylation by the E3 ligase Parkin in order to eliminate damaged mitochondria via selective autophagy (mitophagy) [21]. Pathological dysfunctional mitophagy underlies neurodegenerative Parkinson's disease and is associated not only with K6 ubiquitin linkages but also K29-linked poly-ubiquitin assembled by the E3 ligase TNF receptor associated factor 6 (TRAF6) [22]. The latter type was also detected in protein

aggregates of Huntington's disease patients [23]. The variety of physiological functions conveyed by the distinct lysine-specific poly-ubiquitin linkages gives an example for the complexity of the ubiquitin code. Besides the mentioned linkage specific E2 and E3 enzymes, many ubiquitylating enzymes exist without preferential chain editing, adding another level of complexity. Some examples are the unspecific E2 ubiquitin-conjugating enzyme family UBE2D that interacts with numerous RING-type E3 ligases, or the less linkage-specific E3 ligases SCF and Parkin [7]. Finally, the ubiquitin code is additionally edited by the removal of single ubiquitin molecules by DUBs, offering new opportunities for mixed and branched poly-ubiquitin chains.

2.1.2 Deubiquitylases

As diverse as the multiple ubiquitin-conjugating enzymes with varying poly-ubiquitin linkage specificities are the 98 different ubiquitin-linkage hydrolyzing DUBs in humans. They are divided into six major DUB families that are classified by their structural domain architecture, as nicely reviewed by David Komander and collaborators [24, 25]. Five subfamilies of different size represent cysteine-proteases, e.g.: 54 ubiquitin-specific proteases (USPs), 16 ovarian tumor proteases (OTUs), 4 ubiquitin C-terminal hydrolases (UCHs), 4 Machado-Joseph disease proteases (Josephins) and 4 motif interacting with ubiquitin (MIU)-containing novel DUB family (MINDYs). The sixth known subfamily is represented by 16 Zn-dependent JAB1/MPN/MOV34 metalloproteases (JAMMs). Recently, one additional cysteine-protease DUB family was detected comprising only one member so far, namely zinc finger with UFM1-specific peptidase domain protein (ZUFSP) [26].

The mode of action of DUBs varies among the different subfamilies. The cysteine-protease families cleave the isopeptide linkage between two adjacent ubiquitin molecules through the action of a catalytical triad composed of the active cysteine, a histidine and an asparagine or aspartate residue [25]. Upon a nucleophilic attack of the active cysteine residue towards the carboxy-group of the distal ubiquitin, the newly formed acyl-enzyme intermediate is hydrolyzed, leading to the release of the distal ubiquitin. In contrast, the metalloproteases of the JAMM family position the isopeptide bond of a di-ubiquitin linkage between two zinc ions, followed by a direct water molecule-mediated hydrolysis of the distal ubiquitin [25]. The common prerequisite for all DUBs is the S1 binding pocket, which is composed of different ubiquitin-binding domains (UBDs) [27]. In addition, most USPs comprise additional ubiquitin-binding domains, e.g. zinc finger (ZnF) domains, UBA and UBL domains or domains in USP (DUSP), that assists in ubiquitin-binding at the distal di-glycine motif for proper protease activity [24]. The inter-ubiquitin linkage-dependent topology of the poly-ubiquitin chain determines, whether only the most distal ubiquitin molecule is cleaved (exo-activity) or whether complete ubiquitin polymers are hydrolyzed at once (endo-activity) [25]. Likewise, certain DUBs are specialized to exclusively cleave one chain-linkage type, as in the case of MINDY 1 that has

K48-linkage preference [28], OTULIN with Met1-linear chain selectivity [29] or associated molecule with SH3 domain of signal transducing adaptor molecule STAM (AMSH) with strong K63-linkage specificity [30]. Most USPs on the other hand are rather chain unspecific but provide substrate selectivity by multiple insertions in their catalytic cavity [31].

Substrate selectivity is further achieved by the occurrence of certain DUBs in large multi-enzyme complexes that tightly control regulatory functions towards their substrates. For example, the endosomal sorting complex required for transport (ESCRT) machinery regulates surface receptor endocytosis [32], the BRCC36 isopeptidase complex (BRISC) is active during mitotic spindle assembly [33], the breast cancer associated gene (BRCA1) complex is involved in DNA double-strand break repair [34] or the Spt-Ada-Gcn5 acetyltransferase (SAGA) complex that regulates transcription [35]. Apart from that, DUBs ensure the maintenance of a free ubiquitin pool by recycling ubiquitin molecules from degradative poly-ubiquitin marks upon processing by the 26S proteasome. Therefore, the DUBs UCH-L5, USP14 and RPN11 are directly associated with proteasomal subunits and govern the replenishment of free ubiquitin [36-38].

Finally, some DUBs that structurally resemble ubiquitin-specific DUB classes, are functionally specialized to recognize ubiquitin-like modifiers instead of ubiquitin. These ubiquitin-like proteases (ULPs) share the DUB-specific S1 binding pocket but significantly differ in the constellation of UBDs, conferring specificity towards the surface properties of ubiquitin-like modifiers (UbLs) [39], as for examples the NEDD8-specific JAMM DUB CSN5 [40], the ISG15-specific USP18 [41] or USPL1 with SUMO selectivity [42].

2.2 USP22

USP22 belongs to the DUB family of the USPs that is characterized as cysteine proteases with a highly conserved catalytical triad in the center of the UCH domain. USP22 comprises a single N-terminal ZnF domain, followed by a nuclear localization sequence (NLS) [43] and the C-terminal UCH domain. Interestingly however, USP22 belongs to a group of few USPs that are not able to bind ubiquitin via their ZnF domain but require this structure as an anchor in larger multiprotein complexes [44]. Here, the DUB and its respective substrates are positioned by other complex components to assure hydrolase activity. Within this complex, USP22 preferentially cleaves mono-ubiquitin moieties of histone H2A and H2B [45], but is also described to hydrolyze K63-linked poly-ubiquitin chains on Far Upstream Binding Protein 1 (FBP1) [46] or degradative poly-ubiquitin chains, in the cases of Telomeric repeat binding factor 1 (TRF1) [47] and transcription factor PU.1 [48]. In an indirect manner, USP22 also assists in cleavage of K27-linked poly-ubiquitin chains on STING by recruiting the executive DUB USP13 to its substrate [49]. Transcriptionally, USP22 expression is regulated by binding of the cAMP response element-binding protein (CREB) to the USP22 promoter region [50].

Post-translationally, USP22 activity is downregulated by phosphorylation via cyclin-dependent kinase 1 (CDK1) during mitosis as well as ubiquitylation via the E3 ligase complex APC at the end of the cell cycle [51]. The ZnF domain of USP22 is acetylated which is necessary for the assembly and function within the DUB module of the transcriptional coactivator SAGA complex [52]. Regulation of this transcriptional activity is exhibited by the deacetylase sirtuin-1 (SIRT1) that not only deacetylates USP22, but also other SAGA components [53].

USP22 controls transcriptional regulation and chromatin remodeling as part of the SAGA complex. The SAGA complex occupies active gene loci and enables the elongation by RNA polymerase II during transcription [54]. It comprises an acetyl-transferase module, that marks chromatin for active transcription, a transcription factor interaction module and the DUB module that regulates the euchromatin structure via ubiquitin deconjugation [54]. Within the DUB module, USP22 exerts its ubiquitin hydrolase function in concert with Ataxin 7-like protein 3 (ATXN7L3) and enhancer of yellow 2 homologue (ENY2) towards mono-ubiquitylated K120 of histone H2B (H2Bub1) [45, 55]. H2Bub1 is described as a transcriptional activation mark of genes associated with cell proliferation and cell cycle progression and is associated with carcinogenesis [45]. Within this context, USP22 promotes c-Myc-driven oncogene activation [45], to stabilize the pro-tumorigenic transcription factor FBP1 [46] and the checkpoint regulator Cyclin B1 and Cyclin D1 [51, 56], which together regulate proliferation. By deubiquitylation of FBP1, USP22 induces its persistence on the upstream repressor region of p21, which is an inhibitor of several cyclin-dependent kinases (CDKs) that normally control cell cycle termination [46]. Upon USP22 overexpression, p21 levels are strongly diminished, cell cycle checkpoints are disabled and allow cell cycle progression [54].

In addition, USP22 has critical physiological functions during early embryogenesis, as reflected by embryonic lethality between E10.5 and E14.5 of homozygous *USP22* null mutant mice [57, 58]. Cells isolated from these embryos revealed a high incidence of apoptosis due to strong p53 activity accompanied by the loss of SIRT1. SIRT1 is a deacetylase that suppresses p53 apoptotic signaling and is a direct ubiquitylation target of USP22 [57]. Furthermore, extra-embryonic tissues were affected by loss of USP22 such that reduced vascularization of the murine placenta led to insufficient nutrient and oxygen supply of the mutant embryos [58]. This identifies USP22 as regulator of transforming growth factor ß (TGFß) and several receptor tyrosine kinases that are essential for placental vasculogenesis and vessel migration. In adult mice, USP22 is expressed in all types of tissues, while it was concentrated in brain tissues during early embryonic development [59], stressing the relevance for proper embryogenesis. Interestingly, *in vitro* studies discovered a role for USP22 in governing differentiation of pluripotent embryonic stem cells (ESCs) into all three germ layers by repressing the pluripotency factor sex-determining region Y-box 2 (SOX2) [60]. While this repression is mediated by histone deubiquitylation of the SAGA complex at the SOX2 promoter, USP22 also deubiquitylates and stabilizes the neuronal transcription factor Hairy

and Enhancer of Split 1 (Hes1) that favors the maintenance of neuronal stem cell and progenitor cells during early embryogenesis [61].

In recent years, important roles of USP22 in regulating innate immunity have emerged [49, 62, 63]. The innate immune system mainly regulates the function and activation of innate immune cells such as neutrophils, macrophages and dendritic cells upon unspecific recognition of pathogenic surface proteins, extracellular or cytosolic polynucleotides or fractions of apoptotic or damaged host cells [64]. Sensing of such molecular patterns by pattern recognition receptors (PRRs) results in induction of immunoprotective effects such as inflammation, innate immune killing or activation of adaptive immunity [64]. These effects are mediated by secretion of small signaling molecules like growth factors, chemokines or cytokines, especially interferons (IFN), which act in an autocrine or paracrine manner to activate immune defense-related genes such as IFN stimulated genes (ISGs). Many PRRs as well as IFN-regulatory transcription factors (IRFs) are tightly regulated by the ubiquitin system to ensure surveillance over anti-host autoimmunity [65]. USP22 recently emerged as an immunity-related DUB that regulates constitutive IFN priming as well as anti-viral activation of the type I IFN response. In human intestinal epithelial cells (hIECs), USP22 constitutively represses ISG transcription, IFN secretion and signal transducer and activator (STAT)1 activation [62]. These effects are mediated by USP22-dependent deubiquitylation and inhibition of STING, a cytosolic DNA-sensing PRR. Upon viral infection with SARS-CoV-2, USP22-dependent inhibition of STING results in abrogated type III IFN signaling and upon silencing of USP22, hIECs are protected against SARS-CoV-2 replication due to enhanced ISG and IFN λ expression [62]. Similar effects are reported for USP22-dependent repression of type I IFN in a Herpes Simplex Virus type 1 (HSV-1) infection model in human embryonic kidney cells (HEKs) [49]. Interestingly however, in a murine system, infection of USP22 deficient cells with Vesicular Stomatitis Virus (VSV), HSV-1 or Sendai Virus (SeV) revealed an opposed role of USP22 in immune surveillance [63]. Rather than on the level of STING, USP22 was discovered to associate and deubiquitylate IRF3, the downstream transcription factor of the viral nucleotide-recognition pathway, resulting in enhanced type I IFN and ISG expression. On the other hand, selective depletion of USP22 in the murine hematopoietic lineage resulted in constitutive increase in ISG expression and enhanced priming of adaptive immune cells [66]. Hence, more studies on the role of USP22 in innate immunity are needed to fully elucidate its pro- and antiviral functions.

2.2.1 Roles of USP22 in cancer

Several studies on predictive markers for poor survival prognosis of various cancer types identified USP22 to be highly expressed in a large cohort of cancer tissues, which was positively correlated with poor patient survival [67, 68]. Among the investigated cancer types were solid carcinomas of prostate, lung, breast and urinary tract, as well as several brain tumors and different tumors originated from immune cells. In line with this, high USP22 expression levels correlated with severe cancer progression in additional cancer types including carcinomas of tongue, liver, cervix, pancreas and colon [69-74]. In particular, USP22 expression in colon carcinoma was investigated in great detail with respect to oncogenic USP22 functions, possibly due to its leading occurrence among cancer-related deaths worldwide. Biopsies of colorectal cancer patients with poor survival prognosis revealed significantly higher USP22 expression in immunohistochemical tissue staining and qRT-PCR analyses compared to samples from long disease-free survival patients [73, 75, 76]. Functional analysis of different human colon carcinoma cell lines revealed a positive correlation of USP22 expression with cell proliferation, metastasis and cancer cell stemness mediated by signaling pathways that are regulated by B-cell specific murine leukemia virus integration site-1 (BMI-1) and c-Myc [73, 75-77]. BMI-1 is part of the Polycomb Group (PcG) gene family that regulates cancer stem cell self-renewal and proliferation, favors metastasis and is characterized as a prediction marker for severe cancer progression [67, 78]. In line with the role of USP22 in colorectal cancer cell proliferation, USP22 was discovered to directly deubiquitylate and stabilize Cyclin B1 in human colon cancer cell lines [51]. Cyclin B1 stabilization promotes cell cycle entry and maintenance of mitosis and is likewise correlated with aggressive colorectal cancer progression [79].

In contrast to colon cancer cell lines or expression profiles of human cancerous tissue of advanced stage tumors, a transgenic mouse model for colorectal cancer *in vivo*, however, deciphered a negative correlation of USP22 expression and intestinal tumor burden [80]. Conditional knockout of *USP22* in intestinal tissue resulted in higher colon cell proliferation, increased angiogenesis and enhanced tumor growth, correlating tumor invasiveness and aggressiveness with the loss of USP22. Further mechanistic analysis of intestinal *USP22* knockout *in vitro* and *in vivo* revealed a SAGA-dependent reduction of protein kinase AMP-activated catalytic subunit alpha 2 (PRKAA2) expression, that led to an increase in mammalian target of Rapamycin (mTOR) activity, which is associated with malignant cell growth, proliferation and tumor cell survival in colorectal cancer [80, 81]. Hence, USP22 exerts tumor-suppressive functions *in vivo* by suppressing mTOR signaling. In line with this mouse model and tissue specific tumor-suppressive role of USP22, studies on other tumor entities also delineated contradictions of reported overexpression of USP22 in human tumor tissue

samples and tumor suppressive effects exerted by enhanced USP22 expression, as reviewed recently [54]. One example is the newly identified substrate of USP22, the leukemia-associated transcription factor PU.1. USP22 directly interacts and stabilizes PU.1 via deubiquitylation *in vitro* [48]. Translation into a Kirsten rat sarcoma viral oncogene (KRAS)-mutant mouse model of acute myelocytic leukemia (AML) *in vivo* revealed a positive correlation of USP22 expression, PU.1 stabilization and subsequent lineage differentiation of leukemic progenitor cells. Hence, tumorigenic potential of KRAS-mutant myeloid progenitor cells was suppressed by USP22, revealing another tumor-suppressive function of this multi-facetted DUB.

Finally, USP22 not only affects and regulates tumorigenicity via transcriptional regulation or transcription factor stabilization, but was also found to manipulate the tumor microenvironment by SAGA-independent functions. Recently, USP22 was found to deubiquitylate and stabilize the T-cell inhibitory programmed death ligand 1 (PD-L1) on cancer cells [82], which is a well-known measure of cancer cells to evade tumor immune surveillance. PD-L1 presented on tumor cells binds to its respective PD-1 receptor on cytotoxic T-cells resulting in T-cell inhibition and tumor immune escape. This signaling pathway is successfully exploited by anti-tumor treatment strategies, referred to as immune checkpoint blockade therapy [83]. Regarding tumor therapy, we were recently able to attribute a novel cell death inducing function to USP22 that may assist in cancer cell directed therapy. In detail, we could show, that USP22 expression favors tumor necrosis factor α (TNFα) and Smac mimetic-induced necroptosis in various cancer cell lines *in vitro* via stabilization of the receptor interacting kinase 3 (RIPK3) [84]. This approach is of relevance since many tumor entities manage to evade classical apoptosis-inducing chemotherapy by overexpression of cellular inhibitor of apoptosis proteins (cIAP). This cancer cell-specific resistance to apoptosis can be overcome by inducing necroptotic cell death via cIAP-inhibitors (Smac mimetics) [85]. Hence, Smac-mimetic treatment suggests a reasonable tumor cell death-inducing treatment for entities with high USP22 expression. As we could show, the USP22-RIPK3-axis in necroptosis is selectively active in cancer cell lines but plays a minor role in non-malignant cells *in vitro* [84]. In summary, USP22 is not only ubiquitously expressed in most tissues but also exerts a broad variety of functions that context-specifically either fulfill pro-tumorigenic or tumor-suppressive tasks.

2.3 SUMO and Ubiquitin-like modifications

Apart from modification of substrates by ubiquitin, many proteins are modified by UbL proteins [86]. Some UbLs resemble ubiquitin in protein structure and substrate conjugation mechanisms. Structurally, UbLs share the ß-grasp fold as well as the extended carboxyl-group of the terminal di-glycine motif, which serves as an anchor for covalent

substrate modification [87]. UbL attachment is performed by E1, E2 and E3 enzymes, as described above for the process of ubiquitylation (2.1), with the limitation of only one or two identified UbL-conjugating enzymes per UbL species [39]. Among the most important UbLs are autophagy-related protein 8 (ATG8) and ATG12, ISG15, human leucocyte antigen-F-adjacent transcript 10 (FAT10), NEDD8 and small ubiquitin-like modifier 1-3 (SUMO1-3). Physiologically, the different UbL modifications are linked to precise signaling networks. For example, the ATG proteins are conjugated to proteins involved in the formation and extension of the autophagosome during cellular recycling processes, while ISG15 is upregulated upon IFN-signaling to mark viral proteins during viral infection or host proteins like Janus kinase 1 (JAK1) and STAT1 during innate immune responses [88]. Similarly, FAT10 is induced by IFN-γ upon inflammation and labels proteins for ubiquitin-independent proteasomal degradation [89]. The main substrates for NEDDylation are cullin-RING E3 ubiquitin ligases that are involved in various processes related to cancer, as for example cell cycle dysregulation, stress response or survival signaling [90]. Similar to poly-ubiquitin, FAT10, NEDD8 and SUMO moieties are able to form polymeric chains. Moreover, ISG15, NEDD8 and SUMO are attached to substrate lysine residues and might suggest competition with ubiquitin lysine modifications, although individual UbLs require induction or occur less abundant [91]. SUMOylation for example competes with ubiquitylation of equal lysine residues in about 20 - 30% of all SUMOylated lysine residues detected by proteomics studies [92, 93]. Physiologically, dual use of lysine modifications controls ubiquitin-mediated protein degradation, as known for the inhibitor of NF-κB α (IκBα). While ubiquitylation of IκBα at K21 results in IκBα proteasomal degradation and NF-κB activation, IκBα K21 modification with SUMO1 prevents this degradative signaling and thereby inhibits NF-κB activation [94].

SUMO1 shares 18% of the amino acid sequence with ubiquitin and belongs together with SUMOs 2, 3, 4 and 5 to the SUMO family. SUMO2 and -3 are 97% sequence identical and are therefore grouped as SUMO2/3. All SUMOs share the ubiquitin ß-grasp fold and the C-terminal di-glycine motif that is needed for isopeptide bond formation with lysine residues of an E1 SUMO activating enzyme (SAE). SUMO4 is excluded from protein conjugation due to a C-terminal proline residue that restricts further processing. Together with SUMO5, SUMO4 is only expressed in certain tissues and needs to be characterized in more detail [95].

Compared to the ubiquitylation system with a large pool of interacting E1, E2 and E3 enzymes, the SUMOylation system is less complex. This facilitates the unraveling of SUMOylation-related pathways but also increases the biological vulnerability of the SUMO-conjugation system. Indeed, the SAE1/UBA2 heterodimer is the only known E1 enzyme, that catalyzes the ATP-dependent activation of the C-terminal carboxy-group, followed by the unique E2 SUMO-conjugating enzyme Ubc9, that transfers the SUMO moiety to its own catalytic cysteine. The ligation of SUMO moieties to substrate proteins is facilitated by a few

identified E3 ligases that assure substrate specificity and influence signaling outcome. For example, the RING-type protein inhibitor of activated STAT (PIAS) E3 SUMO ligases govern transcriptional regulation [96], the Ran-binding protein 2 (RanBP2) SUMO ligase regulates nucleoplasmatic transport and nuclear integrity [97] and the Fanconi anemia protein SLX4 ligase complex that is essential during DNA damage and cellular stress response [98], which is the evolutionary most conserved function of SUMOylation [95]. Finally, the deconjugation of SUMO moieties is conducted by six majorly characterized sentrin-specific proteases (SENP) 1-3 and 5-7. These different SENP family members exhibit either chain preference for a certain SUMO paralogue, or promiscuously cleave any SUMO species while being restricted to certain cellular compartments. These SUMO/SENP-dense hotspots are found in the nuclear pore complex, DNA repair foci, the nucleolus or promyelocytic leukemia protein (PML) nuclear bodies [99]. All of these signaling hubs consist of a large number of individual enzymes that together form a macromolecular complex. Essentially, these complexes aggregate via the interaction of SUMOylated proteins with SUMO interaction motif (SIM)-bearing partner proteins. SIMs are composed of a hydrophobic stretch of variable alignments of the amino acids valine, isoleucine and leucine, that interact with hydrophobic residues of the SUMO moieties [100]. Interestingly, SUMO-SIM interactions are of low affinity in the micromolar range, allowing fast signaling switches on the one hand but demanding multiple recognition sites for precise target binding on the other hand [101].

A prominent group of enzymes that comprise multiple SIMs in tandem are SUMO-targeted ubiquitin ligases (STUbLs) that preferentially recognize substrates modified with poly-SUMO-chains which become ubiquitylated and degraded. This mechanism controls the accumulation of SUMOylated effectors in for example DNA repair to prevent cell cycle arrest [95]. Such a regulatory crosstalk of SUMO- and Ub-conjugation is described for PML and the corresponding STUbL RING-finger protein 4 (RNF4) during an acute stress response [102].

2.4 PML

PML is a ubiquitously expressed protein in human cells of all organs with the exception of highly proliferating cells such as cortical thymocytes and germinal center B cells [103]. Its expression is predominantly induced by IFN type I and II-mediated binding of STATs and IRF3 and IRF8 to IFN-stimulated responsive element (ISRE)-sites in the *pml* promoter region [104, 105]. The *pml* gene consists of nine exons located on chromosome 15 with an approximate size of 35kb [106]. During gene expression, alternative splicing leads to seven major PML transcripts, encoding the isoforms PML I – PML VII, with a number of subtypes regulating the cellular localization of each isoform [107]. As depicted in Figure 2, all PML isoforms share exon 1 – 4 of the N-terminus, harboring the RING/B-Box/Coiled-Coil (RBCC)-motif, also known as tripartite motif (TRIM). The zinc-finger containing RING domain does not

interact with DNA but presumably exerts E3 ligase functions towards SUMO moieties [108-110]. Several studies could show, that the RING domain is essential for Ubc9 recruitment and subsequent auto-SUMOylation of PML [109, 111]. The cysteine-rich B-Box domain is in charge for covalent oxidation of PML dimers, while the α-helical coiled-coil domain mediates homo- and hetero-oligomerization of PML isoforms via hydrophobic interactions [112]. The following exons 5 and 6 contain a consensus NLS and are preserved in all isoforms except PML VII, rendering this isoform solely cytoplasmatic [107]. Among the nuclear isoforms, PML I additionally harbors a nuclear export signal (NES) that presumably allows shuttling between cellular compartments [113]. Another motif that is maintained in PML I – PML V is the SIM in exon 7a, encoded by the amino acid sequence VVVISSS at position 556-562. This motif allows interaction with other SUMOylated proteins within nuclear body structures [114].

The isoform-specific domain composition and compartment localization is associated with distinct PML functions. The C-terminus of nuclear PML isoform IV for example directly interacts with the transcription factor p53 and thereby controls senescence and intrinsic apoptosis signaling [115]. On the other hand, cytoplasmatic PML isoforms are responsible for extrinsic death-receptor mediated apoptosis signaling [116]. The most abundant isoform PML I is associated with regulation of angiogenesis [117] and PML V is regarded as structural scaffold of PML nuclear bodies [118].

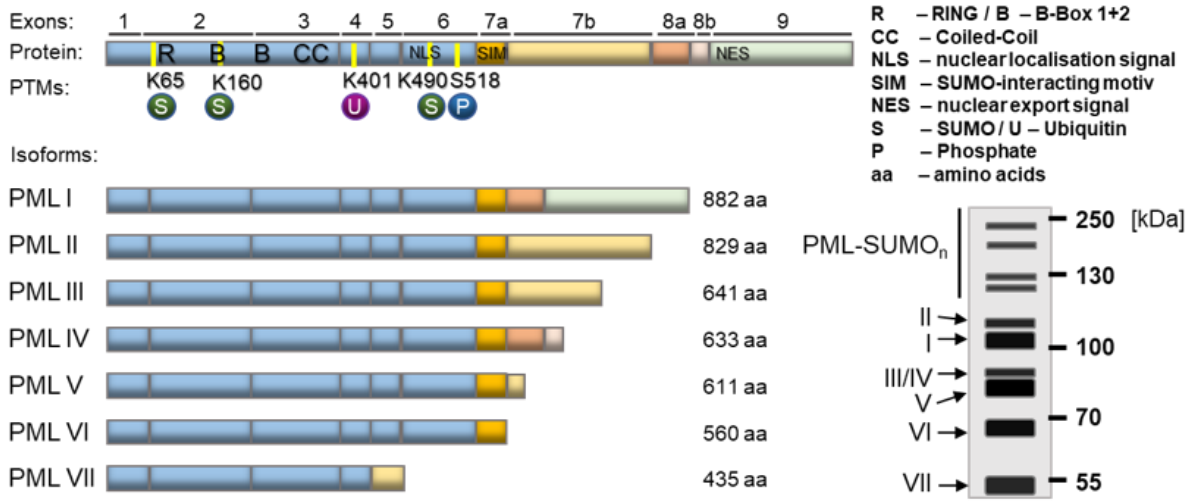

Figure 2: PML isoforms. The PML gene is composed of 9 exons (1-9) with exon 7 and 8 being divided into a and b parts. Exon 2 encodes the RING and B-Box1 domain, exon 3 the B-Box2 and Coiled-Coil domain, forming together the RBCC or Trim-motif. Exon 6 harbors a nuclear localization sequence (NLS), exon 7a a SUMO-interacting motif (SIM) and exon 9 a nuclear export signal (NES). Most important post-translational modification (PTM) during PML protein turnover are indicated at respective protein sidechains (yellow bars). Dependent on the alternative splicing of the full length PML transcript, 7 distinct major isoforms are expressed (PML I – VII) with varying C-termini and protein lengths, as indicated by the number of amino acids (aa). Estimated migration of the distinct PML isoforms in SDS-PAGE are schematically depicted on the right. PML species of high molecular weight are conjugated to multiple SUMO moieties (PML-SUMOn). Schematic representation adapted from [119, 120].

PML nuclear bodies (NBs) are dense nucleoplasmatic, membrane-less granules, consisting of up to 170 different proteins with PML forming the structure-determining core

component [121, 122]. The granules are found in almost all mammalian cells and differ in size and number from 0.2 – 1 µm and 1 – 30 NBs per nucleus, respectively [122]. NB formation is initiated by oxidation of two cysteine residues in the B-Box domain of two adjacent PML proteins, forming a covalent cystine-bridge between the PML dimer (Figure 3) [112]. This dimer then multimerizes via non-covalent hydrophobic interactions between the coiled-coil domains of other PML dimers. This oligomerization process is accelerated under cellular stress conditions, with oxidative reagents like reactive oxygen species (ROS) facilitating the primary dimer formation [114]. As a next step towards mature NBs, SUMO-conjugating E2 enzyme Ubc9 is non-covalently associated to the RING domain of PML, enabling the SUMOylation of PML at various lysine sidechains. SUMOylated PML is than able to further multimerize via the PML internal SIM motif as well as to attract the structurally assisting SIM-bearing protein Sp100 to form mature NBs [118]. Mature NBs differ in size dependent on the PML isoform incorporation and transcriptional stimulus of PML expression [118, 119]. Of note, while PML V is the most stable component of the NB spheres, PML I-IV and PML VI shuttle in and out the spherical structure within seconds and build a depot of nucleoplasmatic, soluble PML [118].

The inside of PML NBs is a soluble, protein-rich inner core with large poly-SUMO2/3 chains, that assembles distinct signaling components via SUMO-SIM interactions, dependent on the cell cycle phase and physiological condition [116, 118, 123]. Termination of PML NB-mediated signaling results from NB disassembly through ubiquitylation of poly-SUMO2/3 chains of PML and associated proteins by the tandem-SIM-containing StUbL RNF4 [102]. PML NB disassembly can be enforced by extrinsic stimuli, as for example the oxidizing agent Arsenic trioxide (Arsenic(III)-oxide; As_2O_3; ATO) that leads to rapid PML degradation [124]. While the PML turnover is physiologically stimulated by an overshooting stress response and the presence of ROS, ATO is able to potentiate the initial oxidative dimerization of PML by directly binding to the di-cysteine motif (aa 212 and 213) of the B-Box2 domain [112]. Thereby, the formation of PML multimers is enhanced, leading to efficient recruitment of Ubc9 and the known downstream catabolism (Figure 3).

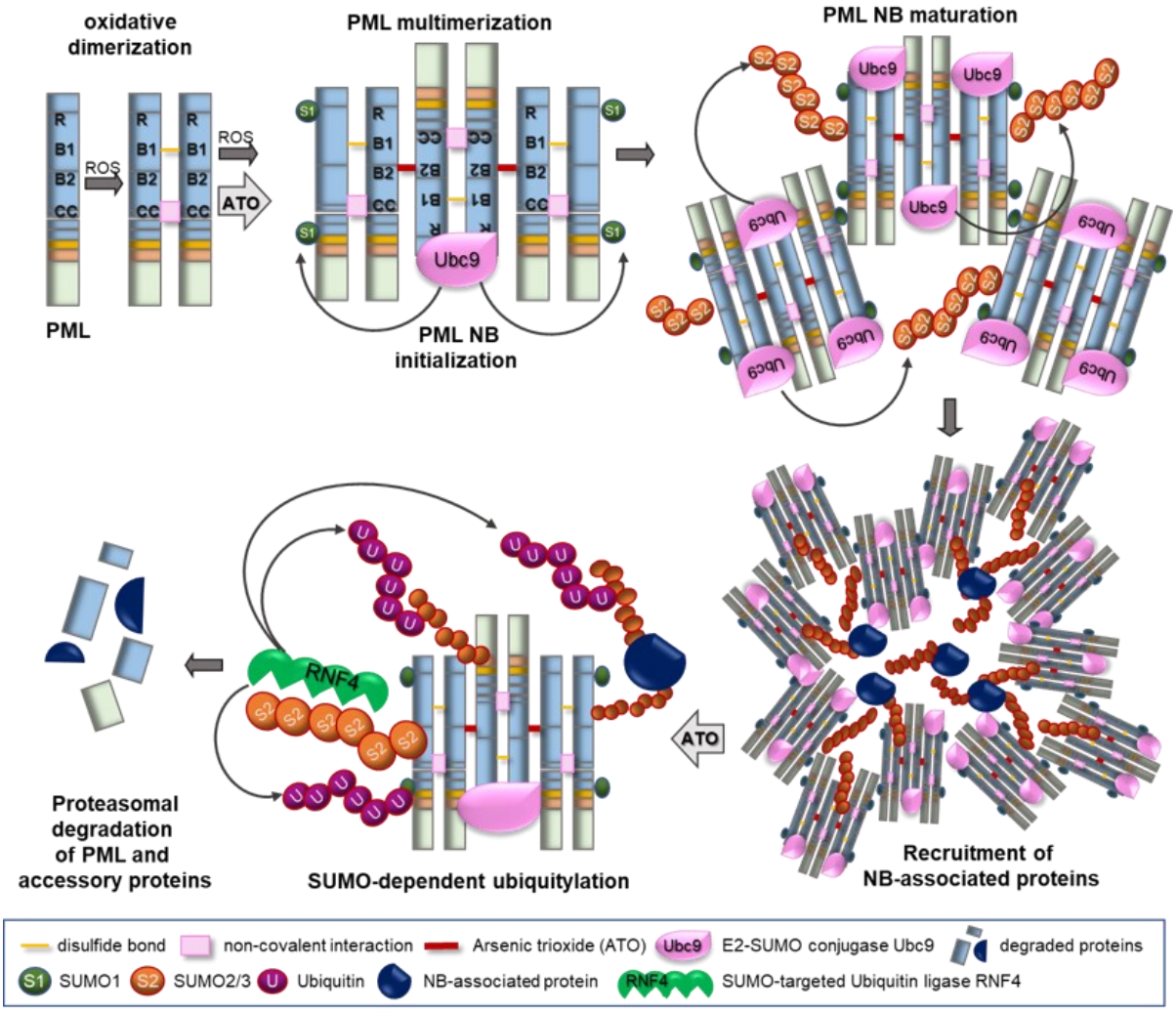

Figure 3: PML nuclear body biogenesis. PML dimerization is induced by oxidative stress (reactive oxygen species, ROS) through the formation of covalent intermolecular disulfide bonds of cysteines in the B-Box 1 domain (B1) and through hydrophobic interactions of apolar amino acid residues in the coiled-coil (CC) region. Constitutive ROS or pharmaceutical arsenic trioxide (ATO) cause further PML multimerization via crosslinking of cysteines or covalent attachment of ATO to a di-cysteine motif in the B-Box 2 domain (B2). PML multimer formation enables the attachment to the nuclear matrix and the engagement of Ubc9 to the PML RING domain (R). Ubc9-mediated conjugation of SUMO1 to PML lysines (K) K65, K160 and K490 initiates PML nuclear body (NB) formation. Further NB maturation occurs upon poly-SUMOylation of PML by Ubc9 and the recruitment of SUMO-interacting motif (SIM)-containing accessory proteins to the inner core of the spherical PML NBs. Hyper-SUMOylation of PML and its associated proteins under persisting ATO influence leads to the recruitment of SUMO-targeted Ubiquitin ligase (StUbL) RNF4. RNF4 binds to poly-SUMO tetramers and transfers poly-ubiquitin chains to PML K401 and onto preexisting poly-SUMO chains of PML and partner proteins causing their proteasomal degradation. Figure adapted from several models of PML NB morphogenesis [112, 114, 118].

Assembly of effector proteins into mature PML NBs constitutes a hub for numerous tumor suppressive signaling pathways including DNA damage response, cell cycle regulation and primary immune response upon viral infection [125, 126]. One well elaborated example is the recruitment of the transcription factor p53 together with its activating acetyltransferases p300 and CREB binding protein (CBP) as well as activating Homeodomain-interacting protein kinase 2 (HIPK2) to enable apoptotic signaling upon cellular stress conditions [115, 116]. Further PML-mediated sequestration of the p53 inactivating E3 ubiquitin ligase mouse double minute 2 homologue (MDM2) and deacetylase SIRT1 balances p53 activity [127, 128].

Additional pro-tumorigenic functions of PML NBs are reported during stem cell maintenance and angiogenesis [125].

2.4.1 PML post-translational modifications

Upon cellular stress conditions, such as DNA damage, UV-irradiation, hypoxia or oxidizing agents, PML protein levels must be rapidly fine-tuned to either ensure DNA repair during cell cycle arrest or to induce apoptosis upon severe genome instability. In this regard, PML phosphorylation was identified to play a critical role in PML activation as well as prerequisite for PML degradation. More than 12 different serine residues are described to be phosphorylated upon different stress stimuli [125]. Kinases involved in PML stabilization and promotion of apoptotic signaling are for example Aurora kinase A, checkpoint kinase 2 (Chk2) and HIPK2 which are all involved in cell cycle regulation [125]. On the other hand, kinases involved in PML-mediated signal abrogation and PML degradation are for example CDK2, extracellular signal-regulated kinase 2 (ERK2) and Casein kinase 2 (CK2) [129, 130]. The latter phosphorylation marks are identified to mediate further PML modification by SUMO and ubiquitin moieties that consequently lead to PML degradation in cancer cells [131].

PML SUMOylation by Ubc9 and Ubc9/E3 ligase complexes is relevant for PML NB dynamics and PML turnover. PML-related E3 SUMO ligases are for example RanBP2, PIAS1 and zinc finger protein (ZNF)451-1 [125]. Early PML research already revealed K65, K160 and K490 as primary SUMOylation sites involved in PML NB formation [132]. Detailed investigations led to the model, that K65 is mono-SUMOylated with SUMO1 moieties, assisting in subsequent SUMOylation of K160, while K160 is poly-SUMOylated with predominantly SUMO2/3-chains, that are needed for PML degradation [109, 124]. Both residues seem to be mutually dependent, since mutation of one or the other impedes SUMOylation of the remaining lysine [124]. K490 is conjugated to the SUMO1 paralogue and appears to be a backup SUMOylation site, since its SUMO-conjugation is enhanced upon mutation of initiator K65 [124]. Mutual mutation of K65 and K490 still allows PML degradation, revealing K160 to be the dominant conjugation site for SUMO2/3 chains. Of note, mutation of individual lysines to arginine (K→R; KR) or collective mutation of all 3 relevant lysines (3KR) does not impair PML NB formation but intervenes with NB maturation, dynamics and PML degradation [124, 132, 133].

In addition to PML SUMOylation, PML protein turnover and NB homeostasis is critically regulated by PML ubiquitylation through the E3 ubiquitin ligase RNF4 for example. RNF4 preferentially binds poly-SUMO2/3-chains of at least 4 SUMO moieties and mutually conjugates poly-ubiquitin chains to the PML sidechain K401 as well as to several lysines of the poly-SUMO2/3 chain [102, 124]. In addition, other E3 ubiquitin ligases like Ubiquitin-like with PHD and RING finger domain 1 (UHRF1), KLHL20 and E6AP ubiquitylate PML with

degradative poly-ubiquitin chains [134-136]. Under hypoxic stress for example, the transcription factor HIF1α is upregulated and induces the expression of the E3 ligase KLHL20, which forms a complex with Cul3 and is sequestered into PML NBs [134]. Here, it ubiquitylates PML upon prior CDK2-dependent PML phosphorylation at serine 518 (S518) but independently of prior PML SUMOylation [134]. The phosphorylation dependency is reported for individual PML isoforms *in vitro* as well as for KLHL20-mediated degradation of the total endogenous PML pool *in vivo* under hypoxic conditions. Under normoxic conditions, the E3 ubiquitin ligase E6AP was discovered to regulate PML stability and proteasomal turnover of distinct isoforms *in vitro* [136]. Additional examinations of tissue samples of E6AP knockout (KO) mice-derived organs revealed an inverse correlation of E6AP expression and PML abundancy as well as an increase in PML NB number and size compared to wild-type samples, supporting E6AP-dependent degradation of PML *in vivo* [136].

2.4.2 Relevance of PML in cancer

Examination of tissue sections of different human cancer types as well as investigations in human B-cell lymphoma samples revealed an overall low to absent abundancy of the PML protein despite detectable expression of PML mRNA, stressing the relevance of PML-degrading PTMs in tumorigenesis [103, 137-139]. Indeed, expression of the PML-degrading E3 ubiquitin ligase E6AP could be correlated to PML protein downregulation, PML NB dysfunction and overall tumor burden in a Myc-induced B-cell lymphoma mouse model [139]. In addition, two studies in breast, central nerval and colon cancer found a decay of PML protein abundance from primary solid tumor sections to invasive metastatic tissues of the same entity, suggesting a role of PML in cancer progression and invasiveness [137, 138]. In line with this, mechanistical *in vitro* analysis revealed a post-translational downregulation of PML protein by KLHL20-mediated ubiquitylation in the human metastatic colon cancer line HCT-116 [140]. This downregulation was favored by the absence of the KLHL20-inhibiting protein KLHL39, which is absent especially in human colorectal metastatic tissue samples. Accordingly, silencing of KLHL39 in the non-metastatic human colon carcinoma HT-29 cell line *in vitro*, as well as in a murine colon cancer model led to downregulation of PML accompanied by an increase in tumor cell migration and invasion [140, 141]. In line with that, detailed *in vivo* analysis of prostate cancer development in mice revealed that loss of PML expression led to areas of invasive prostate protrusions in combination with high-grade intraepithelial metastasis, supporting the correlation of PML deficiency and tumor invasiveness [142].

In addition to post-translationally downregulated PML, global genetic knockout of *PML* in mice causes tumor initiation and progression of multiple tissues, especially the formation of B-cell lymphomas and T-cell-driven leukemias [143]. Interestingly, loss of *PML*

caused an increase in bone marrow progenitor cell proliferation in combination with significantly decreased terminally differentiated granulocytes and monocytes in *PML*$^{-/-}$-mice-derived peripheral blood specimen, resembling the phenotype of leukemogenesis [143]. The most prominent leukemia subtype that is correlated to the loss of PML function is the acute promyelocytic leukemia (APL) that is characterized by the clonal expansion of promyelocytic progenitor cells with a deficiency in differentiation capacity [144]. Driving cause for this phenotype is the genetic monoallelic translocation of the PML gene locus on chromosome 15q22 with the retinoic acid receptor α (RARα)-encoding locus on chromosome 17q21 resulting in the t(15;17) gene product *PML-RARα* and the expression of the respective fusion protein [145]. Transcription of the non-translocated *PML* allele still results in expression of wild-type PML, however with compromised function in PML NB assembly [146-148].

2.5 PML-RARα

The fusion protein PML-RARα was discovered by cDNA sequencing of APL patients and the APL-patient-derived cell line NB4 in the early 1990s [145, 146, 149]. It became apparent, that two major isoforms of the fusion protein (short and long) are expressed in 2 different subclasses of APL, dependent on the translocation break point cluster (bcr) on the PML locus (Figure 4) [146, 149]. NB4-like APL specimen and approximately 55% of APL patients express the long isoform (also bcr1), composed of amino acids 1-552 of PML fused to amino acids 60-462 of RARα with amino acid 60 of RARα being changed from threonine to alanine due to different codon usage at the junction between PML and RARα [145, 150]. The resulting 955 amino acid long isoform has a predicted molecular weight of 106 kDa and appears as two closely running species in SDS-PAGE separation at estimated sizes of 120 kDa and 110 kDa due to an alternative splice site within exon 6 [146, 149, 150]. The residual APL specimen express the second most abundant short isoform (bcr3; 35% of APL patients [150]) with the fusion junction at position 394 of the PML moiety, migrating at approximately 90 kDa in SDS-PAGE. Bcr2 and several less common splice variants of the PML ORF account for approximately 5%-10% of APL patients [149].

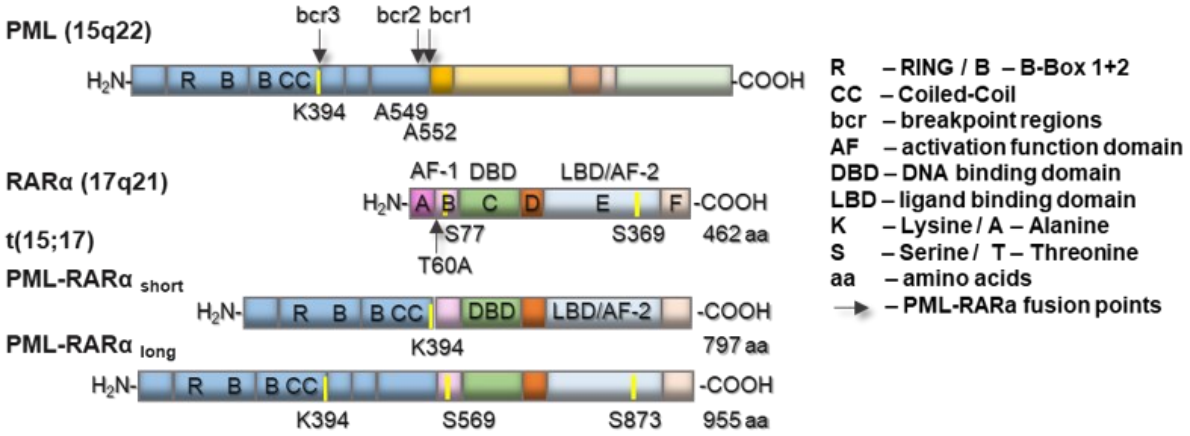

Figure 4: Translocation of PML and RARα in APL. The *PML* gene is encoded on chromosome 15q22 and the *RARα* gene on chromosome 17q21. In APL, chromosomal translocation t(15;17) results in the oncogenic fusion protein PML-RARα. In the PML locus, 3 major breakpoint regions (bcr) are known to be fused to the B – F region of the *RARα* gene. Region A and B compose the activating domain AF-1, which is interrupted in PML-RARα. Region C represents the DNA binding domain (DBD) of the nuclear receptor and region E mediates retinoic acid binding, receptor dimerization and genetic transactivation via the conserved 9aaTAD motif of the AF-2 domain. Upon oncogenic fusion, RARα amino acid threonine (T) 60 is converted into alanine in PML-RARα due to overlapping codon usage at the bcrs. PML-RARα fusion at bcr1 results in the long isoform and fusion at bcr3 results in the short isoform. Indicated serine (S) residues of the RARα moiety become phosphorylated during receptor activation and are mandatory for receptor degradation. Figure inspired by [151]

Functionally, all isoforms preserve the RBCC/TRIM motif of the PML moiety, rendering the fusion protein susceptible to oxidation-induced dimerization of the coiled-coil domain [152], as well as RING-domain mediated recruitment of Ubc9. In terms of the RARα moiety, all isoforms are fused to the B through F regions of the *RARα* locus [150]. The C-region of RARα represents a DNA-binding domain consisting of two zinc finger motifs and the E-region harbors the ligand binding domain with a conserved 9aaTAD motif (also called AF-2 domain) conferring transactivation ability upon ligand binding [153]. RARα belongs to the nuclear hormone receptor family and constitutes a transcriptional repressor upon dimerization with a retinoid X receptor (RXR). RAR-RXR heterodimer formation allows association with direct-repeat motifs (DRs) of DNA (known as RAR-responsive elements/RARE) followed by the recruitment of co-repressor complexes like HDACs or the silencing mediator of retinoid and thyroid receptors (SMRT) [154, 155]. Subsequent ligand binding induces a switch of the repressive towards an activating transcriptional regulation by the recruitment of multiprotein co-activator complexes as for example histone acetyltransferases (HATs) [155]. In PML-RARα-expressing APL cells, RARα-mediated transcriptional repression and ligand-dependent activation are extended by the ability of PML-RARα homodimerization with increased SMRT complex affinity and PML-RARα-RXR multimerization [154, 156]. Those unphysiological PML-RARα dimers bind to conserved RARE motifs with the additional recognition of wide spacings and reverse orientation, resulting in multiple *de novo* target genes, exclusively regulated by PML-RARα in APL [156, 157].

2.5.1 Acute Promyelocytic Leukemia

APL is a subtype of acute myelocytic leukemia (AML), occurring in about 10-15% of all AML-patients. Phenotypically, APL is characterized by an enlarged pool of proliferating promyelocytic progenitor cells that are unable to differentiate into granulocytes of the myelocytic lineage. This leukocytosis develops gradually with the duration of the disease and classifies high-risk APL patients with a white blood cell (WBC) count above $1x10^{10}$/L [158]. Generation of APL-mimicking transgenic mice revealed further insights into hyperproliferating promyelocytes that accumulate in spleen and bone marrow before expanding into peripheral organs like liver, kidneys, lymph nodes and lung [159, 160]. In human APL-patients low thrombocyte count and high coagulation disorder often occurs at the onset of APL development and causes moderate to severe hemorrhagic bleeding which needs to be treated in parallel to the actual leukemia [161, 162]. Standard APL therapy includes pharmacological administration of the endogenous RARα-ligand all-*trans* retinoic acid (ATRA) and the PML-degradative agent ATO in combination with chemotherapeutics like idarubicin or anthracyclines in case of high-risk APL patients [163]. This regimen leads to apoptosis of the proliferating myeloid progenitor pool, relief of the promyelocyte differentiation block and remission of the APL pathology in up to 95% of patients [158, 163].

Individual maturation stages of hematopoietic cells are defined by the presentation of certain clusters of differentiation (CD) on the cell surface as well as lineage-specific gene expression [164]. The population of APL-driving promyelocytic progenitor cells can be characterized by presentation of the myeloid lineage-specific surface markers C-X-C motif chemokine receptors (CXCR)2, CXCR4 and CD62L together with the maturation-dependent ones CD66b and CD15 [165]. In the course of neutrophilic maturation, expression of the ß2-type surface integrins CD11b and CD11c as well as CD18 gradually increases on myelocytes [166]. CD11b is important for neutrophil extravasation out of the bone marrow and for endothelial adherence and vascular transmigration [167]. Master transcription factors involved in surface marker expression and terminal myeloid differentiation are CCAAT/enhancer-binding protein (C/EBP) family members as well as PU.1 and its interacting regulator IRF1 [164, 166, 168]. In APL cells, the oncogenic fusion protein PML-RARα acts as repressor for several lineage-determining genes, resulting in a deficiency of promyelocytic cells to terminally differentiate into mature granulocytes [164] (Figure 5). On the one hand, PML-RARα-binding to RARE sites in the respective promoter regions directly causes repression of *PU.1*, *IRF1* or C/EBPε for example [164, 169]. While on the other hand, RARE-bound PML-RARα was identified to simultaneously occupy adjacent PU.1-binding motifs, resulting in downstream repression of PU.1-inducable genes like *CD11b* or *IRF1* [170].

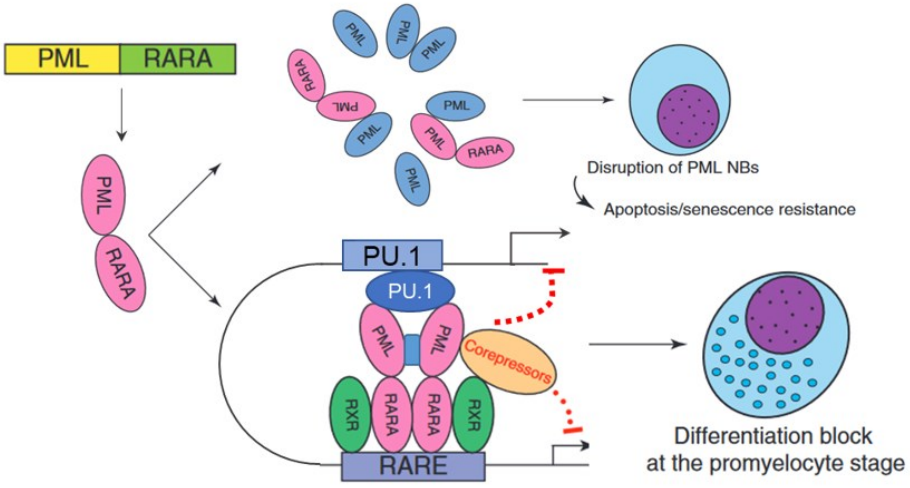

Figure 5: Function of PML-RARα in APL. Transcriptional repression and NB disruption by PML-RARα in APL. The translocated fusion protein PML-RARα interacts with endogenous PML via the coiled-coil domain of PML causing the disruption of PML nuclear bodies (NBs) and the perception of microspeckles. PML-RARα forms homodimers (blue square = hydrophobic interaction) and heterodimers with RXR via the AF-2 domain of RARα. The multimeric nuclear receptor recruits co-repressor complexes like DAXX or SMRT and occupies RAR-response elements (RARE) and PU.1-activated promoter regions to suppress transcription of lineage differentiation gene networks, resulting in the characteristic differentiation block of promyelocytes. Adapted from [170, 171]

During APL treatment, terminal myeloid differentiation is restored by administration of the RAR-ligand ATRA, that binds to promoter-bound PML-RARα dimers and transactivates PU.1- and C/EBP-driven differentiation-associated gene programs [172, 173]. While the respective genetic repression in APL patients is tightly associated to the oncogenic PML-RARα receptor as shown by ectopic PML-RARα expression in non-leukemic myeloblasts [160, 173], loss-of-function mutations of the PU.1 allele also restricts differentiation in a variety of other myeloid leukemia subtypes [174]. Likewise, ATRA- induced expression of IRF1 and STAT1 is associated with myeloid differentiation independent of the leukemic subtype [175, 176]. However, particularly in APL, IFN-signaling-dependent induction of PML expression additionally assists in APL clearance due to PML NB reassembly [177], as further explained below.

2.5.2 Targeting of PML-RARα for APL cure

As mentioned above, the highly efficient standard therapy recommended for APL patients is ATRA in combination with ATO or chemotherapeutics, dependent on the severity of leukocytosis [158]. Biological explanation for the great success of this therapy is based on two major molecular events mediated by direct interference of ATRA as well as ATO with the oncogenic fusion protein PML-RARα. On the one hand, ATRA binding to PML-RARα induces ligand-associated genetic transactivation resulting in relief of the differentiation block of immature promyelocytes. On the other hand, ATRA as well as ATO mediate the degradation of the oncoprotein, resulting in multiple events that collectively lead to promyelocyte apoptosis and the eradication of leukemia-initiating cells (LICs) [178, 179]. This synergism of ATO and

ATRA to induce differentiation and progenitor cell eradication was nicely shown in mice that were subjected to single ATRA treatment only. Despite terminally differentiated myelocyte population, secondary transplantation of the ATRA-treated bone marrow resulted in APL onset in the recipient mice, revealing the persistence of PML-RARα-positive LICs [180]. Similar observations were made in patients with low-dose ATRA therapy that eventually resulted in relapse of the disease due to incomplete deletion of leukemic blasts [181]. On the other hand, isolated APL therapy with ATO led to eradication of the promyelocyte compartment and the presence of CD11b-positive differentiated myelocytes after 6-9 days [182, 183]. However, differentiation was limited to the level of metamyelocytes, lacking features of terminally differentiated neutrophils. Hence, transactivation of differentiation as well as the degradation of PML-RARα are mutually essential for the definite cure of APL (Figure 6).

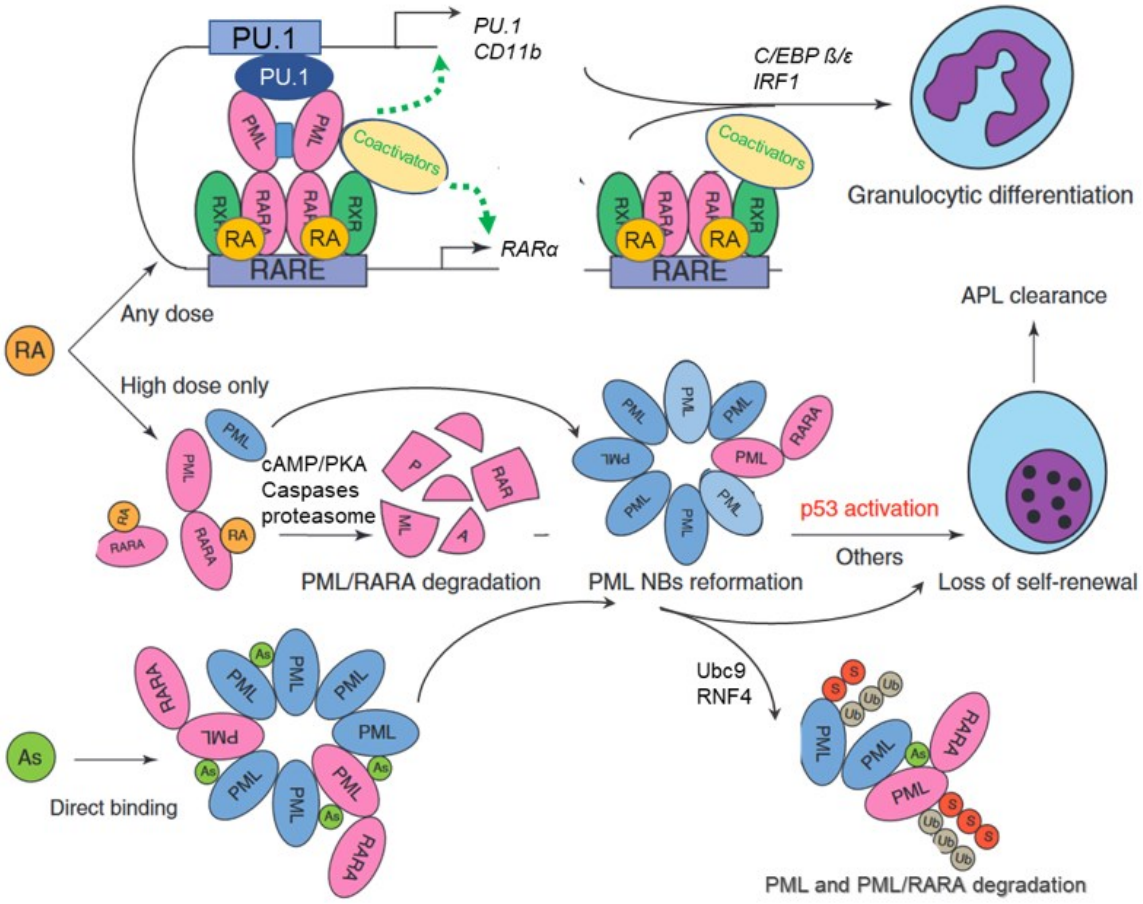

Figure 6: Effect of ATRA and ATO on PML-RARα. Treatment with all-trans-retinoic acid (ATRA/RA) and arsenic trioxide (ATO/As) synergistically leads to APL cure via PML-RARα degradation, NB re-formation, terminal granulocytic differentiation and leukemia initiating cell (LIC) eradication. Retinoic Acid (RA) binds to the ligand binding domain of the RARα moiety, causing the recruitment of co-activator complexes like histone acetyl transferases and the following transactivation of PU.1- and RARα-regulated genes. Endogenous RARα expression participates in transcriptional activation of differentiation-associated genes like C/EBP ß and ε and IRF1. High doses of ATRA cause activated receptor-associated degradation of RARα and PML-RARα involving phosphorylation via cAMP-stimulated protein kinase A (PKA), proteolytic cleavage by caspases and proteasome engagement for protease-mediated degradation. Endogenous PML is released from PML-RARα and able to re-establish NB formation and function like cell fate regulation of leukemic progenitor cells. ATO induces PML multimerization that contributes to NB re-formation. Recruitment of E2 SUMOylase Ubc9 and STUbL RNF4 to NBs cause PML and PML-RARα degradation via the proteasome. Adapted from [170, 171]

Degradative mechanisms targeting the PML-RARα oncoprotein are either directed to the PML moiety and thereby closely related to endogenous PML-degrading pathways, or to the RARα moiety in relation to ligand-dependent receptor degradation. Indeed, as described for PML turnover, ATO covalently binds to the C212/213 motif of PML-RARα which is identified as prerequisite for K160 SUMOylation and subsequent oncoprotein multimerization [112, 124, 133]. This multimer induction is required to re-distribute PML-RARα as well as endogenous PML from irregularly distributed microspeckles into functional NBs with subsequent RNF4-mediated ubiquitylation (Figure 6) [122, 147, 148, 184]. This mechanism is of particular importance for appropriate PML NB-mediated regulation of p53 in APL cells [185]. Interestingly, re-formation of PML NBs could also be observed upon isolated treatment of NB4 cells or APL mice with high doses of ATRA (Figure 6), although in a delayed fashion compared to ATO single treatment [185-188]. In APL mice, ATRA single treatment lead to markedly reduced leukocyte burden in spleens and secondary transplantation experiments revealed the complete absence of newly developed APL in the recipient mice. Those effects were reversed or absent in APL-mice crossed with *PML*$^{-/-}$ mice, supporting the necessity of PML NB re-formation for APL cure [185].

In addition to ATRA-induced PML NB formation, ATRA regulates proteasomal degradation of PML-RARα via phosphorylation of the RARα moiety, excessive ligand binding to the AF-2 transactivation domain as well as caspase-mediated cleavage of the oncogenic receptor [180, 187, 189]. In general, constitutive ligand binding to the AF-2 domain of RARα induces genetic transactivation of RARα target genes and eventually receptor degradation via direct interaction of the ligand-bound AF-2 domain with the SUG-1 subunit of the proteasome [188-190]. Additionally, during ligand activation of RARα transcriptional activity, multiple phosphorylation events are described to increase RARα activity, including a phosphorylation site in the AF-2 domain [191]. This modification is introduced by the cAMP-dependent protein kinase A (PKA) at serine 369. Interestingly, cAMP signaling is a general feature observed to be involved in APL differentiation, maturation as well as progenitor cell clearance *in vitro* and *in vivo* [157, 192]. In line with this, serine 873 of PML-RARα, that corresponds to the PKA-targeted residue in RARα, is phosphorylated upon ATRA treatment in NB4 cells [180]. Furthermore, mutation of the respective residue rendered the protein less sensitive to ATRA-induced proteasomal degradation, implying a role for cAMP signaling in PML-RARα catabolism. In addition to cAMP signaling, APL cells exert constitutive caspase-3 activity that is involved in constitutive turnover of PML-RARα as shown by pan-caspase inhibitors [186-188]. The recovery of PML-RARα protein upon caspase inhibition was even more pronounced upon ATRA-induced degradation [187, 188]. Mutational analyses of distinct PML-RARα domains revealed residue D522 to be the predicted caspase cleavage site responsible for PML-RARα degradation [187, 188]. This is consistent with the report, that the short bcr3-isoform of PML-RARα, lacking PML aa395 - 552 is resistant to ATRA-induced degradation *in*

vitro [193]. Additionally, PML itself becomes catabolized by caspases under basal conditions [188]. However, inactivating mutation of D522 still allowed ATRA-induced degradation of PML-RARα suggesting a co-existence of various PML-RARα catabolizing pathways [194, 195].

Indeed, several studies collected evidence that the PML moiety of PML-RARα becomes ISGylated under ATRA treatment resulting in proteasomal degradation [196, 197]. In detail, microarray analysis detected the ISG15-specific ubiquitin-activating enzyme E1-like (UBE1L) to be a transcriptional target of RARα and to be induced upon ATRA treatment in APL cells [172, 196]. ATRA-induced UBE1L expression could be correlated to the conjugation of ISG15 to the N-terminal region of PML-RARα, resulting in its proteasomal degradation [196, 197]. These findings could be confirmed in APL mice and also partially in patient derived primary APL cells, revealing upregulated UBE1L and ISG15 mRNA levels in response to ATRA treatment. Interestingly, the ISG15-deconjugating enzyme USP18 is also reported to be transcriptionally induced upon ATRA, resulting in increased PML-RARα stability in an N-terminus-dependent fashion which implies a regulatory feedback loop towards global hyper-ISGylation [198]. Finally, the E3 ubiquitin ligases seven in absentia homologue (SIAH)1 and SIAH2 are described to interact with the coiled-coil domain of PML and PML-RARα, regulating the homeostasis of both proteins. Overexpression-based experiments revealed proteasomal targeting of PML and PML-RARα by SIAH1/2 in complex with the E2 ubiquitin-conjugating enzyme UbcH8/UBE2L6 [199-201]. However, details regarding the nature of the ubiquitylation pattern or putative SUMOylation status of the SIAH1/2 targets remain to be identified [200, 201]. Still, physiological implication of the SIAH1/2-mediated PML-RARα degradation was demonstrated by a partial relief of the differentiation block of APL cells *in vitro* [199].

3 Aim of the study

Tumorigenesis is related to multiple aberrations of signaling pathways related to the homeostasis of a cell. Besides genetic alterations, changes in post-translational modifications impact the stability and function of essential signaling components resulting in a pro-tumorigenic cell fate. As member of the ubiquitylation system, the DUB USP22 performs great impact on protein stability of substrates involved in cell cycle regulation and transcriptional regulation. In a broad range of tumor entities, excessively abundant USP22 is associated with enhanced cell proliferation and malignant tumor progression. Simultaneously, the tumor suppressive, cell fate-regulatory protein PML is post-translationally downregulated in progressive stages of various cancer types including colorectal cancer. In APL, PML is fused to the RARα receptor, governing the entire pathogenesis of this leukemia subtype. Interventions with the fusion proteins stability by post-translational modifications is one key concept of APL cure.

With this study, we are intrigued to understand the co-appearance of USP22 overexpression and PML downregulation in colorectal cancer. Does the DUB activity account for PML degradation? Is the PTM pattern of PML altered in the presence or absence of USP22 and which protein sidechains are involved in PML modification? We further aim to investigate an alteration of normal PML function by characterization of PML NB biogenesis in dependence on USP22 expression. Furthermore, we are curious about the implications of USP22-dependent PML regulation on the APL-driving oncoprotein PML-RARα. Are the same sidechains involved in protein stability as in endogenous PML? Does USP22 expression influence PML-RARα turnover and thereby impact the responsiveness of APL cells to standard treatment? With our study, we aim at elucidating novel targets of USP22 in relation to tumorigenesis. We want to extent the knowledge on USP22-related PTMs and particularly gain insight into USP22-governed signaling pathways during leukemogenesis. By that, we envision to generate new treatment strategies for non-responsive or relapsed APL patients.

4 Materials and Methods

4.1 Materials

4.1.1 Material for cloning, DNA transfection and transduction

4.1.1.1 Plasmids

Table 1 List of plasmids

Transgene	Resistance	Vector backbone	Source
(CAT)T7-SB100		pCMV	Addgene #34879
empty	blasticidin	pSBbi-Bla	Addgene #60526
PML-IV-HA	blasticidin	pSBbi-Bla	this work
PML-IV-K394R-HA	blasticidin	pSBbi-Bla	this work
PML-IV-His	blasticidin	pSBbi-Bla	this work
PML-IV-K394R-His	blasticidin	pSBbi-Bla	this work
PML-IV-ER-F	blasticidin	pSBbi-Bla	this work
PML-IV-K394R-ER-F	blasticidin	pSBbi-Bla	this work
PML-IV-ER-F		pSG5	plasmid #6034 of Prof. Müller, IBCII, Frankfurt a.M.
HA-Ubiquitin		pCMV	#5, Prof. Müller
His-Ubiquitin		pCMV	#30, Prof. Müller
Flag-SUMO2-GG		pCI (Promega)	#1281, Prof. Müller
HA-E6AP isoform II		pCMV4	Addgene #8658
empty		pCMV	Our lab
eGFP		pcDNA3.3	Addgene #26822
mCherry		p-C1	Clontech, Cat. No. 632524
PML-RARα$_{long}$		pSG5	Prof. de Thé, College de France, Paris
His-PML-RARα$_{long}$		pSG5	this work
His-PML-K394R-RARα$_{long}$		pSG5	this work
Cas9	Puromycin	plentiCRISPRv2	Addgene #52961
Cas9, sgRNA USP22_1	Puromycin	plentiCRISPRv2	this work
Cas9, sgRNA USP22_2	Puromycin	plentiCRISPRv2	this work
Cas9, sgRNA USP22_3	Puromycin	plentiCRISPRv2	this work

Transgene	Resistance	Vector backbone	Source
Cas9, sgRNA nht_1	Puromycin	plentiCRISPR	this work
Cas9, sgRNA nht_2	Puromycin	plentiCRISPR	this work
Cas9, sgRNA nht_3	Puromycin	plentiCRISPR	this work
VSV-G		pMD2.G	Addgene #12259
HIV-1 gag, HIV-1 pol		psPAX2	Addgene #12260

4.1.1.2 Oligonucleotides for vector cloning

Table 2 List of oligonucleotides for PCR amplification, site directed mutagenesis and sequencing

Oligonucleotide	Internal number	Application	Sequence (5' → 3')
PML K394→R mutation			
PML_K349R_fwd	LK17	mutagenesis PCR	CTTGCATCACCCAGGGGAGAGATGCAG CTGTATCCAAG
PML_K349R_rev	LK18	mutagenesis PCR	CTTGGATACAGCTGCATCTCTCCCCTGG GTGATGCAAG
seq_PML_fwd2	LK21	sequencing	GAGGAGCTGATCCGCGAGCGC
Subcloning pSG5_PML-IV-ER-F → pSBbi_PML-IV-ER-F/-HA/-His			
SfiI muta PML fwd	LK23	mutagenesis PCR	GCAGATGCACGCGGCCGTCGGACAGC TGGGCCGCGCGCGTG
Sfi I muta PML rev	LK24	mutagenesis PCR	CACGCGCGCGGCCCAGCTGTCCGACG GCCGCGTGCATCTGC
SfiI site introduction PML fwd	LK25	PCR	TAACTTGGCCTCTGAGGCCAGATCTAAA CCGAGAATCGAAAC
SfiI site + ER-F-Tag PML IV rev	LK27	PCR	GGACCTGGCCTGACAGGCCGAATTCTC AGACTGTGGCAG
SfiI site + HA Tag PML IV rev	LK28	PCR	GACCTGGCCTGACAGGCCTCATCCTGC GTAATCTGGAACATCGTATGGGTAAGAA GGAATTAGAAAGGGGTG
SfiI site + His tag PML IV rev	LK29	PCR	GACCTGGCCTGACAGGCCTCATCCGTG ATGGTGGTGATGGTGAGAAGGAATTAG AAAGGGGTGG
seq_PML_fwd	LK19	sequencing	GACTTCTGGTGCTTTGAGTGCGAG
seq_PML_rev	LK20	sequencing	GCTCACTGTGGCTGCTGTCAAG
seq_PML_fwd3	LK22	sequencing	GAGGAGGGGAAGGAGGCAAGGTTG

Oligonucleotide	Internal number	Application	Sequence (5' → 3')
His-tag insertion into pSG5_PML-RARα			
His6x-PML fwd	LK46	mutagenesis PCR	CATCACCATTCCATGGAGCCTGCACCC GCC
5-UTR-His6x rev	LK47	mutagenesis PCR	GTGGTGATGCATGGACCCCAGCTTAGT TTCGATTCTC
T7-Promoter (rev)	P195	sequencing	TAATACGACTCACTATAGGG
sgRNA insertion into plenti_CRISPRv2			
hUSP22_1	C2.1_fwd	ligation	**CACC**GCCATTGATCTGATGTACGG
	C2.1_rev	ligation	**AAAC**CCGTACATCAGATCAATGGC
hUSP22_2	C2.2_fwd	ligation	**CACC**GCCTCGAACTGCACCATAGGT
	C2.2_rev	ligation	**AAAC**ACCTATGGTGCAGTTCGAGGC
hUSP22_3	C2.3_fwd	ligation	**CACC**GACCTGGTGTGGACCCACGCG
	C2.3_rev	ligation	**AAAC**CGCGTGGGTCCACACCAGGTC
nht_1/eGFP#4 (Addgene #51763)	C29.1_fwd	ligation	**CACC**GGAGCGCACCATCTTCTTCA
	C29.1_rev	ligation	**AAAC**TGAAGAAGATGGTGCGCTCC
nht_2/eGFP#3 (Addgene #51762)	C29.2_fwd	ligation	**CACC**GGCCACAAGTTCAGCGTGTC
	C29.2_rev	ligation	**AAAC**GACACGCTGAACTTGTGGCC
nht_3/eGFP#1 (Addgene #51760)	C29.3_fwd	ligation	**CACC**GGGCGAGGAGCTGTTCACCG
	C29.3_rev	ligation	**AAAC**CGGTGAACAGCTCCTCGCCC
U6		sequencing	GGGCAGGAAGAGGGCCTAT

All oligonucleotides were designed individually and purchased from Eurofins in HPLC purity

4.1.1.3 Cloning reagents and kits

Table 3 List of cloning and transfection reagents

Reagent	Company/Composition
***In silico* cloning**	
BsmBI restriction enzyme	NEB
CutSmart® restriction buffer	NEB
Fast Alkaline Phosphatase	NEB
GeneArt™ Site-Directed Mutagenesis Kit	Thermo Fisher Scientific
GenElute PCR clean-up Kit	Sigma

Reagent	Company/Composition
peqGOLD Gel Extraction Kit	peqlab
Phusion polymerase Kit	NEB
Platinum PCR Super Mix High Fidelity	Thermo Fisher Scientific
Q5® Site-Directed Mutagenesis Kit	NEB
SfiI restriction enzyme	NEB
T4 Ligase and buffer	Thermo Fisher Scientific
Taq polymerase Kit	NEB
TOPO™ TA Cloning™ kit	Thermo Fisher Scientific
Bacterial transformation	
Glycerol	Carl Roth
Ampicillin	Carl Roth
Kanamycin	Carl Roth
LB medium	10 g Tryptone, 5 g Yeast extract, 5 g NaCl 1 ml 1M NaOH in 1L ddH_2O
LB agar	15 g agar dissolved in 800 ml LB medium
S.O.C. medium	Thermo Fisher Scientific
DH5α competent *E.coli*	Thermo Fisher Scientific
Top10 One Shot competent *E.coli*	Thermo Fisher Scientific
Stabl3 competent *E.coli*	Thermo Fisher Scientific
GeneJET plasmid Miniprep Kit	Thermo Fisher Scientific
GeneJET plasmid Midiprep Kit	Thermo Fisher Scientific
PureLink™ HiPure Plasmid filter Maxiprep Kit	Thermo Fisher Scientific
Cellular transfection/transduction	
FuGENE® HD Transfection Reagent	Promega
Lipofectamin 2000	Thermo Fisher Scientific
OptiMEM transfection medium	Thermo Fisher Scientific
Polybrene	Sigma

4.1.2 Cell lines and cell culture reagents

All cell lines were authenticated by STR profiling/DNA fingerprinting at the Leibniz Institute, German Collection of Microorganisms and Cell Cultures (DSMZ, *Deutsche Sammlung von Mikroorganismen und Zellkulturen*) and regularly tested for mycoplasma contamination by PCR.

Table 4 Parental human cell lines

Cell line	Specification	Source	Culture medium
HT-29	Non-metastatic colorectal adenocarcinoma	ATCC	McCoy's 5A (Modified) Medium GlutaMAX™-I
HEK293T	embryonic kidney with SV40 large T-antigen expression	ATCC	Dulbecco's Modified Eagle Medium (DMEM) GlutaMAX™
HELA/PML	HeLa (cervical adenocarcinoma) with stable expression of pSG5_PML-III-6xHis-HA	Prof. Müller, IBCII, Frankfurt a.M.	DMEM GlutaMAX™
NB4	acute promyelocytic leukemia	DSMZ	Roswell Park Memorial Institute (RPMI) 1640 Medium

Cell culture media were purchased from Thermo Fisher Scientific and supplemented with 10% FCS, 1% Pen/Strep (all cell lines) and additional 1% Sodium Pyruvate (HEK293T and HeLa/PML cells).
All listed cell lines were transformed into Cas9/sgRNA_n.h.t.(1-3) and Cas9/sgRNA_USP22(1-3) expressing monoclonal cell lines cultured in the same medium as parental cell lines.

Table 5 Media supplements, additional cell culture reagents and consumables

Reagent	Company
Fetal calf serum (FCS)	Thermo Fisher Scientific
Penicillin/Streptomycin (pen/strep)	Thermo Fisher Scientific
Sodium pyruvate (100 nM)	Thermo Fisher Scientific
Puromycin	Clontech Laboratories
Blasticidin	Sigma
Trypan blue solution	Thermo Fisher Scientific
0.05%Trypsin/EDTA	Thermo Fisher Scientific
Cell culture flasks (25 cm², 75 cm², 175 cm^2 tissue culture)	Greiner Bio-One
Cell culture dishes (100 mm/145 mm diameter, tissue culture)	Greiner Bio-One
Cell culture plates (96-well, 24-well, 12-well, 6-well)	Greiner Bio-One
Cryogenic vials	Starlab

Table 6 List of drugs and inhibitors used as cell treatment

Reagent	Company
Arsenic Trioxide, As_2O_3, ATO	Merck
all-*trans* retinoic acid, ATRA	Sigma
Cycloheximide, CHX	Sigma
MG-132	Merck Millipore
Ruxolitinib	Selleckchem
Z-Val-Ala-DL-Asp-fluoromethylketone, zVAD.fmk, zVAD	Bachem

4.1.3 Material for RNA analysis

4.1.3.1 Oligonucleotides for quantitative real-time PCR (qRT-PCR)

Table 7 List of oligonucleotides for qRT-PCR of cDNA

mRNA target	Internal number	Sequence (5' → 3')
CD11b fwd	LK54	ACTTGCAGTGAGAACACGTATG
CD11b rev	LK55	AGAGCCATCAATCAAGAAGGC
DRAM1 fwd	LK56	TGTCTGTGCTTCACTAATTTCCA
DRAM1 rev	LK57	TCACAGATCGCACTCACTACG
h28S fwd	P53	TTGAAAATCCGGGGGAGAG
h28S rev	P54	ACATTGTTCCAACATGCCAG
IFI27 fwd	P915	GTGGCCAAAGTGGTCAGG
IFI27 rev	P916	CCAATCACAACTGTAGCAATCC
IFI6 fwd	P913	AACCGTTTACTCGCTGCTGT
IFI6 rev	P914	GGGCTCCGTCACTAGACCT
IFN-α fwd	P817	TCCATGAGVTGATBCAGCAGA
IFN-α rev	P818	ATTTCTGCTCTGACAACCTCCC
IFN-ß fwd	P813	ATGACCAACAAGTGTCTCCTCC
IFN-ß rev	P814	GGAATCCAAGCAAGTTGTAGCTC
IFN-λ1 fwd	P811	GGA CGC CTT GGA AGA GTC AC
IFN-λ1 rev	P812	AGC TGG GAG AGG ATG TGG T
IRF1 fwd	P151	ACAGCACCAGTGATCTGTACAAC
IRF1 rev	P152	TTCCCTTCCTCATCCTCATCT
IRF9 fwd	P280	AGCCTGGACAGCAACTCAG
IRF9 rev	P281	GAAACTGCCCACTCTCCACT
ISG15 fwd	P911	GAGGCAGCGAACTCATCTTT
ISG15 rev	P912	AGCATCTTCACCGTCAGGTC
OAS2 fwd	P659	TGCAGGGAGTGGCCATAG
OAS2 rev	P660	TCTGATCCTGGAATTGTTTTAAGTC
OAS3 fwd	P661	TCCCATCAAAGTGATCAAGGT
OAS3 rev	P662	ACGAGGTCGGCATCTGAG
PML fwd	LK19 [202]	GACTTCTGGTGCTTTGAGTGCGAG
PML rev	LK20 [202]	GCTCACTGTGGCTGCTGTCAAG
PML-RARα fwd	LK50	GCCCCGTCATAGGAAGTGAG
PML-RARα rev	LK51	TGACCCCATAGTGGTAGCCT

mRNA target	Internal number	Sequence (5' → 3')
USP18 fwd	P653	TCCCGACGTGGAACTCAG
USP18 rev	P654	CAGGCACGATGGAATCTCTC
USP22 fwd	P346	GAAGATCACCACGTATGTGTCC
USP22 rev	P347	CATTCATCCTGCTCTCTTTGC

All oligonucleotides were purchased from Eurofins in HPLC purity.

Table 8 List of reagents used for qRT-PCR

Reagent/consumable	Company
Nuclease-free water	Thermo Fisher Scientific
SYBR™ Green PCR Master Mix	Thermo Fisher Scientific
RevertAid H Minus First Strand cDNA synthesis kit	Thermo Fisher Scientific
MicroAmp™ Optical 384-Well Reaction Plate	Thermo Fisher Scientific

4.1.4 Buffers and reagents for protein analysis

4.1.4.1 Western blot and immunoprecipitation reagents

Table 9 Western Blot and pulldown reagents

Reagent	Company
Western Blot	
Albumin Fraction V (BSA)	Carl Roth
Ammonium persulfate (APS)	Carl Roth
Bromohenolblue	Amersham
cOmplete™ Protease Inhibitor Cocktail (PIC)	Roche
Dithiothreitol (DTT)	Merck
Ethylenediaminetetraacetic acid (EDTA)	Carl Roth
Hybond ECL nitrocellulose membrane	GE Healthcare
Hyperfilm™ ECL	GE Healthcar
N-ethylmaleimide (NEM)	Sigma
Nonidet P-40 (NP-40)	Carl Roth
PageRuler™ Plus Prestained Protein Ladder	Thermo Fisher Scientific
Pierce™ BCA Protein Assay	Thermo Fisher Scientific
Pierce™ ECL Western Blotting Substrate	Thermo Fisher Scientific
Pierce™ Universal nuclease	Thermo Fisher Scientific
Rotiphorese® Gel 30, Acrylamide	Carl Roth

Reagent	Company
Sodium dodecyl sulfate (SDS)	Carl Rotjh
Sodium orthovanadate	Sigma
Starter for x-ray developer	TETENAL
Superfix MRP x-ray fixing solution	TETENAL
Tetramethylethylenediamine (TEMED)	Carl Roth
Whatman paper	Carl Roth
ß-glycerophosphate	Sigma
IP	
HisPur™ Ni^{2+}-NTA beads	Thermo Fisher Scientific
Pierce™ Anti-HA Magnetic Beads	Thermo Fisher Scientific
Glutathione agarose beads	GE Healthcare Bio-Sciences

4.1.4.2 Lysis and IP buffers

Table 10 buffers for cell lysis and immunoprecipitation

Buffer	Composition
Whole cell lysis	
RIPA	50 mM Tris HCl pH 8.0 1% NP-40 0.5% Nα-deoxycholate 150 mM NaCl 2 mM $MgCl_2$ **2% SDS** EDTA-free protease inhibitor cocktail (PIC) 2 mM DTT 250 U/ml Pierce Universal Nuclease
HA-IP and GST-TUBE pulldown	
Cell wash buffer	25 mM NEM in PBS
Lysis buffer	RIPA/**1% SDS** 1 mM Sodium orthovanadate 5 mM Sodium fluoride 1 mM ß-glycerophosphate 25 mM NEM
IP buffer	20 mM Tris HCl, pH 7.5 50 mM NaCl 1 % NP-40 10 % Glycerol 5 mM EDTA Protease Inhibitor Cocktail (PIC) 1 mM Sodium orthovanadate 5 mM Sodium fluoride 1 mM ß-glycerophosphate 250 U/ml Pierce Universal Nuclease

Buffer	Composition
HA-IP washing buffer	As IP buffer above
TUBE washing buffer	1x TBST: 20 mM Tris-HCl 0.15 M NaCl 0.1 % Tween-20, pH 8
elution buffer	2X Laemmli loading buffer
NiNTA affinity pulldown	
Cell washing buffer	25 mM NEM in PBS
Lysis buffer	6 M Guanidine HCl 0.1 M NaH_2PO_4 100 mM Tris, pH 8.0
washing buffer #1	6 M Guanidine HCl 0.1 M NaH_2PO_4 10 mM Tris 0.05 % TritonX-100, pH 8
washing buffer #2	8 M UREA 0.1 M NaH_2PO_4 10 mM Tris 0.05 % TritonX-100, pH 8
washing buffer #3	8 M UREA 0.1 M NaH_2PO_4 10 mM Tris-HCl 0.05 % TritonX-100, pH 6.3
Elution buffer	3X Laemmli loading buffer 200 mM Imidazole

All chemicals as buffer components were purchased from Carl Roth or Sigma unless stated otherwise

4.1.4.3 Buffers for SDS-PAGE and Western blotting

Table 11 List of buffers for Western blotting

Buffer	Composition
Blocking buffer	5% milk powder in PBS-Tween (0.1% Tween)
Blotting buffer	5.8 g/l Tris Base 2.9 g/l Glycine 0.04% SDS 20% methanol
Loading buffer, Laemmli (6x)	350 mM Tris Base, pH 6.8 3.8% Glycerol 10% SDS 0.12 mg/ml Bromphenolblue
Phosphate-buffered saline (PBS, 10x, pH 7.4)	80 g/l NaCl 2 g/l KCl 2 g/l KH_2PO_4 14.4 g/l Na_2HPO_4

Buffer	Composition
Running buffer (5x)	15.1 g/l Tris Base 94 g/l Glycine 0.5% SDS
Separation gel	10% Acrylamide (Rotiphorese) 0.1% SDS 250 nM Tris HCl, pH 8.8 0.1% APS 0.04% TEMED
Stacking gel	5% Acrylamide (Rotiphorese) 0.1% SDS 125 mM Tris HCl, pH 6.8 0.1% APS 0.04% TEMED
Stripping buffer	0.4 M NaOH
Wash buffer	PBS-T, 0.1% Tween in PBS

All chemicals as buffer components were purchased from Carl Roth or Merck unless stated otherwise

4.1.4.4 Antibodies for Western blotting

Table 12 Primary and secondary antibodies for Western blotting

Target protein	Dilution	Species/ Conjugate	Company and order number
Primary antibodies			
Caspase 3	1:1000	Rabbit	Cell Signaling, 9662S
CDK1	1:1000	Rabbit	Abam, ab133327
E6AP	1:1000	Rabbit	ProteinTech, 10344-1-AP
ER-F-region-tag	1:500	mouse	Euromedex, ERF3-AS
FLAG-tag	1:5000	Mouse	Sigma, F1804-200UG, clone M2
GAPDH	1:5000	Mouse	Biotrend, 5G4cc
GFP	1:1000	Rabbit	ChromoTek, 632592
HA-tag	1:5000	Mouse	Santa Cruz, sc-7392x, clone F-7
His_{6x}-tag	1:500	Mouse	Santa Cruz, sc-53073
Lamin B1	1:10000	Rabbit	Abcam, ab16048
phosphoSTAT-1	1:000	Rabbit	Cell Signaling, 9167L, clone 58D6
PML	1:000	Rabbit	Abcam, ab179466
RARα	1:000	rabbit	Cell Signaling, 62294S
RFP	1:1000	Rabbit	ChromoTek, 5f8-20
ß-Actin	1:5000	Mouse	Sigma, A5441-0.2mL

Target protein	Dilution	Species/ Conjugate	Company and order number
STAT-1	1:000	Mouse	Cell Signaling, 9176S, clone 9H2
SUMO2/3	1:000	Mouse	MBL, M114-3, clone 1E7
UBE2L6	1:000	rabbit	ProteinTech, 17278-1-AP
Ubiquitin	1:5000	Mouse	Santa Cruz, sc-8017, clone P4D1
USP22	1:2000	Rabbit	Abcam, ab195289
Vinculin	1:10000	Mouse	Sigma, V9131
Secondary Antibodies			
Goat-anti-mouse-IgG	1:10000	Horseradish peroxidase	Abcam, ab6789
Goat-anti-rabbit-IgG	1:10000	Horseradish peroxidase	Abcam, ab6721

All primary antibodies were diluted in PBS-Tween (0.1 %) with 2 % BSA.
Secondary antibodies were diluted in PBS-Tween (0.1 %) with 5 % milk powder.

4.1.5 Immunofluorescence-related materials

4.1.5.1 Buffers and reagents for immunofluorescence and flow cytometry

Table 13 Buffers for IF and FACS

Buffer	Composition
IF	
Fixation buffer	3.7% PFA in PBS
Permeabilization buffer	0.1% TritonX-100 in PBS
Antibody dilution buffer	0,9 % NaCl 10 mM Tris HCl, pH 7.5 5 mM EDTA 1 mg/ml BSA
FACS	
Blocking buffer	3% FCS in PBS

Table 14 Reagents and special consumables for IF and FACS

Reagent/Consumable	Company
CellEvent Caspase 3/7 Green Detection Reagent	Thermo Fisher Scientific
CELLSTAR© microclear black plate (96-well)	Greiner Bio-One
4',6-Diamidino-2-Phenylindole (DAPI)	BD Biosciences
Hoechst 33342	Thermo Fisher Scientific

Reagent/Consumable	Company
Paraformaldehyde (PFA)	Sigma
SB-Shi-fix™ 96well plate	Everest Biotech

4.1.5.2 Antibodies for immunofluorescence and flow cytometry

Table 15 Primary and secondary antibodies for IF and FACS

Target protein	Dilution	Species/ Conjugate	Company and order number
Primary antibodies IF			
HA-tag	1:500	Mouse	Santa Cruz, sc-7392x
His-tag	1:200	Mouse	Santa Cruz, sc-53073
PML (in HeLa)	1:100	Rabbit	Abcam, ab179466
PML (in NB4)	1:100	Mouse	Santa Cruz, sc-966, clone PG-M3
RARα	1:100	Rabbit	Cell Signaling, 3965S
SUMO2/3	1:100	mouse	MBL, M114-3, clone 1E7
Secondary antibodies IF			
Goat-anti-mouse	1:800	FITC	Jackson ImmunoResearch, 115-097-003
Donkey-anti-rabbit	1:800	Cy™3	Jackson ImmunoResearch, 711-165-152
FACS			
CD11b, mouse	1:100	PE	BD Bioscience, 555388

4.1.6 Equipment and Software

Table 16 List of equipment

Equipment	Company
Autoclave VX150	Systec
Balances Kern 770/EW	Kern
Biowizard Goldenline biosafety cabinet	Kojair
Centrifuge MIKRO 200 R	Hettich
Centrifuge ROTIXA 50 RS	Hettich
CO_2 Incubator MCO-19AIC	Sanyo
Easypet© 3	Eppendorf
Electronic analytical balance EW	Kern
Electronic precision balance 770	Kern

Equipment	Company
FACS Canto II	BD Biosciences
Heating magnetic stirrer ARE	VELP scientifica
ImageXpress micro XLS system	Molecular Devices
Infinite M100 microplate reader	Tecan
Innova 4230 bacteria shaker	New Bruinswick Scientific
Inolab© pH 7310	WTW
Magnetic microtube tack	AMS Biotechnology
Mastercycler® pro	Eppendorf
Micro Centrifuge SD	Carl Roth
Microscope CKX41	Olympus
Mini-PROTEAN Tetra Cell electrophoresis system	Bio-Rad
Multipipette© 4	Eppendorf
Nalgene © Mr Frosty	Sigma
NanoDrop 1000	Peqlab
Neubauer improved counting chamber	Carl Roth
PerfectBlue™ Gel system	Peqlab
Pipette Research plus (2.5 µl, 10 µl, 20 µl, 100 µl, 200 µl, 1000 µl)	Eppendorf
PowerPac™ Universal power supply	Bio-Rad
QuantStudio 7 Flex Real-Time PCR system	Thermo Fisher Scientific
Roller	neoLab
Shaker	neoLab
Sonoplus HD 2070.2	Bandelin
Sonotrode MS 73	Bandelin
Thermomixer comfort	Eppendorf
Trans-Blot© SD Semi-Dry Transfer Cell	Bio-Rad
Vacuum Pump HLC	Ditabis
Vortex mixer ZX classic	VELP scientifica
Water bath WBT 22	Carl Roth
X-Ray cassette type G	Rego

Table 17 List of software

Software (Version)	Company
EndNote (X7.8)	Thomson Reuters
FACSDiva™ (6.1.3)	BD Bioscience
FlowJo (10.6.2)	BD Bioscience
GraphPad Prism® (7)	GraphPad Software
i-control™ (1.10)	Tecan
ImageJ (1.52e)	National Institute of Health
Magellan Data Analysis (7.2)	Tecan
MetaXpress© (6.5.1.347)	Molecular Devices
Microsoft Office 2013	Microsoft GmbH
NanoDrop Software (3.8.1)	Peqlab
NEBaseChanger™ (1.3.2)	NEB
Paint.net (4.3.7)	dotPDN LLC
PrimerX (2006)	Carlo Lapid, Bioinformatics.org
SnapGene Viewer (6.0.2)	GSL Biotech LLC

4.2 Methods

4.2.1 Molecular Biology techniques

4.2.1.1 Bacterial plasmid amplification

Mammalian expression plasmids were transformed into *E. coli* bacteria for DNA amplification. For transformation of plasmids generated with the Q5 Site-directed mutagenesis PCR kit (NEB) or GeneArt™ Site-directed mutagenesis kit (Thermo Fisher Scientific), OneShot® MAX Efficiency® DH5α™-T1R competent *E. coli* (Thermo Fisher Scientific) were used. For transformation of Platinum™ Taq polymerase-generated PCR products, OneShot® TOP10 competent *E. coli* (Thermo Fisher Scientific) were chosen and finally, for upscaling or re-transformation of correctly sequenced plasmids, OneShot® Stbl3™ competent *E.coli* (Thermo Fisher Scientific) were employed. In all cases, 2-5 µL of PCR product or purified plasmid DNA were incubated with 50 µL competent bacteria on ice for 30 minutes (min), followed by a heat shock at 42°C for 42 seconds (sec) and a recovery phase of 2 minutes on ice. Pre-expansion of transformed bacteria was performed in 250 µL prewarmed S.O.C.-medium for 1 h at 37°C and 220 rpm. Subsequently, bacterial suspension was spread on prewarmed LB-agar plates with the respective antibiotic of the target plasmids resistance (ampicillin in all cases except

TOPO vectors using kanamycin resistance) and placed upside down in an incubator for 16 h - 20 h at 37°C to assure single colony formation. Afterwards, 3 – 5 single colonies were picked in the vicinity to a gas flame and further expanded individually in 5 mL LB medium with respective antibiotic for 24 h at 37°C shaking. Amplified plasmid DNA was purified from 4/5 of the bacterial culture using the GeneJET plasmid Miniprep Kit (Thermo Fisher Scientific) according to manufacturer's instructions. DNA elution was performed in 30 µL prewarmed nuclease free ddH_2O. Finally, DNA amount was determined spectro-photometrically using a NanoDrop 1000 device. For DNA quality control, 1 µg purified DNA was prepared for Sanger Sequencing service (LGC genomics) together with 1 µM of the respective sequencing oligonucleotide (see 4.1.1.2). If the correct plasmid DNA sequence was verified, the residual 1/5 of the bacterial pre-culture was transferred into 250 mL of LB medium supplemented with antibiotic, incubated over night at 37°C shaking and finally subjected to plasmid isolation using the PureLink™ HiPure Plasmid Maxiprep Kit (Thermo Fisher Scientific). DNA elution was performed in 500 µL nuclease free prewarmed ddH_2O and stored at -20°C for downstream applications.

4.2.1.2 Cloning of PML expressing pSB_bi vectors

For transient, as well as constitutive expression, full-length human PML isoform IV (mRNA transcript variant 6, NM_002675.4) was subcloned from the pSG5 backbone (provided by Stefan Müller, IBCII, Frankfurt) into the pSBbi-blasticidin backbone of the Sleeping Beauty (SB) vector system ([203], Addgene plasmid #60526) via *SfiI*-restriction sites.

Site-directed mutagenesis (GeneArt™)

An internal *SfiI*-digestion site was deleted by silent C-A point mutation at Gly266 of the PML ORF using the GeneArt™ Site-Directed Mutagenesis Kit (Thermo Scientific) and the corresponding oligonucleotides LK23 and LK24 (4.1.1.2). PCR was performed as follows:

Table 18 GeneArt site-directed mutagenesis PCR composition

Template DNA	20 ng in dH_2O	DNA methylation	37°C	20 min
Mutagenesis primer pair	0.3 µM each	Initial denaturation	94°C	2 min
AccuPrime™ *Pfx* Reaction mix	1X	Amplification x18 cycles	94°C	20 sec
Enhancer	1X		57°C	30 sec
DNA Methylase	4U		68°C	3 min
SAM	1X	Final extension	68°C	5 min
AccuPrime™ *Pfx* polymerase	1U		4°C	hold

The PCR product was subjected to the Kit-associated recombination reaction for DNA template digestion for 10 minutes which was terminated by addition of 50 mM EDTA. Bacterial transformation and plasmid purification was performed as described above (4.2.1.1).

Platinum™ PCR and TOPO™ TA Cloning™

As a next step we inserted the pSB-required *SfiI*-digestion sites to the CDS of PML-IV by PCR using the Platinum™ PCR SuperMix Kit (Invitrogen). Simultaneously, different protein detection tags were inserted at the 3' end of PML Exon 8b after a Pro-Ser spacer. In detail, PCR oligonucleotide LK25 as *SfiI*-encoding forward primer was combined with either LK27, LK28 or LK29, encoding the Estrogen Receptor F-region (ER-F)-tag, the human influenza hemagglutinin epitope (HA)-tag or the hexa-histidine (His)-tag, respectively (see 4.1.1.2 for primer sequences). Insert amplification was conducted by Platinum™ PCR as follows:

Table 19 Platinum™ PCR composition

Template DNA	50 ng in dH_2O	Initial denaturation	94°C	2 min
Tag-insertion primer pair	0.2 µM each	Amplification x30 cycles	94°C	30 sec
Platinum™ PCR Super Mix	45 µL		58°C	30 sec
			68°C	2 min
			4°C	hold

The fresh PCR product was immediately processed for TOPO™ vector ligation for a maximum of 30 minutes using the TOPO™ TA Cloning™ Kit (Thermo Scientific) according to manufacturer's recommendations. 2 µL of the ligated TOPO vector reaction mix were transformed into DH5α competent bacteria in the presence of kanamycin as described (4.2.1.1) and TOPO vector DNA was isolated of multiple 5 mL cultures per primer pair using the GeneJet Miniprep Kit as recommended. Before DNA sequencing, a control digest was conducted using the *SfiI* restriction enzyme to select for successfully integrated inserts:

Table 20 Conditions of *SfiI* control digest

Miniprep plasmid DNA	500 ng in dH_2O	DNA restriction	50°C	30 min
Cutsmart buffer	1X		4°C	hold
SfiI restriction enzyme	1U			

For preparative *SfiI*-restriction digest of correctly sequenced TOPO_PML vectors with varying protein tags, Miniprep-DNA was amplified by retransformation into Stbl3 competent bacteria supplemented with kanamycin and isolated from 5 mL cultures. The empty target vector pSBbi-blast (Addgene #60526) was included for backbone preparation. Preparative digest was conducted as follows:

Table 21 Conditions of *SfiI* preparative digest

plasmid DNA	5 µg in dH_2O	DNA restriction	50°C	3h
Cutsmart buffer	1X		4°C	hold
SfiI restriction enzyme	20U			

Before agarose gel separation and DNA gel extraction of digested pSBbi backbone and *Sfi*I-flanked PML inserts with peqGOLD Gel Extraction Kit (peqlab), pSBbi backbone was dephosphorylated with 2U Fast alkaline phosphatase (FastAP) for 15 minutes at 37°C, followed by 5 minutes inactivation at 75°C. Gel purified DNA was eluted in 30 µL prewarmed dH_2O and directly processed for ligation as follows:

Table 22 Conditions of pSBbi plus PML-tag ligation

backbone DNA	50 ng in dH_2O	DNA ligation	16°C	over night
insert DNA (5:1 molar ratio)	100 ng in dH_2O	heat inactivation	65°C	10 min
T4 ligase buffer	1X			
T4 ligase	2.5U			

Ligation reactions were processed for transformation into Stbl3 competent bacteria in the presence of ampicillin followed by DNA amplification, isolation, sequencing and upscale amplification of correctly cloned plasmids pSBbi_PML-IV-ER-F, pSBbi_PML-IV-HA and pSBbi_PML-IV-His.

Finally, the K394R mutant of PML-IV was generated of all pSBbi_PML-IV plasmids by introducing a point mutation within the AAA-sequence of K394 to AGA, encoding for Arg394 using the primer pair LK17 and LK18 and following the instructions of the GeneArt™ Site-directed mutagenesis Kit as described in detail above (Table 18).

4.2.1.3 Cloning of PML-RARα expressing pSG5 vector

Site-directed mutagenesis (Q5®)

Transient expression of the long form of the fusion protein PML-RARα in HEK293T cells was conducted with a pSG5_PML-RARα expression plasmid, kindly provided by Hugues de Thé (College de France, Paris). For protein detection, a 6x-His-tag was inserted to the 5' end of the PML ORF by conducting a PCR following the instructions of the Q5® Site-Directed Mutagenesis Kit (NEB). Oligonucleotides were designed to contain a Met-START Codon, the complete 6x-His sequence, followed by a di-cysteine linker and an 18-nucleotide complementary sequence of the 5' PML-RARα ORF (see LK46 and LK47 in 4.1.1.2). Site-directed mutagenesis PCR was assembled and conducted as follows:

Table 23 Q5 Site-directed mutagenesis PCR composition

Template DNA	25 ng in dH_2O
Mutagenesis primer pair	0.5 µM each
Q5 Hot Start Master Mix	1X

Initial denaturation	98°C	30 sec
Amplification x25 cycles	98°C	10 sec
	70°C	30 sec
	72°C	3 min 40 sec
Final extension	72°C	2 min
	4°C	hold

The PCR product was subjected to the combined kinase-ligase-*DpnI* (KLD)-reaction for template DNA digestion, as proposed by the Q5 protocol. The KLD-reaction mix was then transformed into OneShot® MAX Efficiency® DH5α™-T1R competent *E. coli* (Thermo Fisher Scientific) and cultured in the presence of ampicillin as described above (4.2.1.1). The correct sequence of the plasmid DNA isolated from bacterial colonies was verified with Sanger Sequencing by LGC genomics before upscaled bacterial amplification and purification with PureLink™ HiPure Plasmid Maxiprep Kit (Thermo Fisher Scientific). In addition, the K394 to Arg394 mutation of the PML sequence was introduced into pSG5_His-PML-RARα with GeneArt™ site-directed mutagenesis as described for the pSB_PML-IV plasmids (4.2.1.2).

4.2.1.4 Cloning of sgRNA expressing plentiCRISPR_v2 vectors

For the generation of CRISPR/Cas9-mediated genetic knock out cell lines, Cas9 encoding plentiCRISPRv2 vectors were cloned to encode for single guide (sg)RNAs targeting either USP22 or eGFP as non-human-target (n.h.t.) control. For each target, 3 individual sgRNAs were designed to anneal next to a genomic PAM sequence (a NGG nucleotide motif). For plentiCRISPRv2 cloning, the sgRNA sequences were ordered as complementary forward and reverse oligonucleotides with *BsmBI* restriction site overhangs as proposed by the Zhang lab protocol (retrieved from www.genome-engineering.org/gecko on 23.04.2018). Oligonucleotide sequences are listed in Material section (4.1.1.2). 10 µM of each oligonucleotide of a corresponding pair were annealed by 5 minutes heating at 95°C followed by 1h recovery at ambient temperature. Immediately after, the annealed oligo pairs were subjected to ligation into *BsmBI*-digested, not-dephosphorylated plentiCRISPRv2 backbone. Digestion and ligation were set up as follows:

Table 24 Conditions of *BsmBI* preparative digest

plasmid DNA	1 µg in dH_2O
Buffer 3.1 (NEB)	1X
BsmBI restriction enzyme	10U

DNA restriction	55°C	1h
	4°C	hold

Table 25 Conditions of plentiCRISPRv2 and sgRNA ligation

digested backbone DNA	100 ng in dH_2O	DNA ligation	21°C	30 min
annealed oligo pair	1 µmol	no heat inactivation, because *BsmBI* is active at 55°C		
T4 ligase buffer	1X			
T4 ligase	5U			

Ligation reaction was directly transformed into recombinase deficient Stbl3 competent bacteria and plated onto LB-Amp agar plates for colony selection. Downstream DNA amplification, isolation and verification was performed as described above (4.2.1.1). The U6 standard sequencing primer was applied for plentiCRISPRv2_sgRNA validation.

4.2.2 Cell culture techniques

4.2.2.1 Culturing of cell lines

All cell lines were cultured in recommended medium (see section 4.1.2) in humidified incubators with 5 % CO_2 at 37°C. Cells were split every 48-72 hours when 90% confluent and passaged into fresh culture flasks once a week. Splitting factors varied among cell lines between 1:3 (NB4 cells), 1:10 (HT-29 and HeLa cells) and 1:20 (HEK293T cells). For passaging of adherent cells, cell layer was washed with pre-warmed PBS and adhesion was inhibited with trypsin/EDTA solution at 37 °C, 5 % CO_2 for 5 to 10 minutes. Upon detachment of cells, fresh culture medium was added to inhibit trypsin activity. Cell suspension was collected in 50 mL tubes for counting and downstream experimental seeding. Respective proportion of cells was re-transferred into culture flask and diluted with fresh medium. Cell culture was terminated at a number of 30 passages or 3 months of permanent culture.

4.2.2.2 Cryo-preservation of cells

Stocks of immediate early cell passages after purchase or genetically engineered cell lines were stored in liquid nitrogen tanks for long-term preservation. Per cryogenic vial, approximately 1x10^6 healthy confluently grown cells were harvested in collection tubes, separated from culture medium by centrifugation for 5 minutes at 1200 rpm and resuspended in 1 mL pure FCS/10% DMSO. Cryo-vials were immediately stored in isopropanol-cooled racks (Mr Frosty) and stored at -80°C for 48h for gradual freezing before transfer into liquid nitrogen tanks.

4.2.2.3 Seeding and treatment of cells

Cell density of all experiments was kept the same in order to achieve comparable cellular performance throughout this work. In detail, adherent cells were seeded 24h prior to cell treatment at a density that reaches confluency at the timepoint of treatment. That is 0.5 x 10^5/cm² for HT-29 cells and 0.3 x 10^5/cm² for HEK293T and HeLa/PML cells. NB4 suspension cells were pre-seeded 4h before treatment at a density of $1/10^{th}$ of confluency for 96 h and 120 h treatment regimen and at $1/5^{th}$ of confluency for 72 h treatment, that is 0.1 x 10^6/mL and 0.2 x 10^6/mL, respectively. Cell counting was performed using a Neubauer Counting chamber and cell suspension was diluted 4:1 with Trypan Blue for optical dead cell exclusion while counting. For immunoprecipitation, one 100 mm/145 mm cell culture dish was used per condition, for protein or RNA extraction, one well of a 6-well plate was used per condition and for immunofluorescence staining, 1 well of a 96-well glass bottom plate was used per condition. For FACS assays of NB4 cells, 2 mL of pre-seeded cultures were processed as technical duplicates of 2 x 1 mL. Experiments that represent different timepoints of the same treatment were seeded simultaneously but treated in reciprocal order to allow simultaneous harvest of different conditions. Appropriate dilutions of drugs and inhibitors were prepared in the culture medium of the respective cell line and added dropwise the day after seeding. As control condition, equal amount of medium used for drug dilution was added to the cells. In case of 120 h incubation of NB4 cells with all-trans retinoic acid, 2 mL of fresh culture medium supplemented with the appropriate concentration of ATRA were added to each condition after 72 h due to the reported half-live of ATRA in cell culture [204, 205].

4.2.2.4 Transfection of cells

HEK293T cells with transient PML expression

Transient expression of PML and PML mutant variant in HEK293T cells was conducted using FuGENE® HD transfection reagent according to the manufacturer's instructions. For CHX-chase experiments, 0.3 x 10^5/cm² cells were seeded in 6 wells 24h before transfection in the absence of Pen/Strep. At the day of transfection, 1 µg of the target vector (pSBbi-blast_PML-IV-HA or pSG5_PML-RARα-His or respective K394R mutants) were mixed with 0.3 µg of a reporter plasmid (pCMV_GFP or pCMV_mCherry) and FuGENE® reagent at a 3:1 ratio in relation to the total DNA amount and diluted in 200 µL Opti-MEM® medium per condition. The reaction mix was incubated 15 minutes at room temperature after careful inversion. Next, the suspension was added dropwise to the cells and left to incubate for 24h at 37°C/5%CO_2 before treatment of the cells with CHX.

For immunoprecipitation experiments, the same transfection procedure as described for CHX experiments was applied using 100 mm culture dishes per condition and 12 µg DNA per transfected plasmid (deviations noted in the respective figure legends) in a total amount of 1000 µL Opti-MEM® medium.

HT-29 with stable PML expression

Constitutive expression of PML and PML mutants in HT-29 cells was generated using the Sleeping Beauty (SB) transposon system [203], existing of pSB-target vectors and the transposase enzyme needed for genomic insertion at specific internal- and direct-repeat (IR/DR) motifs. For this, 0.2 x 10^5/cm² HT-29 cells were seeded in 6-well dishes 24 h prior to transfection in the absence of Pen/Strep. At day of transfection, 1.8 µg of the respective pSB-target vector (pSBbi-blast_empty, pSBbi-blast_PML-IV-His, pSBbi-blast_PML-K394R-His) was mixed with 0.2 µg of the transposase-expressing vector pCMV-(CAT)T7-SB100 and diluted in 100 µL Opti-MEM® medium per condition. Simultaneously, Lipofectamin2000® was diluted in 100 µL Opti-MEM® medium per condition, at a 2.5:1 ratio in relation to the total DNA amount and incubated 5 minutes at room temperature. Next, both dilutions were mixed by careful inversion and incubated again for 20 minutes at room temperature before dropwise addition to the cell culture wells. After 4 h the transfection medium was changed to regular growth medium supplemented with Pen/Strep. Upon 48 h incubation at 37°C/5%CO_2, cells were re-seeded into T25 culture flasks with fresh culture medium supplemented with 10 µg/mL blasticidin. Culture expansion was continued in the presence of blasticidin selection agent for 14 days before immunofluorescent and immunoblot validation of target gene expression. For further experiments cells were maintained in regular culture medium.

4.2.2.5 Generation of CRISPR/Cas9-derived *USP22* KO cell lines

Viral particle generation

All parental cell lines listed in the Material section (Table 4) were genetically modified with the CRISPR/Cas9 system to express single guide (sg)RNAs targeting either eGFP as non-human target (n.h.t.) control or USP22 as gene of interest (GOI). Per target gene, three sgRNA sequences were designed to anneal to 3 different PAM regions of the GOI in order to provoke a DNA double strand break by the Cas9 endonuclease. Multiple breaks either cause the genetic deletion of the intersection or result in false nucleotide sequences due to incorrect base repair by non-homologous end joining, leading to a frame shift and consequent genetic knockout of the GOI. Mutant cell lines were generated by lentiviral transduction. For this, VSVG-coated, psi-deficient HIV-1-derived viral particles were generated in HEK293T. Cells were seeded 24h in advance in 6 well plates, followed by co-transfection of 1 µg packaging

plasmid pMD2.G and 2.7 µg psPAX2 with 1.1 µg of 3 Cas9- and sgRNA-encoding pLentiCRISPRv2 vectors (nht#1,_#2,_#3 or USP22#1,_#2,_#3) with the help of FuGENE® transfection reagent, as described above (4.2.2.4). The transfection medium was replaced by fresh culture medium after 24 h. Lentiviral particle containing supernatants were then collected after 24 h and 48 h, sterile filtered with 45 µm syringe filters, pooled and stored at 4°C until further use.

Target cell transduction

Adherent target cells were seeded at a high density one day in advance in 6 well dishes and transduced with 1 mL of viral particles plus 2 mL fresh culture medium in the presence of 8 µg/mL polybrene. After 48 hours of transduction, medium was exchanged and supplemented with 12 µg/mL puromycin as selection agent for 10 – 14 days until target cell expansion allowed immunoblot analysis for knock out verification. NB4 suspension cells were prepared in 2 mL growth medium per 6 well 24h before addition of 500 µL viral particles and 8 µg/mL polybrene followed by spin-transduction. Culture plates were rotated at 1200 x *g* (plate rotor = 177 mm, acceleration 1, brake 0) for 2 hours at room temperature as suggested in literature [206] and placed at 37°C/5%CO_2 for 24 h. For target cell selection, 10 µg/mL puromycin were added directly into the culture for 4 days before medium exchange and target cell expansion into bigger flasks under selection pressure for 3 – 4 passages. Protein expression was analyzed 21 days post transduction. Next, puromycin resistant cell pools were diluted to 0.5 cells per 100 µL and cultured in 96 well plates for 2 – 3 weeks until expansion allowed immunoblot analysis of monoclonal-derived cells.

4.2.3 RNA analysis by qRT-PCR

Gene expression analysis was performed using quantitative real-time (qRT) PCR. For this, total RNA extracts were isolated either from 3x10^6 untreated cells, or from individually seeded and treated cells at the end of an experiment with the peqGOLD Total RNA Kit (Peqlab) as proposed by the manufacturer. During cell harvest, growth medium was washed out by resuspension of pelleted cells in 600 µL PBS and centrifugation for 3 minutes at 2000 rpm. Washed cell pellets were directly incubated with peqGOLD RNA lysis buffer and either directly processed for RNA isolation or stored at -20°C. At the end of RNA isolation, optional DNAse-digest was performed on-column before RNA elution. RNA was eluted in nuclease-free ddH_2O and was strictly kept on ice until storage at -80°C for long-term preservation. Reverse transcription of 1 µg isolated RNA was conducted according to the manufacturer's recommendations of the RevertAid H Minus First Strand cDNA synthesis Kit (Thermo Scientific). Following conditions were applied:

Table 26 Conditions of RNA reverse transcription

Isolated RNA	1 µg in dH_2O	primer annealing	25°C	5 min
Random primer	10 µM	Reverse transcription	42°C	60 min
RevertAid reaction buffer	1X	inactivation	70°C	4 min
Ribolock RNAse inhibitor	20U		4°C	hold
dNTP mix	2 mM			
Reverse transcriptase	200U			

Generated cDNA was diluted 1:10 in nuclease-free water and stored at -20°C until further use. qRT-PCR reaction on the obtained cDNA was performed using the SYBR™ Green PCR Master Mix (Applied Biosystems) with the QuantSudio™ 7 Flex Real-Time PCR System (Applied Biosystems) and assembled as follows in MicroAmp® Optical 384 well plates:

Table 27 Conditions of SYBR™ Green PCR

Template cDNA	50 ng cDNA	Primer annealing	50°C	2 min
qPCR primer pair	250 nM each	Polymerase activation	95°C	10 min
SYBR™Green Master Mix	1X	Amplification	95°C	15 sec
		x40 cycles	60°C	1 min
			4°C	hold

Amplification quality was judged by melting curve observation of individual primer pairs. As endogenous mRNA expression reference, oligonucleotides against the rRNA sequence of human ribosomal subunit 28s were incubated with each cellular condition. Expression level quantification was conducted using the $2^{-\Delta\Delta CT}$ method [207] after normalization of the target Cycle Threshold (CT) values to the CT values of 28s rRNA of each sample. Each PCR reaction was conducted as technical triplicates.

4.2.4 Protein analysis

4.2.4.1 SDS-PAGE and Western Blot

Cell lysis

Protein extracts were obtained by whole cell lysis of cells, that were washed once in PBS to remove residual growth medium and subsequently incubated with 50 – 100 µL lysis buffer per treatment condition. Cell lysis samples were kept on ice for 20 minutes before determination of protein content. In this work, mainly the protein level of PML or PML-RARα was analyzed in whole cell lysates. PML is a nuclear matrix-associated protein that clusters in nuclear bodies composed of covalently and non-covalently linked PML multimers. Protein analysis of PML

monomers thus needed to be performed under harsh denaturing and reducing conditions in order to solve dense nuclear protein aggregates. Therefore, standard RIPA lysis buffer was supplemented with 2% SDS (4.1.4.2). For easier handling of the denatured lysates, Pierce™ Universal Nuclease was added to degrade DNA. Final breakup of insoluble proteins was achieved by 5 minutes incubation of the lysates at 96°C. Residual cell debris was collected at the tube bottom by centrifugation at 17500 x *g* for 15 minutes. Protein content was immediately determined in the cleared supernatants with the Pierce™ BCA protein assay kit. Colorimetric measurement of the BCA reagent was done at a wavelength of 560 nm and protein quantification occurred in comparison to a linear BSA standard curve that was freshly prepared for each lysate analysis. Samples for gel electrophoresis were assembled by mixing 40 µg of determined protein with 6X Laemmli loading buffer and dH_2O to a maximum of 18 µL followed by 5 minutes incubation at 96°C.

SDS-Polyacrylamide Gel Electrophoresis (PAGE)

Prepared protein samples were separated by size using SDS-PAGE. SDS-polyacrylamide gels were self-prepared and consisted of a lower separating part (10% acrylamide) and an upper stacking part (5% acrylamide). Gels were positioned in electrophoretic running buffer (see Table 11 for chemical composition). As protein size reference, the standard pre-stained protein ladder PageRuler™ Plus was administered in every gel, ranging from 10 – 250 kDa molecular weight proteins. During sample assembly in the stacking gel, electrophoresis was run at 80 V – 100 V, followed by 120 V – 140 V during the separation phase.

Western Blot

Transfer of separated proteins from the gel onto a nitrocellulose membrane was achieved using a semi-dry blotting system in the presence of methanol containing blotting buffer (see Table 11 for chemical composition). Protein transfer was achieved in 1 hour 45 minutes at 1 mA/cm² of the gel. Afterwards, the membrane background was blocked with milk protein using a 5% milk-containing blocking buffer for 3x 5 minutes. After membrane washing with PBST, primary antibodies were incubated with membranes over night at 4°C on a rolling device (see Table 12 for antibody dilutions). Next day, antibody-solutions were re-collected and membranes washed in PBST 3x 5 minutes before incubation with horse-reddish peroxidase (HRP)-coupled secondary antibodies for one hour at room temperature. After another washing step, membranes were wetted with Pierce™ ECL Western Blotting substrate for 5 minutes. Finally, membranes were covered with X-ray films in the dark for enhanced chemiluminescent detection of HRP-conjugates. X-ray film development was performed manually in appropriate solutions.

Quantification of immunoblot signals

Comparison of protein levels in different treatment conditions was assessed by quantification of the band intensities on developed immunoblot films. For this, grey-level intensities of housekeeping proteins and proteins of interest were determined with ImageJ software from scanned films. POI signals were normalized to one reference protein of the same blot and calculated as fold intensity of untreated or control samples. For statistical evaluation, at least four individual immunoblots of biological replicates were analyzed.

4.2.4.2 Pulldown and immunoprecipitation (IP)

TUBE pulldown of ubiquitylated proteins

HEK293T cells were seeded at a density of 0.3x10^5/cm² in 10 cm dishes and transfected with 12 µg of plasmid DNA as described above (4.2.2.4). 24 h post transfection, plates were washed 3x with PBS supplemented with 25 mM N-ethylmaleimide (NEM), a pan-cysteine protease inhibitor that blocks deubiquitylase activity. Then, cells were detached by scraping and centrifuged for 5 minutes at 1800 rpm. Cell pellets were suspended in RIPA lysis buffer, supplemented with 1% SDS, 1 mM Sodium orthovanadate, 5 mM Sodium fluoride, 1 mM ß-glycerophosphate and 25 mM NEM for 15 minutes on ice (for buffer formulation see Table 10). Next, lysates were subjected to 2 x 10 seconds pulse-sonification at 40 % amplitude for complete shearing of genomic DNA and breakup of insoluble protein aggregates. After 20 minutes centrifugation at 14000 rpm protein content was determined by BCA reaction. 300 µg protein were prepared with 6X Laemmli loading buffer as input fraction and 3 mg total protein suspension were diluted 1:10 in TUBE lysis buffer without supplements to decrease SDS concentration to 0.1 %. For the ubiquitin-affinity pulldown, tandem ubiquitin binding entities (TUBE) tagged with glutathione S-transferase (GST), were purified from *E. coli* bacteria as described by Hjerpe and colleagues [208] and coated on glutathione agarose beads. GST-TUBE beads were pre-washed 3x in SDS-free IP buffer followed by addition of 50 µL beads to the diluted lysates. After rotating bead incubation overnight at 4°C, beads were washed 4-6 times in 600 µL TUBE wash buffer (1X TBST) by 90 seconds centrifugation at 3500 rpm. Residual wash buffer was separated from beads by short centrifugation at 14000 rpm. Finally, proteins of interest were eluted from the beads by heating to 96 °C in 60 µL reducing and denaturing 2X Laemmli buffer and analyzed by Western blot.

IP of HA-tagged proteins

HEK293T cells were prepared, washed, harvested and lysed as described for TUBE-pulldown. Enrichment of HA-tagged proteins was performed using 50 µL Pierce™ α-HA magnetic beads per 3 mg extracted protein suspension. Beads were pre-washed 3x in SDS-free IP buffer and incubated with diluted lysates overnight at 4°C rotating. Next day, HA-beads were washed 4-

6 times with 600 µL SDS-free IP buffer by inversion and with the help of a magnetic rack. One final washing step was performed in 1XTBST before incubation of the dried beads with 2X Laemmli loading buffer and sample propagation to Western blot analysis.

Ni^{2+}-NTA affinity purification of His-tagged proteins

HEK293T cells were seeded, transfected, washed and scraped as described for TUBE-pulldown. For harsh denaturation, cells were lysed in 500 µL RIPA buffer supplemented with 2% SDS and 25 mM NEM for 10 minutes on ice, followed by 2 x 10 seconds pulse-sonification at 40 % amplitude and centrifugation at 14000 rpm for 15 minutes and 4°C. Protein content was determined in cleared lysates by BCA. As input samples, 100 µg protein suspension was prepared for Western blot with 6X Laemmli loading buffer. For Ni^{2+}-NTA affinity purification, 1200 µg protein suspension were filled up to 5 mL volume with 6M guanidinium chloride-containing Ni^{2+}-NTA lysis buffer in 5 mL Eppendorf cups. Per sample, 30 µL HisPur™ Ni^{2+}-NTA magnetic beads were equilibrated 2x in Ni^{2+}-NTA lysis buffer and added to the diluted lysates for rotating incubation overnight at room temperature. Next day, bead suspension was transferred stepwise into 1.5 mL tubes and separated from the supernatant by 2 minutes centrifugation at 5000 rpm. Collected beads were washed by sequential incubation for 2 minutes with 2x 900 µL Ni^{2+}-NTA washing buffer #1, #2 and #3 (Table 10) using a magnetic rack. Final washing step was performed in 1X PBS followed by centrifugation for 2 minutes at 3000 rpm and careful removal of the supernatant. For His-tagged protein elution, dried beads were mixed with 200 mM imidazole-containing elution buffer for 30 minutes at room temperature, while vortexing.

4.2.4.3 Proteomics and mass spectrometry

Identification of ubiquitylated proteins was prepared by Dr. Jens Rödig, as published recently [84]. Briefly, HT-29 n.h.t. and HT-29 USP22 KO cells were cultured in stable isotope containing SILAC culture medium for 6 passages, labeling n.h.t. cells with Lys^0 and Arg^0 light isotopes and USP22 KO cells with Lys^8 and Arg^8 heavy isotopes. Next, equal amounts of cells were mixed and subjected to protein precipitation in the presence of ice-cold acetone. Denatured protein extracts were sequentially digested with trypsin and endoproteinase Lys-C, followed by enrichment of ubiquitin remnants with α-Gly-Gly-antibody-coupled resin. Resulting ubiquitylated peptide fractions were subjected to tandem mass spectrometry (UHPLC-MS/MS) by a quadrupole Orbitrap mass spectrometer (Q Exactive Plus, Thermo Scientific). Peptide identification and lysine site localization was processed by the MaxQuant quant software [209], employing the PTM scoring algorithm with posterior error probability filter. Mass spectrometry, the corresponding analysis and ubiquitin remnant profiling was performed by Thomas Juretschke and Petra Beli at the Institute of Molecular Biology (IMB) in Mainz.

4.2.5 Cellular phenotype analysis

4.2.5.1 Immunofluorescence microscopy

Protein imaging was performed using immunofluorescence (IF) and microscopic analysis. Adherent cells were seeded and treated in Cellstar® black micro-clear 96-well plates for the required duration of an experiment. IF staining and microscopic analysis was performed in-well without prior detachment. NB4 suspension cells were seeded and treated in 6-well plates for the required duration of an experiment. At the end of a treatment, cells were split up into appropriate portions for lysate preparation, FACS staining and IF staining. Here, 150 µL of treated cells was transferred into one well of Shi-fix™ coated 96-well plates, that allow attachment of suspension cells as a monolayer. Attachment was allowed for 30 minutes at room temperature. Following IF staining steps were performed in-well as for adherent cells. For intracellular staining, cells were fixed in pre-warmed 3.7% PFA in PBS solution for 10 minutes followed directly by 10 minutes permeabilization in 0.1% TritonX in PBS. Afterwards, wells were washed 3 x 1 minute with PBS. To assure proper cell attachment, all reagents were changed using multichannel pipettes and careful handling. Next, plate background was blocked for 30 minutes with 1 mg/mL BSA-containing antibody-dilution buffer (ADB, see Table 13 for complete formulation) followed by administration of 30 µL/well primary antibodies diluted in ADB and incubated overnight at 4°C (see Table 15 for antibody dilutions). Next day, antibody dilutions were recollected, stored at -20°C and used up to 5 times for IF staining. After careful washing, 50 µL of secondary, fluorophore-conjugated antibodies diluted in ADB was added to the wells together with 1:10,000 diluted DAPI for 90 minutes at room temperature in dark surrounding. Finally, wells were washed again 3 x in PBS and plates were kept at 4°C in the dark until microscopic analysis with the ImageXpress Micro XLS Widefield High-Content Analysis System by using the 60x objective and the DAPI, TRITC or FITC filter system.

IF image quantification

Automated IF image analysis was performed using the MetaXpress® analysis software. Absolute cell numbers per image were determined using the DAPI channel, average nucleus size was set to range from 5 – 30 µm in diameter. Signal intensity above background was determined manually for individual channels for each experiment. Relative amounts of cells of interest were determined using the Cell Scoring algorithm, that calculates the number of TRITC- or FITC-positive cells in relation to all DAPI-positive nuclei. Quantification of dot-like structures was conducted by the Granularity algorithm with dot size set to range from 0.7 – 5 µm in diameter. Per well of a 96-well plate, multiple sites distributed across the well were recorded for analysis. The respective algorithms calculated an average of all sites resulting in one value per condition. Blurry sites were excluded from the calculation manually and the

average was adapted accordingly. Analysis of PML-Cy3 and SUMO-FITC double stained HeLa/PML cells was conducted using the Custom Module Editor. In detail, cells were identified by DAPI-positive objects with the above-mentioned diameter range and a maximum area of 600 µm². Next, within the defined areas of cells, round objects were identified and marked per channel with a pre-set size of 0.1 – 1 µm². Then, the percentage of identically marked objects was determined as double-positive SUMO-PML punctae. To reduce potential spill-over into other channels, signal intensities were calibrated until no signals were detected in the partner channel anymore. Finally, single channel pictures were exported per recorded site and formatted with the ImageJ software for representative overlay graphics.

Caspase activity assay

Relative caspase-3 and caspase-7 activity was assessed using the CellEvent™ Caspase-3/7 Green Detection Reagent as suggested by the manufacturer. In detail, the detection reagent is a fluorophore-conjugated peptide harboring the caspase-3 and -7 specific cleavage motif DEVD (Asp-Glu-Val-Asp). Upon caspase activation, the peptide is cleaved and the fluorescent signal becomes released as detectable signal in the FITC channel. 2 µM of the reagent were co-incubated with cellular treatment agents throughout the complete period of treatment on cells seeded in 96-well plates. At the day of microscopic analysis, 1 µg/mL Hoechst-33342 DNA dye was added per well for 10 minutes at 37°C/5% CO_2 as total cell reference.

4.2.5.2 Flowcytometric analysis

Evaluation of cell surface protein presentation was assessed by flow cytometry using a fluorescence activated cell sorting (FACS) device (BD, FACS Canto II). Here, a cellular phenotype is characterized by laser-supported determination of cellular size, granularity and surface protein presentation of fluorescently labeled proteins. The cellular size and granularity are determined by optical detectors of forward light scatter (FSC) and sideward light scatter (SSC), respectively. Fluorophore detection is enabled by multiple lasers at distinct excitation wavelengths. Here, the Argon laser was used to detect PE-conjugated CD11b surface protein at an excitation wavelength of 488 nm. Laser voltage was adjusted before each experiment for appropriate distribution of the main cell population in the FSC/SSC plot.

Treatment of cells was conducted as described above (4.2.2.3). Briefly, NB4 cells were seeded one day before treatment followed by incubation with all-trans retinoic acid (ATRA) for 120 hours. After 72 hours, treatment concentration was refreshed. Cells were then collected as technical duplicates in FACS tubes and washed 1x with PBS in-tube by centrifugation for 5 minutes at 1800 rpm and 4°C. Afterwards, cell surface was blocked with 3 % FCS in PBS for 30 minutes on ice. For direct fluorophore labelling, samples were incubated with PE-conjugated CD11b-ms-IgG1 antibody in a 1:40 dilution for 30 minutes on ice, washed again

and directly subjected to flow cytometric analysis. Recorded cells were first restricted to single cells by gate-enclosing the main population of and FSC-area(A)/FSC-height(H) plot. Next, cell debris was excluded from the analysis by FSC/SSC-dependent gating. In addition, mean fluorescence intensity (MFI) of the PE-fluorescence signal was quantified after size-dependent exclusion of dead cells from the main cell population. The analysis gate was set around the main cell population in untreated NB4 wildtype cells and transferred to all samples and conditions.10,000 events of this main cell population were acquired per sample. The experiment was performed in biological triplicates. Statistical analysis was applied on the normalized changes of the MFI of treated samples relative to the MFI of untreated samples.

4.2.6 Statistical analysis

All experiments were performed in at least 3 biological replicates reflecting cell samples of individual cell passages with at least 48 h proliferation rest in between. All results are shown as means with standard error of means (SEM) and were analyzed for statistical significance with GraphPad Prism (v7). For qRT-PCR, FACS-based determination of CD11b expression and protein quantification of the CHX experiments, an unpaired 2-way ANOVA without repeated measures was conducted. The assumption of normal distribution was implied to assess the influence of the treatment concentration or duration on the read-out variable among the different cell lines. The Sidak's multicomparison post-test was applied to generate individual *p*-values for each treatment condition. *P*-values indicated in CHX-quantification graphs describe the overall significance between variances of both transfected cell lines. Comparisons of USP22 KO cells with n.h.t. cells in immunofluorescence image quantifications were analyzed by two-tailed, unpaired student's t-test, indicated with stars for significance representing the following *p*-values: *p <0.05; **p <0.01; ***p <0.001. All tests are based on a 95 %-confidence interval.

5 Results

5.1 PML stability is controlled by USP22

The tumor-suppressive promyelocytic leukemia protein (PML) is a key regulator of DNA damage responses and a mediator of cellular senescence and apoptosis [210]. In a variety of human cancers, including carcinomas of prostate, lung, breast and colon, the reduction in PML protein levels has been described [137] and is generally associated with aberrantly regulated proteasomal degradation rather than genetic alteration of PML expression. Human colon adenocarcinoma tissues, for example, expresses 31% less PML protein compared to healthy colon tissues [137]. Oncogenic signaling networks that are involved in post-translational modifications of PML stability include kinases, E3 ubiquitin ligases, E3 SUMO ligases and SUMO-dependent E3 ubiquitin ligases, as reviewed by Rabellino and colleagues [130]. Less is known however, how deubiquitylases (DUBs) regulate PML ubiquitylation and degradation. Interestingly, the tumor-associated DUB USP22 controls the degradation of several cell cycle-regulating proteins and DNA damage response mediators and promotes pro-tumorigenic survival [51, 56, 211]. Strikingly, human colorectal cancer represents a tumor entity with a clear correlation of USP22 overexpression and malignant cancer progression [74, 75], providing and ideal model to test the hypothesis of overlapping signaling networks between USP22 expression levels and PML protein stability.

5.1.1 Basal PML protein abundance is regulated by USP22

To investigate a potential role of USP22 in controlling the stability and function of the tumor suppressor protein PML in human colorectal cancer-derived HT-29 cells, we generated constitutive genetic knockout cell lines of *USP22* (USP22 KO) with CRISPR/Cas9-mediated gene editing established by the Zhang laboratories [212]. Selection marker resistant cell pools were further sub-cultured into monoclonal KO cell lines by limited dilution. All experiments in this work were conducted with a monoclonal HT-29 cell line (clone #62), generated by Dr. Jens Rödig [84]. As transduction control, HT-29 cells were infected with non-human-target gRNA containing viral particles (n.h.t.) and sub-cultured as selection resistant monoclonal cell lines. Confirming experiments or analyses of mutated proteins were conducted in CRISPR/-Cas9-mediated monoclonal HEK293T n.h.t. and USP22 KO cell lines (clone #32), which were generated by myself.

Immunoblot analysis of HT-29 n.h.t. and USP22 KO denatured whole cell lysates revealed the expression of a variety of PML isoforms of different molecular weights (Figure 7A), which reflects the well described alternative splicing events of the *PML* gene locus into up to 14 different transcripts (see Figure 2, Introduction) [107]. Among these, one protein band of approximately 120 kDa was dominantly present in both cell lines, presumably reflecting the size of PML isoforms I or II [119]. The protein level of PML isoform I/II in HT-29 USP22 KO cells was increased up to 3-fold compared to n.h.t. cells (Figure 7B). In contrast to studies on reduced protein levels of USP22-targeted proteins [46, 48, 61], the inverse correlation of USP22 and PML expression levels suggests a rather indirect regulation of USP22 on PML. By deubiquitylation of mono-ubiquitylated histone H2B, USP22 regulates transcriptional activation and elongation as a member of the SAGA complex [45]. Analysis of mRNA levels however, revealed no striking increase of PML mRNA levels in USP22 KO cells (Figure 7C), suggesting that the USP22-dependent increase in PML protein levels is most likely not mediated by transcriptional upregulation. Of note, this includes all PML transcript variants, since the PCR-primers were designed to amplify the conserved 3'-end of pan-PML mRNA.

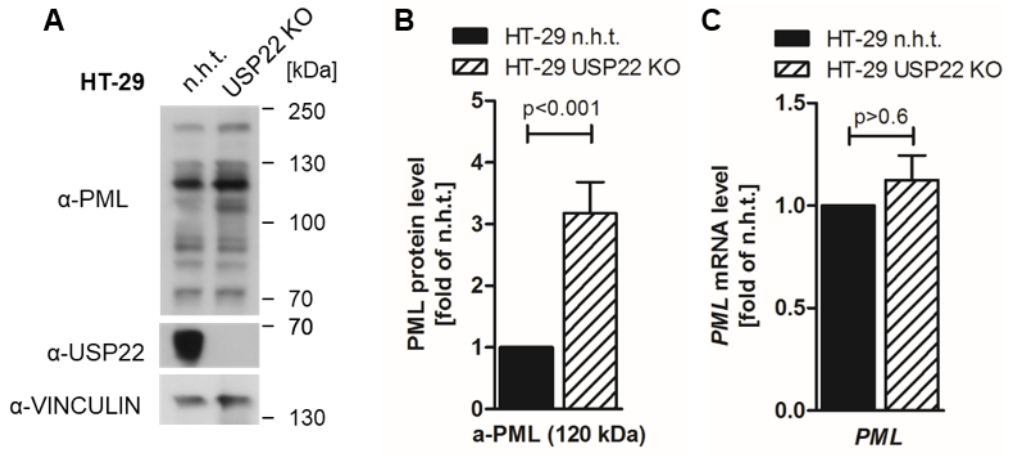

Figure 7: PML protein levels are inversely correlated with USP22 expression. A: Denatured lysates of CRISPR/Cas9-modified non-human-target (n.h.t.) and monoclonal *USP22* knockout (USP22 KO) HT-29 cells were analyzed by Western blotting using the indicated antibodies. Vinculin served as loading control. B: PML protein levels in Figure A were quantified by normalizing Western blot signal intensities of PML (120 kDa) against loading control. C: qRT-PCR analysis with pan-PML-recognizing primers in n.h.t. and USP22 KO HT-29 cells.

Stabilization of PML is associated with cell protective mechanisms, like senescence induction or gene repression as consequence of tumorigenic aberration or viral infection. In addition, infection with the human cytomegalovirus induces type I IFN signaling, which contributes to PML upregulation [126]. Vice versa, PML itself is able to trigger IFN responses by stabilizing activated phospho-STAT1, suggesting an IFN-driven feed-forward loop that potentiates PML expression and stabilization [213]. Intriguingly, recent work from our group established a mechanistic link between USP22 and IFN signaling, in that we could show a

significant upregulation of IFNs type I and III upon lack of USP22 expression [62]. In detail, a basal 4-fold upregulation of *IFNα* and 1.5-fold upregulation of *IFNβ* was detected in HT-29 USP22 KO cells (Figure 8A), accompanied with an increase in total and phosphorylated forms of the IFN-induced transcription factor STAT1 (Figure 8B). To investigate the relation between a global increase in interferon signaling upon USP22 deficiency and increased PML levels, pharmacological inhibition of the IFN system was applied. Blockade of the JAK-STAT-signaling axis by the JAK1/2-inhibitor ruxolitinib caused a partial reduction in PML protein levels in USP22 KO cells (Figure 8B), suggesting a regulation of interferon signaling and PML protein abundance by USP22.

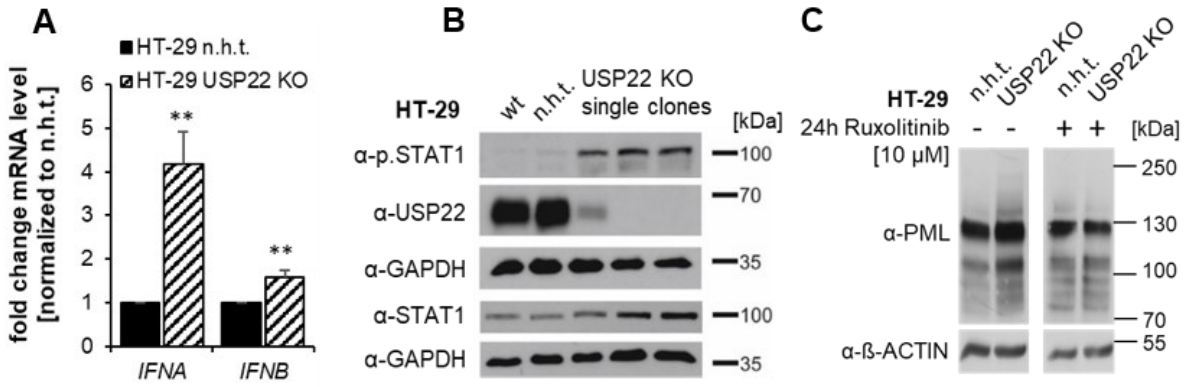

Figure 8: USP22 negatively regulates IFN signaling. A: qRT-PCR analysis of indicated mRNA levels in monoclonal USP22 KO HT-29 cells, normalized to n.h.t. HT-29 cells. 28s mRNA levels served as internal reference. B: Western blot analysis of total and phosphorylated (p.) STAT1 in parental wild-type (wt), n.h.t. and three monoclonal USP22 KO HT-29 cell lines. GAPDH served as loading control. Figures A and B were performed by Rebekka Karlowitz. C: Western blot analysis of PML protein levels in n.h.t. and USP22 KO HT-29 cells that were incubated with 10 μM JAK1/2-inhibitor ruxolitinib for 24h. ß-ACTIN served as loading control.

5.1.2 Basal PML protein stability is controlled by USP22

Since interferon signaling only slightly affected PML protein abundance in USP22 KO cells, we investigated a potential influence of USP22 on PML protein stability. Transient transfection of HEK293T n.h.t. and USP22 KO cells with PML isoform IV resulted in a prominent increase of PML protein levels in USP22 KO cells (0h CHX samples in Figure 9A), comparable to the increase in endogenous PML levels observed in HT-29 cells (Figure 7A). Blocking the *de novo* protein synthesis with the ribosomal inhibitor cycloheximide (CHX) [214] for 12, 18 and 24 hours, followed by monitoring of the remaining PML protein level, revealed a significant USP22-dependent effect on PML protein stability (Figure 9A). While PML half-life was $t_{1/2}$ = 18 hours in HEK293T n.h.t. cells, PML turnover was prolonged to approximately $t_{1/2}$ = 21 hours (interpolated value) upon USP22 deficiency (Figure 9B).

Simultaneous expression of the red fluorescent reporter protein (RFP) mCherry revealed no general alteration of protein degradation pathways in USP22 KO cells (Figure 9C). Therefore, we conclude that USP22 could affect PML expression by regulating degradation, perhaps though post-translational modifications (PTMs) that control protein stability.

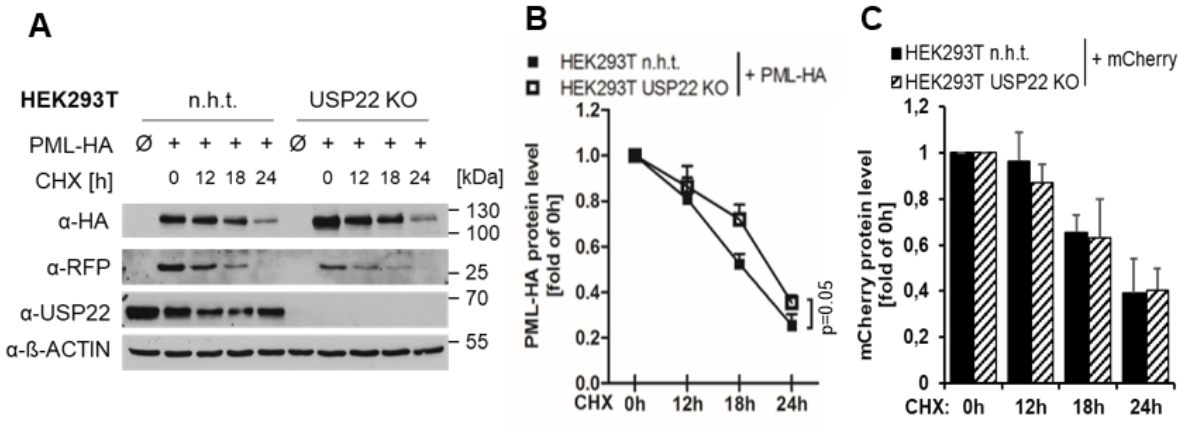

Figure 9: USP22 controls PML protein stability. A: Western blot analysis of n.h.t. and monoclonal USP22 KO HEK293T cells that were co-transfected with 1 µg HA-tagged PML (isoform IV) and 0.3 µg mCherry (RFP) plasmids 24h before incubation with 20 µg/mL cycloheximide (CHX) for the indicated periods of time. Ø = untransfected control. ß-ACTIN served as loading control. B: PML protein levels in Figure A were quantified by normalizing Western blot signal intensities of HA against loading control. Half-lives of the transfected proteins were calculated by polynomic approximation: $t_{1/2}$(n.h.t.) = 18 h and $t_{1/2}$(USP22 KO) = 21 h. C: mCherry protein levels in Figure A were quantified by normalizing Western blot signal intensities of RFP against loading control

Since ubiquitylation is important for proteasomal degradation and protein stabilization [11], we next set out to elucidate the role of USP22-mediated PML ubiquitylation. Ubiquitin pulldowns with GST-coupled tandem ubiquitin binding entities (TUBE) in denatured lysates of HEK293T cells that transiently expressed HA-tagged PML isoform IV (PML-HA) or the corresponding empty vector (EV) revealed a subtle decrease in TUBE-bound PML-HA in USP22 KO cells at a size of approximately 120 kDa (Figure 10A). Since the exogenously overexpressed PML protein is detectable at an approximate size of 120 kDa, the observed ubiquitylated PML species could represent PML modification with mono-ubiquitin. We further supported this finding by immunoprecipitation of PML-HA (Figure 10B), where the knockout of *USP22* also resulted in a reduction of ubiquitin-conjugated PML detectable at 120 kDa (arrowhead in Figure 10B). These findings support the notion of mono-ubiquitylated PML under homeostatic conditions and suggest a role of USP22 in ubiquitylation of PML isoform IV.

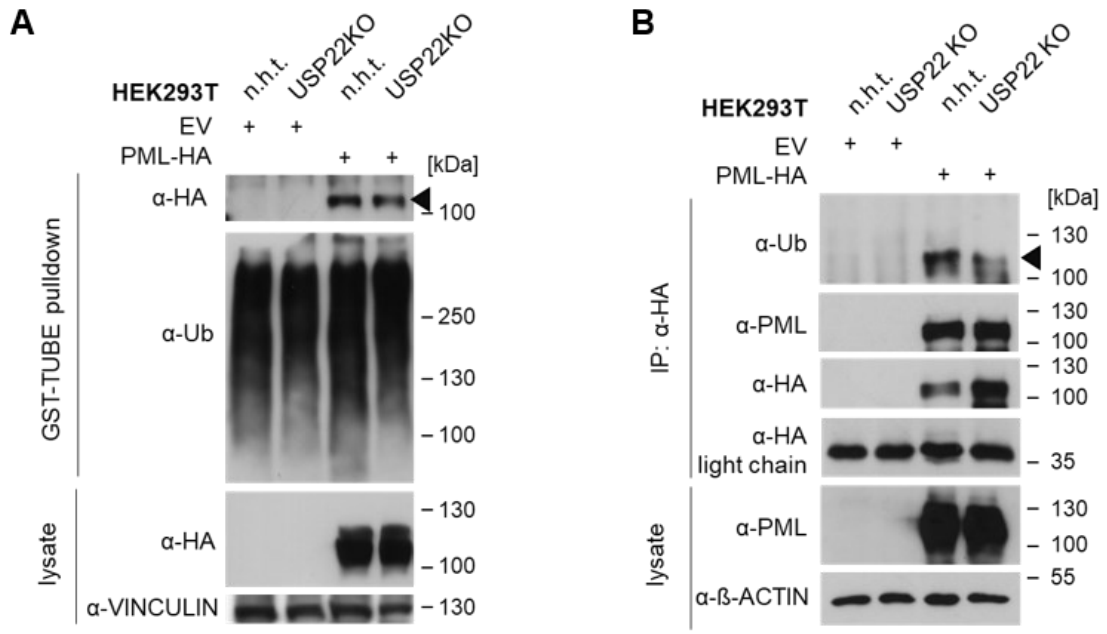

Figure 10: Loss of USP22 might affect PML ubiquitylation. A: Transient transfection of 12 µg PML-HA (isoform IV) or empty vector (EV) plasmids for 24h in n.h.t. and USP22 KO HEK293T cells. Enrichment of ubiquitylated PML proteins in denatured lysates with GST-TUBE beads. Western blot analysis of total and ubiquitylated PML-HA protein levels (α-HA). Ubiquitin-probing served as bead control, VINCULIN served as loading control. B: Cells were prepared as in A. PML-HA protein immunoprecipitation (IP) in denatured lysates with α-HA-coupled magnetic beads. Western blot analysis of total PML protein levels (α-PML) and ubiquitylated PML-HA protein levels (α-Ub). α-HA light chain detection served as bead control, ß-ACTIN served as loading control. One of two biological replicates is shown for each experiment.

5.1.3 USP22 regulates ATO-mediated post-translational modification of PML

Ubiquitylation of PML is best understood in response to cellular stress conditions, like DNA damage or oxidative stress, that induce aggregation of PML into PML nuclear bodies (NBs), in which PML becomes heavily post-translationally modified and ultimately degraded [130]. The chemical compound arsenic trioxide (ATO) mimics and enhances this stress induced PTM-cascade on PML and triggers PML degradation *in vitro* and *in vivo* [114]. Since we were able to detect small, USP22-dependent changes in ubiquitylated PML under steady-state conditions, we assessed whether USP22 might also be involved in stress-induced alteration of PML-PTMs upon ATO treatment. For this, several monoclonal USP22 KO HEK293T and HeLa/PML cell lines were generated and treated with 5 µM ATO for one and six hours (Figure 11). In contrast to endogenous PML levels that were monitored in HEK293T cells, HeLa/PML cells constitutively express HA-His-tagged PML isoform III (kindly provided by Prof. Stefan Müller, IBCII, Goethe-University, Frankfurt).

As delineated by the PML-pioneers Valérie Lallemand-Breitenbach, Hugues de Thé and colleagues, ATO treatment induces a rapid conjugation of PML with multiple SUMO2/3 moieties at the lysine residue K160 [133], followed by SUMO-dependent ubiquitylation via the STUbL RNF4 and subsequent proteasomal degradation [124]. PML conjugation with one or

multiple SUMO molecules can be monitored by Western analysis as distinct protein species of higher molecular weights (see Figure 2, introduction). While this is already detectable after 15 minutes of ATO incubation, additional ubiquitylation peaks after 4-6 hours upon ATO incubation, culminating in complete PML degradation between 12-16 hours [124]. Accordingly, the detection of various endogenous PML isoforms in HEK293T cells shifted from below 120 kDa to high molecular weight signals between 130 kDa and 250 kDa upon one hour ATO incubation (Figure 11A), representing SUMOylated PML [120]. Compared to HEK293T n.h.t. cells, SUMO-conjugated PML levels were increased in HEK293T USP22 KO cells. The dominant PML species appearing at approx. 120 kDa presumably represents incompletely degraded PML isoform I, which is located in the cytoplasm where it is excluded from ATO-mediated PML modification, as observed by others [113, 114, 120].

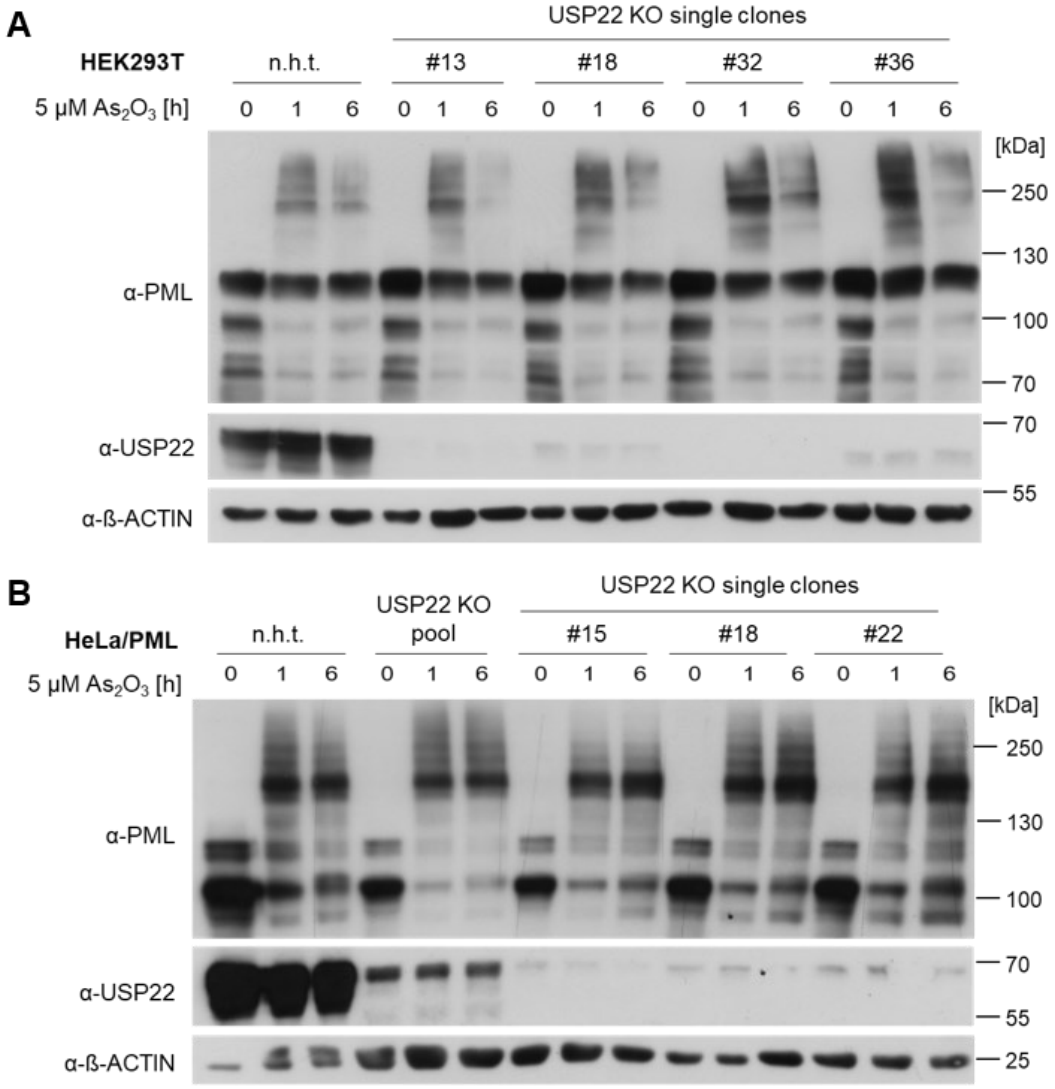

Figure 11: ATO-induced PML modifications are maintained upon loss of USP22. A: Incubation of n.h.t. and different monoclonal USP22 KO HEK293T cell lines with 5 µM arsenic trioxide (As_2O_3, ATO) for the indicated periods of time. Western blot analysis of total PML protein levels in whole cell lysates; ß-ACTIN served as loading control. B: Incubation of n.h.t., polyclonal USP22 KO (pool) and different monoclonal USP22 KO HeLa/PML cells with 5 µM As_2O_3 for indicated periods of time. Western blot analysis as in described in Figure A.

After six hours, SUMO-conjugated PML species were strongly diminished according to the onset of protein degradation (Figure 11A). Despite slightly increased SUMOylated PML levels after one-hour ATO incubation, the levels of degraded PML after six hours ATO incubation were comparable in HEK293T USP22 KO and n.h.t. cells, suggesting a minor effect of USP22 on ATO-mediated PML degradation. Similar results were observed in HeLa/PML n.h.t., polyclonal 'pooled' USP22 KO and monoclonal USP22 KO cells with ectopic expression of tagged PML isoform III (Figure 11B), detectable at approximately 110 kDa as reported by others [119]. The basal band shift at approximately 120 kDa presumably reflects single SUMOylated PML independent of ATO treatment, as described in literature [124]. Incubation of HeLa/PML n.h.t. cells with 5 µM ATO for one hour induced transition of PML III towards high-molecular weight species in a ladder-like fashion, representing ATO-dependent conjugation of multiple SUMO moieties. Of note, six hours incubation with ATO did not suffice to degrade SUMOylated PML which might result from the high total PML protein amount due to the strong T7 promoter activity used for exogenous PML expression. Knockout of *USP22* in these cells resulted in varying basal expression levels of PML III and mono-SUMOylated PML III (Figure 11B). ATO-dependent SUMOylation of PML III was detectable in all monoclonal USP22 KO cell lines with an overall increase in SUMO-conjugated PML levels after six hours compared to HeLa/PML n.h.t. cells. Together, ATO-induced alteration of PML modification was slightly affected by the loss of USP22 expression, without major effects on PML stability.

According to the PML modification upon one-hour ATO treatment and PML degradation after six hours ATO in HEK293T n.h.t. and USP22 KO cell lines, we analyzed the presence of SUMOylated PML as well as ubiquitylated SUMO-PML species at the respective timepoints. HEK293T n.h.t. and monoclonal USP22 KO cells (clone #32) were transfected with His_6-tagged PML isoform IV ('PML-His') and co-transfected with Flag-tagged SUMO2 ('Flag-SUMO') in the presence of one hour ATO incubation or with HA-tagged Ubiquitin ('HA-Ub') for a duration of six hours ATO (Figure 12A and B, respectively). Exogenously expressed PML-His was enriched from denatured cell lysates on Ni^{2+}-NTA-coupled magnetic beads and probed for conjugated Flag-SUMO or HA-Ubiquitin on Western blot. Estrogen receptor F-region (ER-F)-tagged PML IV was expressed as specificity control of the His-tag purification on Ni^{2+}-NTA beads.

Of note, PML-His enrichment was equally efficient in untreated HEK293T n.h.t. and USP22 KO cells (Figure 12A+B). Co-expression of Flag-SUMO already resulted in SUMO-conjugated PML under untreated conditions, reflecting the physiological level of mono-SUMOylated PML in PML NBs [124]. Stimulation with ATO for one hour enhanced the basal SUMOylation pattern and induced additional conjugation of multiple SUMO moieties as reflected by the high-molecular weight ladder, indicated with arrowheads (Figure 12A).

Interestingly, basal as well as ATO-induced PML SUMOylation appeared to be slightly reduced in the absence of USP22. Intriguingly, co-expression of ubiquitin in untreated cells resulted in the detection of discrete ubiquitylated PML species at the same molecular weight as mono-SUMOylated PML (arrowheads in lanes 5 + 6 in Figure 12B). Since ubiquitin and SUMO are of approximately same molecular weight, these PML species might reflect mono-ubiquitylated PML, as already observed in TUBE experiments before (Figure 10A+B). The co-existence of both PTMs under homeostatic conditions is known as regulatory cross-talk and is described for PML as well as a variety of other proteins [92, 112]. Treatment with ATO for six hours revealed the disappearance of mono-ubiquitylated PML and the prominent presence of poly-ubiquitylated PML (lowest arrowhead and smear in lanes 7 + 8 in Figure 12B).

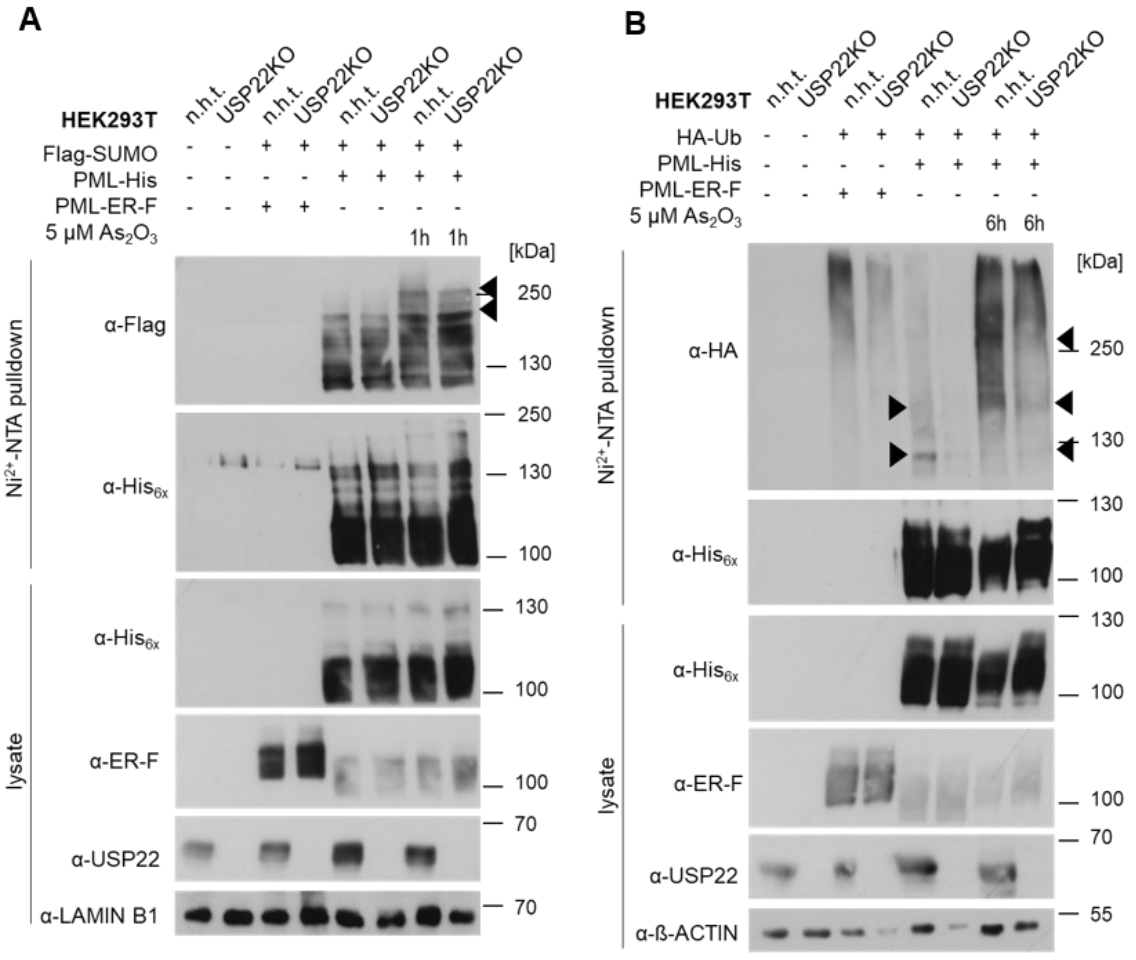

Figure 12: USP22 affects ATO-induced PML modifications. A: Transient co-transfection of 6 µg PML-His (isoform IV) and 6 µg Flag-SUMO2/3 plasmids for 24h in n.h.t. and monoclonal USP22 KO HEK293T cells. Co-transfection with PML-ER-F (Estrogen Receptor F region) served as negative bead control. Additional incubation of transfected cells with 5µM As_2O_3 for 1h as indicated. Enrichment of total PML-His proteins with Ni^{2+}-NTA-coupled magnetic beads in denatured lysates. Western blot analysis of total and SUMOylated PML-His protein levels. LAMIN B1 served as loading control. Arrowheads indicate poly-SUMO-conjugated PML species. B: Cells were transfected and processed as in A with co-transfection of 6 µg HA-Ubiquitin plasmids (HA-Ub). Incubation with As_2O_3 as indicated. Western blot analysis of total and ubiquitylated PML-His protein levels. ß-ACTIN served as loading control. Arrowheads indicate mono- and poly-ubiquitylated PML species. One of two biological replicates is shown for each experiment.

Interestingly, faint bands of ubiquitylated PML were detectable at approximate sizes of SUMOylated PML, pointing to the fact that ubiquitin chains are most likely added to pre-existing SUMO chains in response to ATO, as consistent with published findings [102]. Of note, unspecific HA-Ubiquitin was detectable to a certain extent in bead-control samples (lane 3+4 in Figure 12B). In line with the degradative signal conferred to PML by the ATO-induced poly-ubiquitin conjugation, overall PML protein levels were reduced in HEK293T n.h.t. cells (Figure 12B, lysate fraction). This onset of PML degradation could not be observed in HEK293T USP22 KO cells, correlating with less pronounced poly-ubiquitylation signals. Together, these findings confirm conjugation of SUMO and ubiquitin moieties to PML in response to ATO, with a slight loss of basal and ATO-induced PTM modifications in the absence of USP22. Therefore, we conclude that USP22 partly affects ATO-induced post-translational modifications on PML.

5.1.4 ATO-mediated PML nuclear body formation partly relies on USP22

One hallmark of ATO-mediated PML modification is the assembly and subsequent degradation of PML nuclear bodies (NBs). ATO-induced oxidative stress results in the formation of covalently linked PML dimers, which further form multimers via non-covalent interactions [112]. Long-term ATO exposure further oxidizes PML, which results in stable PML multimers and growing PML NBs that eventually become hyper-SUMOylated and ubiquitylated, causing PML degradation and PML NB disassembly [112, 133]. To understand the role of USP22 in this kinetics, we monitored the ATO-induced NB formation in HeLa/PML n.h.t. and polyclonal USP22 KO cells (Figure 13).

Interestingly, overexpression of PML III in HeLa cells resulted in the formation of NB-like structures in the absence of ATO (Figure 13A). These PML-positive clusters co-localized with SUMO2/3 in 50 – 75% of HeLa/PML cells, reflecting physiologically SUMOylated PML NBs (Figure 13A+B). This finding is in line with the observation of discrete PML-SUMO species in Western blot analysis of untreated HeLa/PML cells (Figure 11B). Consistently, the outer shell of PML III-formed NBs is described to assemble SUMO2/3 molecules under basal conditions [120]. The same study describes PML NB SUMOylation to increase within the first hour of ATO treatment. Consistently, treatment of HeLa/PML cells with ATO led to an almost complete overlap of α-PML and α-SUMO immunofluorescent signals within 30 minutes of ATO incubation (Figure 13A+B). In addition, SUMOylated NBs are described to undergo maturation by increased association of regulatory proteins and SUMO-conjugating enzymes, as well as ATO-mediated redistribution of free PML towards NBs, leading to an increase in NB size [114, 184]. In line with that, we observed an increase in NB diameter throughout the course of ATO treatment (Figure 13C). While constitutive PML NBs were calculated to measure an average of 0.7 µm diameter in HeLa/PML n.h.t. cells and 0.65 µm in USP22 KO cells, the average size of NBs increased to 1.1 µm and 0.96 µm, respectively, after 24 hours ATO incubation (Figure

13C). Finally, hyper-SUMOylated PML NBs are degraded via the recruitment of proteasomal subunits together with SUMO-dependent poly-ubiquitylation of PML and accessory proteins [133]. Likewise, the overall number of PML-positive granules decreased in n.h.t. cells from an average of 18 granules per nucleus in untreated condition to 8 granules per nucleus after 24 hours ATO treatment (Figure 13D). The number of NBs measured in USP22 KO cells declined from 13 granules per nucleus at zero hours treatment to an average of 6.7 granules at 24 hours ATO treatment. Our findings of size and number of NBs were in the range of 5-30 punctae with a size of 0.2 µm – 1 µm, as described for PML isoform-specific NB morphology in a cell type-dependent manner [119, 122].

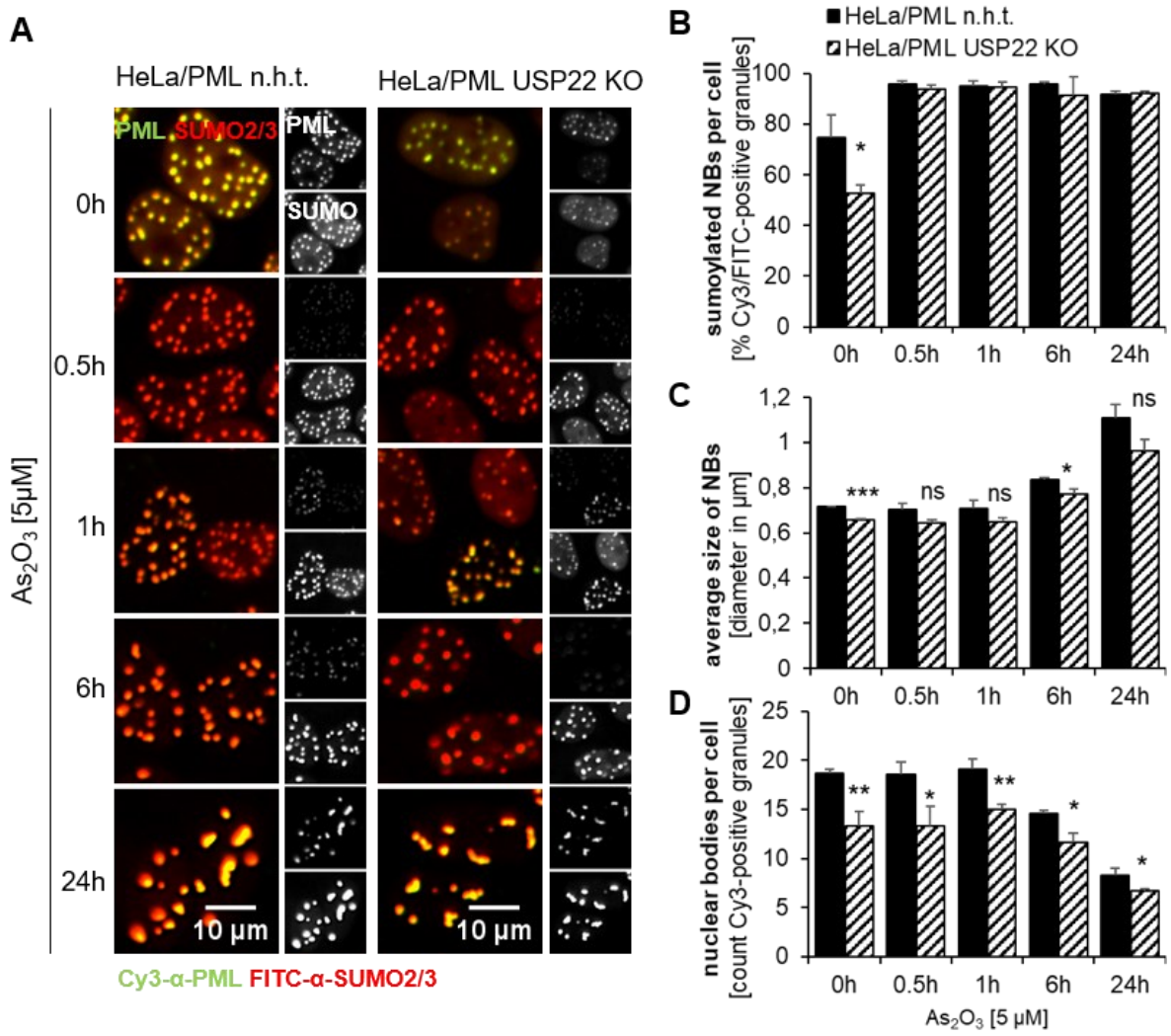

Figure 13: ATO-mediated PML nuclear body formation partly relies on USP22. A: Incubation of n.h.t. and polyclonal USP22 KO HeLa/PML cells with 5 µM As_2O_3 for the indicated periods of time. Intracellular immunofluorescence imaging of PML (Cy3/green) and SUMO2/3 (FITC/red) proteins. DAPI served as nuclear DNA staining (not shown). Magnification 60x; scalebar 10 µm. B-D: Quantification of immunofluorescence signals in A. Fraction of SUMOylated PML proteins relative to total PML proteins (B), average granule size in µm (C) and granule number in absolute count per cell (D) of total PML proteins (Cy3). Quantification based on 9 sites per condition with approx. 100 nuclei per site.

Taken together, these results show that the ATO-induced mechanism of PML SUMOylation with subsequent NB maturation and PML degradation is most likely not impaired upon USP22 deficiency. However, we were able to observe subtle differences in NB morphology under homeostatic conditions. Immunofluorescence imaging revealed that HeLa/PML USP22 KO cells comprised less PML-positive granules per nucleus (Figure 13D) accompanied by a marginally smaller diameter (Figure 13C) and a diminished degree of initial SUMOylation (Figure 13B), compared to HeLa/PML n.h.t. cells. The latter observation correlates with the slightly decreased levels of PML SUMOylation determined by His-purification in USP22 KO cells (Figure 12A).

5.1.5 USP22-dependent ubiquitin modification of PML at residue K394

To investigate whether ubiquitylation of PML is dependent on USP22 expression, we performed a global ubiquitylome profiling of USP22 deficient cells, as published recently [84]. As depicted in Figure 14A, HT-29 n.h.t. and USP22 KO cells were cultured in SILAC medium with distinct amino acid isotope composition. Ubiquitylated proteins in pooled lysates were then sequentially digested with proteases to produce peptides with isopeptide-linked di-glycine (GG) remnants on lysine residues (K-ε-GG), which were enriched by immuno-precipitation (IP) and analyzed by tandem mass spectrometry.

We identified an ubiquitylated PML residue K394 in a peptide sequence that was 2.1-fold more abundant in HT-29 USP22 KO cells compared to n.h.t. cells (Figure 14B-D). PML K394 is located right behind the RBCC domain at the very end of exon 3, which is conserved in all human PML isoforms (Figure 14C). Consistently, PML ubiquitylation at position 394 is reported in several high-throughput ubiquitylome datasets that identified ubiquitylated proteins in a global fashion upon treatment with proteasome inhibitors [215-218]. This suggests ubiquitylation of PML K394 to be involved in proteasomal turnover. Indeed, studies on PML-specific ubiquitylation also reported PML K394 to be ubiquitylated in response to ATO treatment [102, 219]. Together with our findings on USP22-dependent PML modification, we hypothesize that USP22 is involved in regulating PML turnover.

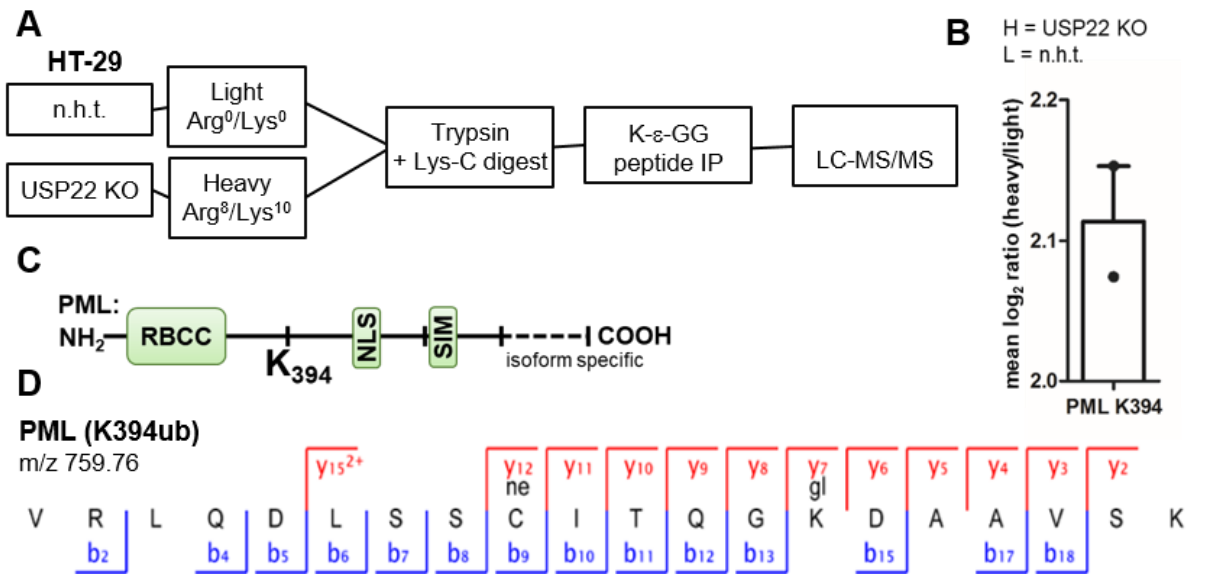

Figure 14: Identification of the USP22-dependent ubiquitylation site K394 of PML. A: Schematic experimental workflow of quantitative ubiquitylome analysis in n.h.t. and monoclonal USP22 KO HT-29 cells. Culturing of cells in SILAC medium with isotopes of arginine and lysine. Combined digest of lysates with Lys-C and trypsin proteases. Immunoprecipitation (IP) of ubiquitylated peptides with antibodies against the lysine-glycine-glycine motif (α-K-εGG) followed by liquid chromatography-tandem mass spectrometry (LC-MS/MS). B: Quantification of PML K394-peptide abundance in USP22 KO HT-29 cells (H, heavy labelled) relative to peptide abundance in n.h.t. HT-29 cells (L, light labelled). Andromeda score of the PML K394 site was 183,09 with a PEP = 4,45867E-53. C: Schematic depiction of the PML protein with indicated ubiquitylation site K394. RBCC: Ring-B-Box-Coiled-Coil domain; NLS: nuclear localization signal; SIM: SUMO-interacting motif; ----: PML isoform specific C-terminus. D: Ion spectrum and amino acid sequence of the PML peptide comprising a di-gly-remnant at position K394. m/z, mass/charge ratio of identified y- and b-ions. Sample preparation was performed by Dr. Jens Rödig and mass spectrometric experiments were performed and analyzed by Thomas Juretschke and Petra Beli (IMB, Mainz).

5.1.6 PML residue K394 is associated with PML protein stability

For validation of ubiquitylated PML K394 in HT-29 cells, we generated stable HT-29 cell lines, constitutively expressing His-tagged PML isoform IV (PML-His), the lysine (K) to arginine (R) mutant (PML-K394R-His) or the respective empty vector (EV). Immunofluorescence imaging of blasticidin selected polyclonal cell lines revealed homogeneous expression of the transfected plasmids (Figure 15A). In addition, Western blot analysis confirmed wild-type and K394R His-tagged PML at approximately 120 kDa, accompanied by faint high molecular weight species at typical sizes of SUMOylated PML (Figure 15B). Since K394 is described to be involved in basal and ATO-mediated degradation of PML, we analyzed the ATO-induced modification of PML K394 by Ni^{2+}-NTA-affinity purification under basal and ATO conditions in the presence of proteasome inhibition (Figure 15C). Enrichment of His-tagged PML variants was achieved to comparable levels in all cell lines. Application of proteasome inhibitor MG132 efficiently rescued ATO-treated PML from degradation, allowing analysis of the ATO-induced PTM pattern.

As expected, probing of the pulldown fractions for SUMO2/3 revealed a subtle decrease of SUMOylated PML K394R mutant species under basal conditions and even more pronounced in the presence of ATO (arrowheads in Figure 15C). In addition, discrete poly-ubiquitylated PML species were detected at molecular weights corresponding to SUMOylated PML variants (upper arrowheads in Figure 15C), despite a strong background detection of poly-ubiquitylated proteins in MG132-treated samples. In line with reduced poly-SUMO conjugation of ATO-treated PML K394R, the PML mutant also displayed a reduced ubiquitylation pattern in response to ATO. Together, our findings confirm a role for PML K394 in post-translational modification of PML, particularly in the context of protein degradation.

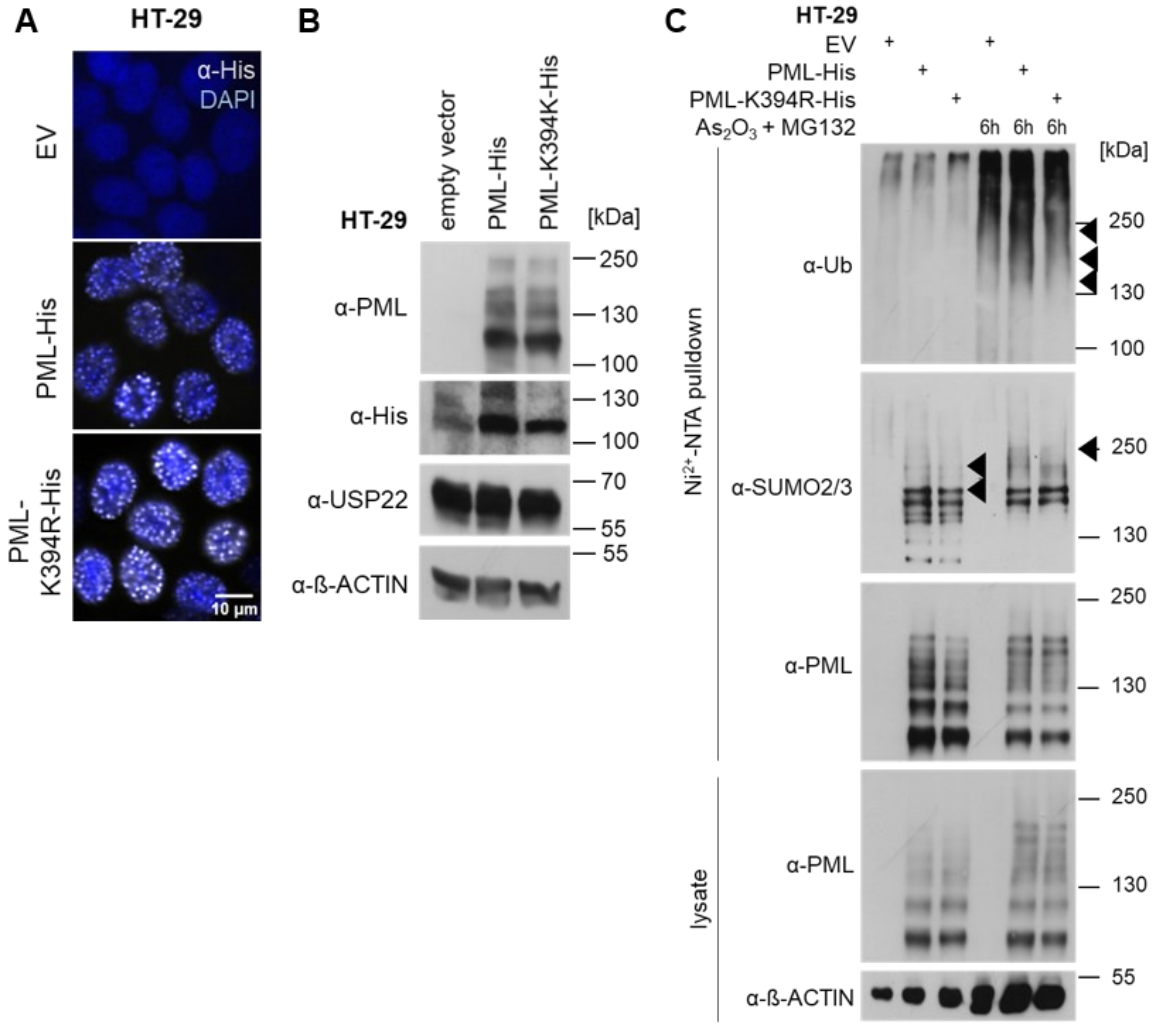

Figure 15: PML K394 is involved in PML post-translational modifications A: Immunofluorescence imaging of wild-type and K394R PML-His proteins (FITC/α-His, white) in stably transfected HT-29 cells. Empty vector (EV) served as negative control, DAPI served as nuclear counter staining (blue). Magnification 60x; scalebar 10 µm. B: Western blot analysis of PML-His protein levels of cells shown in Figure A. ß-ACTIN served as loading control. C: Incubation of indicated cells shown in Figure A + B with 10 µM MG132 1h prior to incubation with 5 µM As_2O_3 for 6h. Enrichment of PML-His proteins with Ni^{2+}-NTA-coupled magnetic beads in denatured lysates. Western blot analysis of total, SUMOylated and ubiquitylated PML-His protein levels. ß-ACTIN served as loading control. Arrowheads indicate differences in conjugated PML species. One of two biological replicates is shown.

Further analysis of the relevance of PML K394 modification for basal PML protein turnover was performed in a transient expression model. Here, HEK293T cells were transfected with equal amounts of wild-type or K394R HA-tagged PML isoform IV together with eGFP as transfection control (Figure 16A). Noteworthy, in contrast to constitutively PML expressing HT-29 cells, transient expression revealed elevated PML K394R protein levels compared to its wild-type homologue. This expression level discrepancy was not observable for eGFP expression, pointing to a PML K394R mutant-specific increase in protein level. Consistently, incubation of these cells with cycloheximide for increasing periods of time revealed a notable increase of PML K394R protein abundance compared to wild-type PML (Figure 16B). Curve-fitted calculation of PML half-life revealed a significant prolongation of PML K394R stability by approximately 9 hours to $t_{1/2}$ = 25.5 hours (extrapolated value) compared to $t_{1/2}$ = 16.5 hours for wild-type PML (Figure 16C). In accordance, post-translational modifications of PML K394R were reduced compared to wild-type PML (Figure 16D). In line with increased PML K394R protein levels detected in the input fraction, SUMOylated PML species were reduced in PML-enriched pulldown fractions (arrowheads in Figure 16D). Likewise, ubiquitylations of poly-SUMO conjugated PML species were reduced as well in PML K394R expressing cells (upper arrowhead in Figure 16D). In summary, increased protein abundance correlates with prolonged PML half-life and reduced modification of PML K394R, which reveals a direct role of K394 in basal turnover of PML.

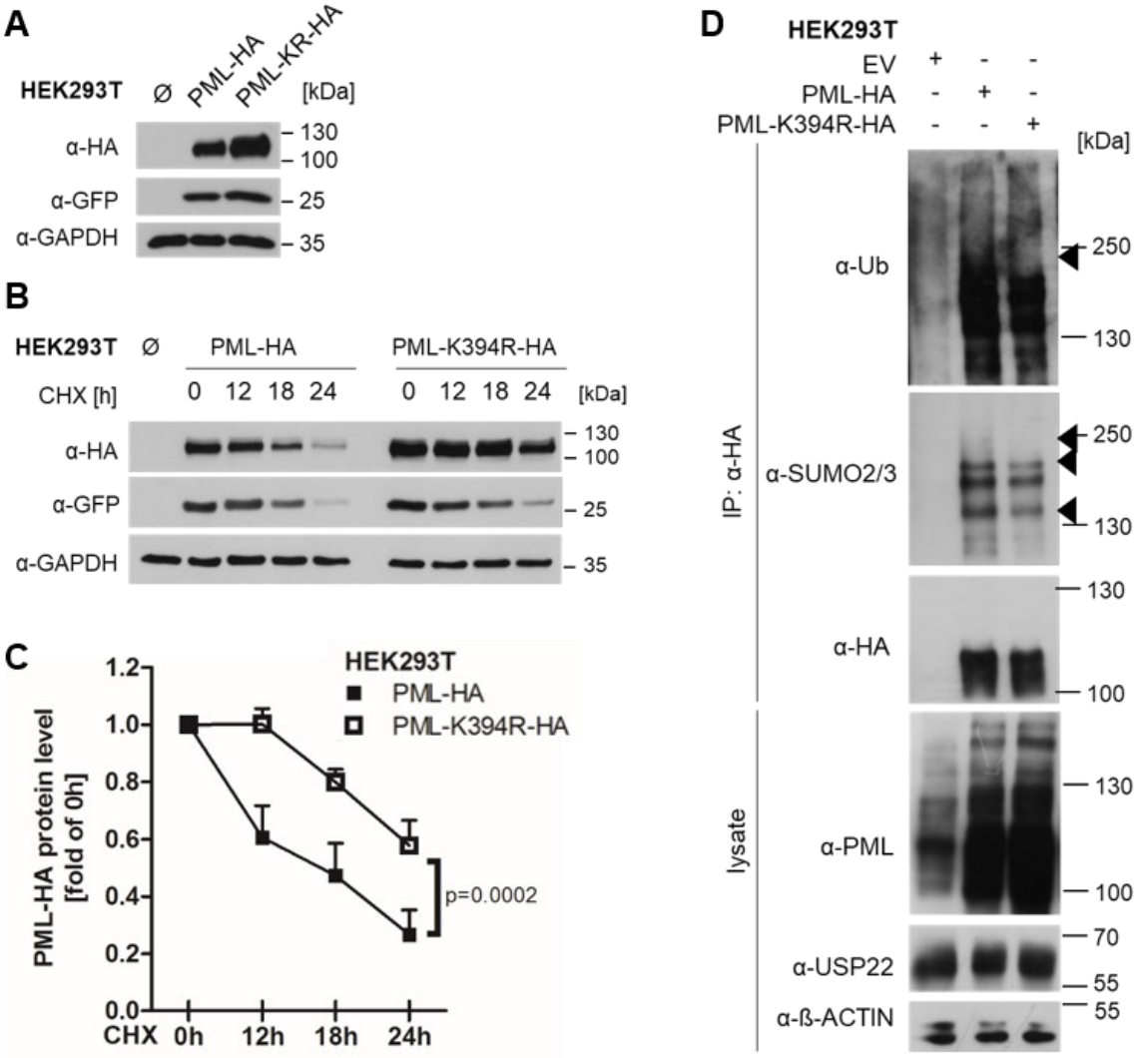

Figure 16: PML K394 is important for PML protein stability. A: Transient transfection of wild-type or K394R mutant PML-HA (isoform IV) plasmids for 24h in HEK293T cells. Untransfected cells served as expression control (Ø). Co-transfection with eGFP plasmids served as transfection control. Western blot of total PML-HA proteins; GAPDH served as loading control. B: Cells were prepared and processed as in Figure A and incubated with 20 µg/mL cycloheximide (CHX) for the indicated periods of time. C: Quantification of total PML-HA protein levels shown in Figure B normalized to loading control. Half-lives calculated by polynomic approximation: $t_{1/2}$(PML-HA) = 16.5 h and $t_{1/2}$(PML-K394R-HA) = 25.5 h. Statistical analysis was performed on 3 independent biological replicates. D: Transient transfection as in Figure A. Empty vector (EV) served as negative control. Immunoprecipitation (IP) of total PML-HA proteins with α-HA-coupled magnetic beads in denatured lysates. Western blot analysis of total, SUMOylated and ubiquitylated PML-HA proteins. ß-ACTIN served as loading control. Arrowheads indicate differences in conjugated PML species. One of two biological replicates is shown.

5.2 Functional regulation of the PML-RARα oncoprotein by USP22

Having deciphered a role for USP22 in basal turnover of the tumor suppressor PML, we were intrigued to elucidate whether this regulatory function also applies to the oncogenic PML fusion protein PML-RARα. In acute promyelocytic leukemia (APL), the N-terminal part of PML is fused to the C-terminal region of retinoic acid receptor α (RARα) due to chromosomal translocation [149]. Dependent on the chromosomal break point, two major isoforms are expressed in APL patients with PML-RARα$_{short}$ being fused behind PML residue K394 and PML-RARα$_{long}$ behind PML A552 [146]. Both isoforms harbor the complete RBCC motif of PML, allowing homo-dimerization of the fusion protein as well as heterodimerization with wild-type PML [152]. Dimerization of PML-RARα allows RARα-directed binding of the fusion protein to RAR-responsive elements (RARE) present in multiple promoter regions of RARα-regulated target genes involved in progenitor cell differentiation, regulation of apoptosis and immune response signaling pathways [156]. Transcriptional regulation occurs via engagement and release of physiological RARα ligand all-*trans*-retinoic acid (ATRA) that either induces genetic activation or repression, dependent on the recruitment of co-regulatory complexes [155]. In the case of APL however, the fusion of RARα to PML results in a dominant negative effect over endogenous RARα signaling, such that physiological levels of ATRA are not sufficient to transactivate genes occupied by the PML-RARα dimer [154]. Because of that, multiple RARα-regulated genes involved in cellular differentiation and cell cycle regulation are constitutively repressed by PML-RARα, resulting in the inhibition of proliferating APL progenitor cells to terminally differentiate [172]. Stimulation of APL cells with exceeding concentrations of ATRA leads to PML-RARα-mediated transactivation and subsequent induction of granulocyte differentiation. Under constitutive ATRA administration, PML-RARα becomes eventually degraded, leading not only to a release of the differentiation block but also to the ability of differentiated myelocytes to undergo apoptosis [178]. To which extent USP22 is involved in PML-RARα turnover and whether a potential regulation of protein stability affects APL cell fate will be addressed in the following part of this thesis.

5.2.1 USP22 controls basal PML-RARα protein stability

Degradation of PML-RARα in response to ATO or ATRA treatment involves post-translational modifications like SUMOylation, ISGylation, phosphorylation and ubiquitylation [124, 188, 197, 199]. In contrast, few studies address the mechanism of basal PML-RARα turnover and the responsible PTM-modulating enzymes and target residues. Since we demonstrated USP22-dependent regulation of PML stability in a K394-related manner, we hypothesize that these effects might be conserved in the PML-RARα fusion protein.

The patient-derived APL cell line NB4 dominantly expresses the long isoform of the PML-RARα fusion protein [145], which is detectable at approximately 130 kDa in Western blot analysis. The dependence of the PML-RARα protein levels on USP22 expression was analyzed in monoclonal CRISPR/Cas9-modified NB4 USP22 KO cells and compared to wild-type and CRISPR/Cas-9-modified NB4 n.h.t. cells (Figure 17A). Consistent with our observations of increased PML protein levels in USP22 KO HT-29 cells (Figure 7A), we detected an approximate 2-fold increase of the PML-RARα fusion protein levels in USP22 KO NB4 cells (Figure 17A + B). In addition, no transcriptional regulation of PML-RARα mRNA levels could be observed in dependence on USP22 in NB4 cells (Figure 17C), suggesting a role for USP22 in regulating post-translational protein stability of PML-RARα. Of note, detection of the fusion protein with an antibody directed against the C-terminus of RARα revealed an additional band at the size of approximately 90 kDa (asterisk in Figure 17A). According to literature, this RARα-positive species represents a PML-RARα cleavage product that lacks the PML RING and B-Box domains and occurs in untreated NB4 cells and increases upon ATRA treatment [179, 194, 220].

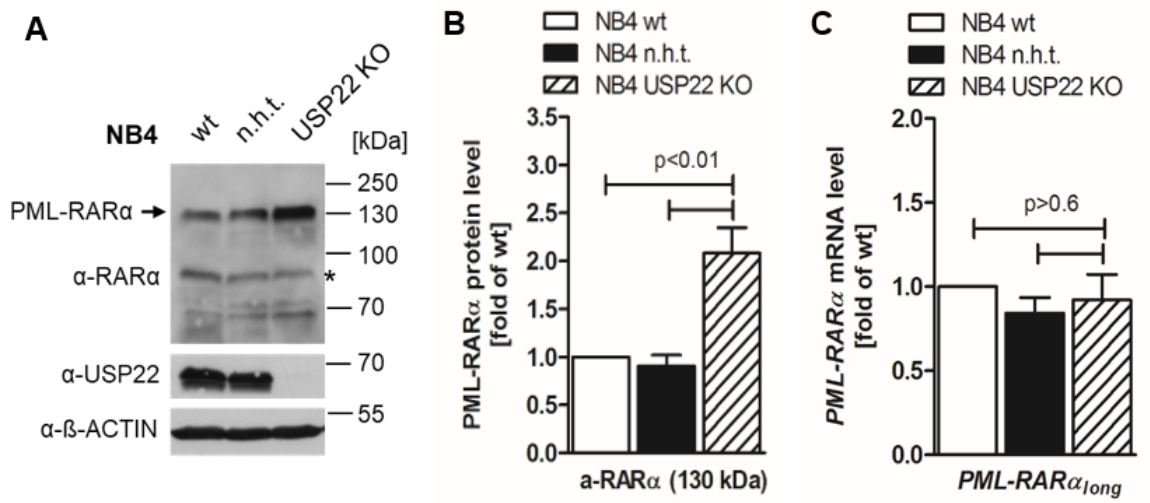

Figure 17: Endogenous PML-RARα expression in APL cells is USP22-dependent. A: Western blot analysis of PML-RARα protein levels in parental (wild-type, wt), n.h.t. and monoclonal USP22 KO NB4 cell lysates. ß-ACTIN served as loading control. B: Quantification of PML-RARα protein levels of n.h.t. and USP22 KO NB4 cells shown in Figure A (approx. 130 kDa signal) normalized to wt NB4 cells. C: qRT-PCR analysis with primers recognizing the bridge region of the fusion transcript *PML-RARα* (long isoform) in n.h.t. and USP22 KO NB4 cells normalized to wt NB4 cells.

In agreement with the USP22-dependent increase in PML-RARα protein abundance in NB4 USP22 KO cells, we detected alterations in PML-RARα stability upon loss of USP22 (Figure 18A). Inhibition of *de novo* protein synthesis with cycloheximide revealed a reduction of PML-RARα protein levels to approximately 40 % after 24 hours in wild-type and NB4 n.h.t. cells (Figure 18B), which is consistent with the reported turnover rate of physiological PML-RARα [221]. Ablation of USP22 lead to an extension of the endogenous PML-RARα half-life to a protein amount of approximately 80 % after 24 hours (Figure 18B).

To analyze the kinetics of these effects in more detail, we ectopically expressed PML-RARα$_{long}$ in n.h.t. and USP22 KO HEK293T cells and monitored the reduction of exogenous PML-RARα$_{long}$ protein levels upon CHX incubation (Figure 18C). The PML-RARα$_{long}$ protein half-life was $t_{1/2}$ = 5 hours in n.h.t. cells and significantly extended to $t_{1/2}$ = 10 hours in USP22 KO HEK293T cells (interpolated values, Figure 18D). Of note, the turnover rate of co-transfected red fluorescent reporter protein (RFP) did not differ in both cell lines (Figure 18C), indicating a specific role for USP22 in controlling the stability and degradation of the chimeric oncoprotein PML-RARα in APL NB4 cells.

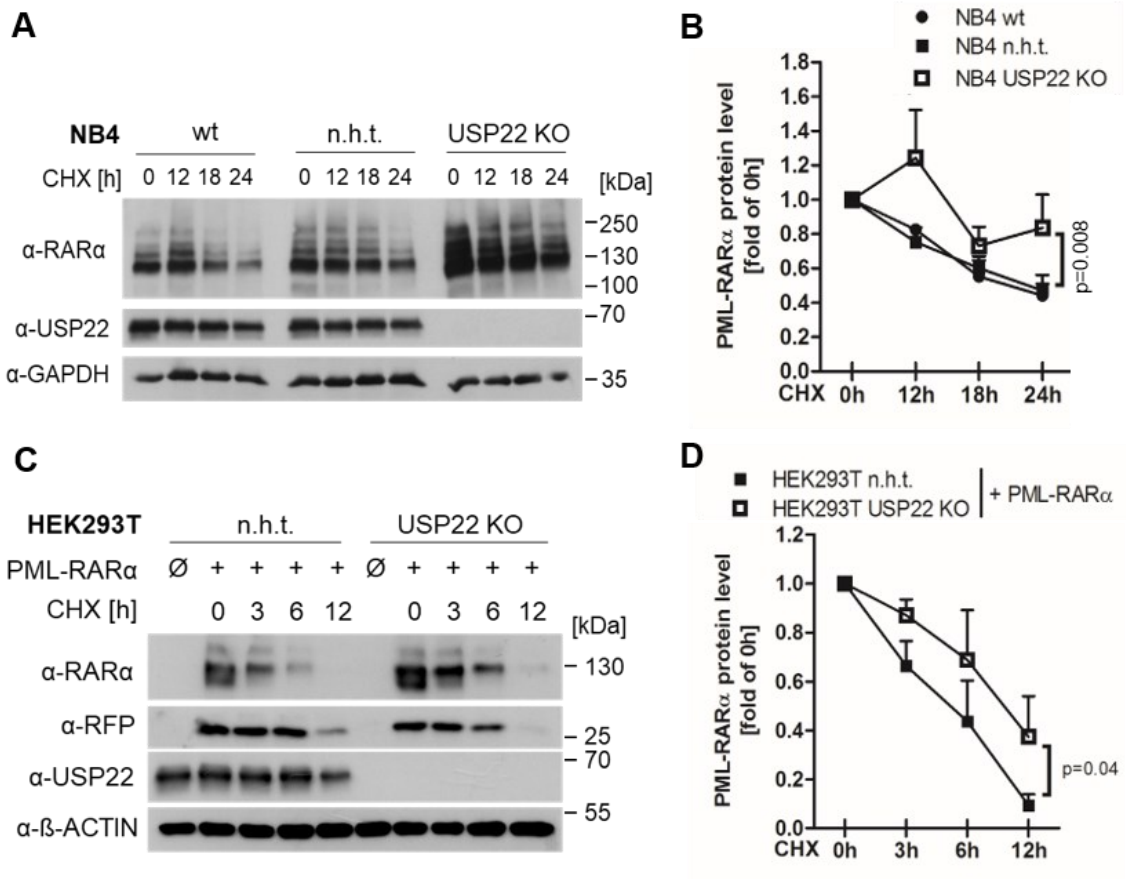

Figure 18: USP22 controls stabilization of PML-RARα. A: Incubation of parental (wt), n.h.t. and monoclonal USP22 KO NB4 cells with 20 µg/mL cycloheximide (CHX) for the indicated periods of time. Western blot analysis of PML-RARα protein levels in whole cell lysates; GAPDH served as loading control. B: Quantification of PML-RARα protein levels in cells shown in Figure A (approx. 130 kDa signal) normalized against loading control. Half-lives calculated by polynomic approximation: $t_{1/2}$(wt) = 21.5 h, $t_{1/2}$(n.h.t.) = 23 h, half-life of PML-RARα in USP22 KO NB4 cells could not be determined. C: Transient transfection of His-PML-RARα (long isoform) plasmids for 24h in n.h.t. and monoclonal USP22 KO HEK293T cells. Untransfected cells served as expression control (Ø). Co-transfection with mCherry (RFP) plasmids served as transfection control. Incubation with CHX and Western blot analysis as described in Figure A. ß-ACTIN served as loading control. D: Quantification of His-PML-RARα protein levels shown in Figure C (approx. 130 kDa signal) normalized against loading control. $t_{1/2}$(n.h.t.) = 5 h and $t_{1/2}$(USP22 KO) = 10 h. Statistical analysis was performed on 3 independent biological replicates.

5.2.2 PML-RARα residue K394 is important for PML-RARα protein stability

Given the conservation of USP22-mediated regulation of PML and PML-RARα degradation, we investigated the role of USP22-related PML residue K394 in regulating PML-RARα stability. PML K394 is not only conserved in all isoforms described for the human PML protein, but also in the different isoforms of the oncogenic fusion protein PML-RARα (see Figure 4, introduction). Exogenous expression of wild-type and K394R PML-RARα$_{long}$ in HEK293T cells revealed a 1.2-fold increase in basal protein expression of the PML-RARα$_{long}$ K394R proteins compared to the wild-type homologue (Figure 19A, 0h CHX samples). Of note, co-expression of an eGFP reporter plasmid revealed equal transfection efficiency, independent of USP22 expression. As expected, the degradation of PML-RARα K394R was delayed within six hours of CHX treatment compared to the degradation of wild-type PML-RARα, followed by a nearly complete degradation after 12 hours translational inhibition (Figure 19A+B). The calculated half-life of PML-RARα K394R was increased 5 hours compared to wild-type PML-RARα (Figure 19B). Interestingly, these effects correlate with the extended stability of exogenous PML-RARα in HEKT293T USP22 KO cells compared to n.h.t. cells (Figure 18C+D). Based on these findings, we conclude that the residue K394 controls PML-RARα protein stability in a USP22-dependent manner.

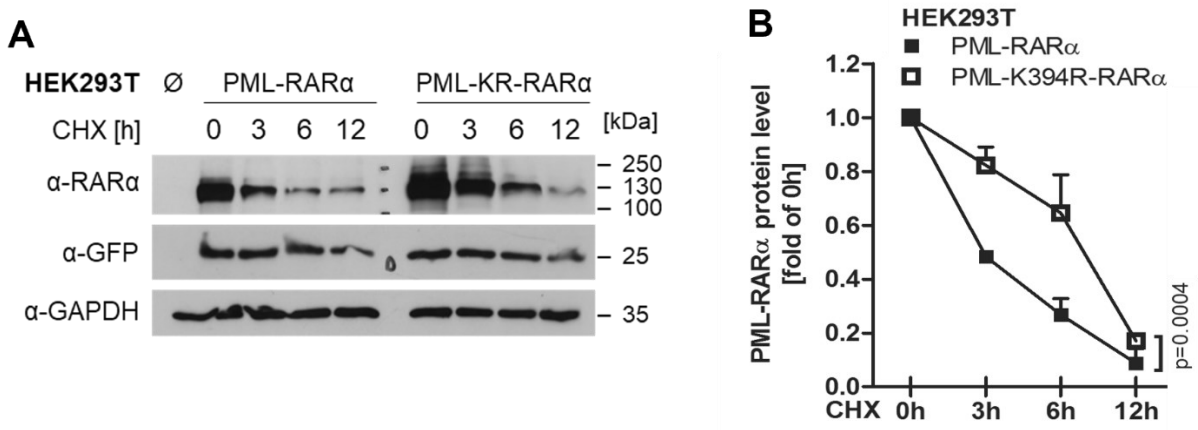

Figure 19: PML-RARα residue K394 is important for protein stability. A: Transient transfection of wild-type and K394R His-PML-RARα plasmids for 24h in HEK293T cells. Untransfected cells served as expression control (Ø). Co-transfection with eGFP plasmids served as transfection control. Incubation with 20 µg/mL cycloheximide (CHX) for the indicated periods of time. Western blot analysis of His-PML-RARα protein levels in whole cell lysates; GAPDH served as loading control. B. Quantification of PML-RARα protein levels shown in Figure A (approx. 130 kDa signal) normalized against loading control. Half-lives calculated by polynomic approximation: $t_{1/2}$(PML-RARα) = 3 h and $t_{1/2}$(PML-KR-RARα) = 8 h. Statistical analysis was performed on 3 independent biological replicates.

5.2.3 ATRA-induced degradation of PML-RARα is controlled by USP22

Stabilization of the PML-RARα fusion protein is a central determinant for the molecular phenotype of APL due to its dominant repressive effect on differentiation-associated genes [170, 222]. In APL therapy, high therapeutic doses (1 µM) of ATRA reverse the repressive functions of PML-RARα into transcriptional activation and subsequently induce terminal myelocyte differentiation [173]. In addition, ATRA facilitates the proteasomal degradation of PML-RARα via stimulation of cellular caspase activity and induction of several post-translational receptor modifications [187-189]. Both ATRA-mediated mechanisms are considered individual modes of action, both required for APL cure although not necessarily interlinked [178]. Here, we analyzed USP22-dependent functions on ATRA-mediated destabilization of PML-RARα and on ARTA-induced terminal differentiation of APL NB4 cells.

ATRA-induced degradation of PML-RARα occurs within 12-48 hours in NB4 cells at a clinical concentration of 1 µM [188], while granulocytic differentiation occurs within 72-96 hours with ATRA concentrations greater than 100 nM [223, 224]. We applied a dose range of subclinical to clinical concentrations of ATRA ranging from 0.1 nM to 1 µM and compared the degradative effect of ATRA in control and USP22 KO NB4 cells over a period of 4 days (Figure 20).

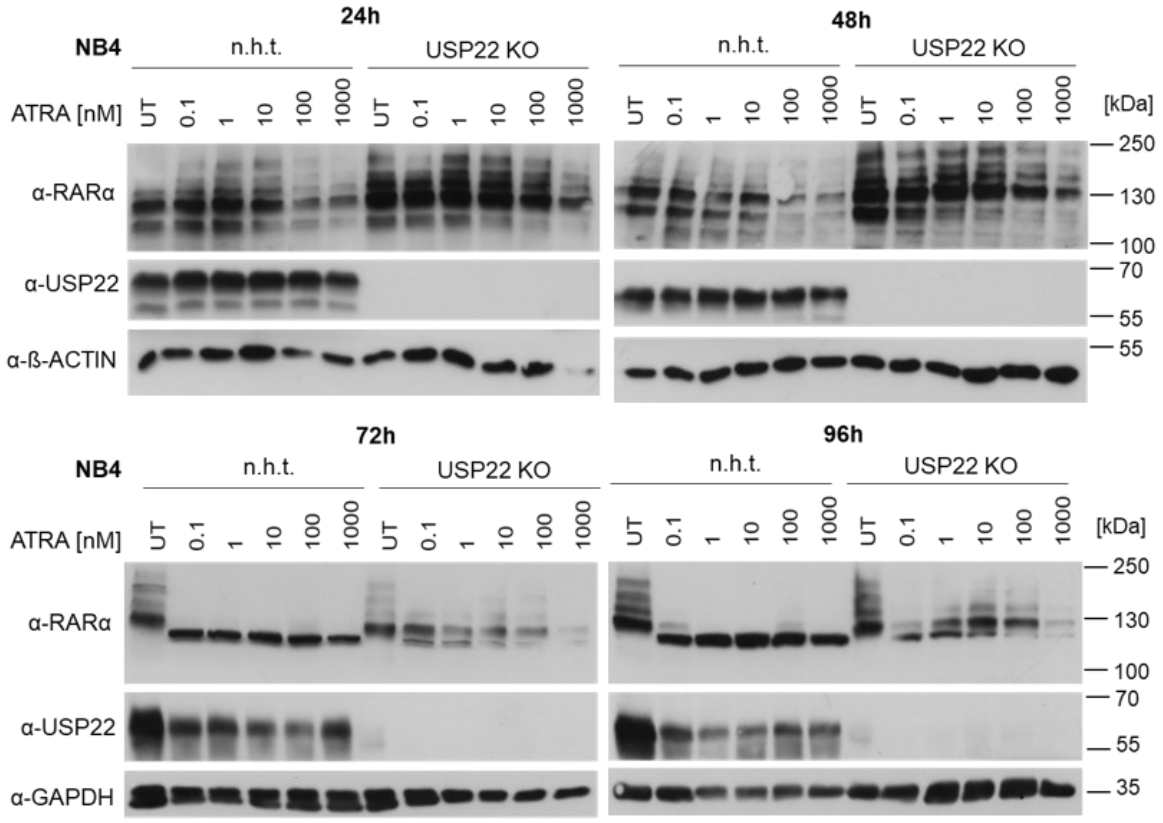

Figure 20: USP22 controls ATRA-mediated degradation of PML-RARα. Western blot analysis of PML-RARα protein levels in n.h.t. and monoclonal USP22 KO NB4 cells incubated with increasing concentrations of all-*trans*-retinoic acid (ATRA) for indicated periods of time. ß-ACTIN and GAPDH served as loading controls.

In line with the reported onset of PML-RARα proteolysis within 2 days, we observed a marked decrease of PML-RARα protein levels in NB4 n.h.t. cells after 24h and 48h in the presence of the highest ATRA concentrations (Figure 20 upper panels). Extension of ATRA treatment to 72 h or 96 h revealed a nearly complete reduction of PML-RARα protein levels already at physiological doses of 0.1 nM – 1 nM ATRA in NB4 n.h.t. cells (Figure 20 lower panels). Interestingly however under these conditions, a distinct, ATRA-insensitive PML-RARα cleavage product appeared approximately 10 kDa lower than the full-length PML-RARα protein in NB4 n.h.t. cells. According to literature, this protein most likely either resembles a C-terminal PML-RARα cleavage product [194] or an alternative PML-RARα isoform that is transcribed from an internal initiation codon [146]. As anticipated, USP22 deficiency induced a prominent increase in basal PML-RARα protein levels, accompanied by an increased protein stability in untreated NB4 cells (see Figure 18A for comparison). Accordingly, exposure to 1 µM ATRA was not sufficient to degrade PML-RARα in NB4 USP22 KO cells until an incubation time of 72 hours, representing a major delay in PML-RARα degradation compared to NB4 n.h.t. cells. Of note, the ATRA-induced PML-RARα cleavage product at approximately 120 kDa was also detectable in NB4 USP22 KO cells, although only in the presence of low ATRA concentrations (Figure 20 lower panels). These results clearly indicate a role of USP22 in regulating ATRA-mediated degradation of PML-RARα that involves alternative protein cleavage efficacy.

The appearance of an PML-RARα cleavage product in response to ATRA treatment is consistent with the reported involvement of proteases that are implicated in PML-RARα degradation [187, 188]. Pan-caspase inhibition, as well as caspase-3 and -7 specific inhibition has been reported to counteract ATRA-dependent PML-RARα cleavage and corresponds with ATRA-induced caspase-3 activity in NB4 cells [187]. We investigated if ATRA-induced caspases are involved in PML-RARα degradation in an USP22-dependent manner. For this, caspase-3 and -7 activities were determined via fluorescence-mediated quantification of fluorophore-coupled DEVD-peptide cleavage during ATRA treatment (Figure 21A). Intriguingly, USP22 KO cells showed less caspase-3 and -7 activity after 3 days of ATRA incubation compared to n.h.t. cells (Figure 21B). In line with that, cleaved pro-caspase-3 levels were altered in an USP22-dependent manner in ATRA-treated NB4 cells (Figure 21C). Consistently, increased ATRA-dependent pro-caspase-3 activation in n.h.t NB4 cells correlated with the appearance of the PML-RARα cleavage product at 120 kDa in these cells, which was absent in USP22 KO NB4 cells that did not reveal increased pro-caspase-3 activation upon ATRA exposure (Figure 21C). In addition, we observed an uncharacterized cleavage product of approximately 30 kDa that presumably results from ATRA-induced PML-RARα cleavage but not from endogenous RARα, whose ATRA-dependent degradation occurs caspase-independent [188].

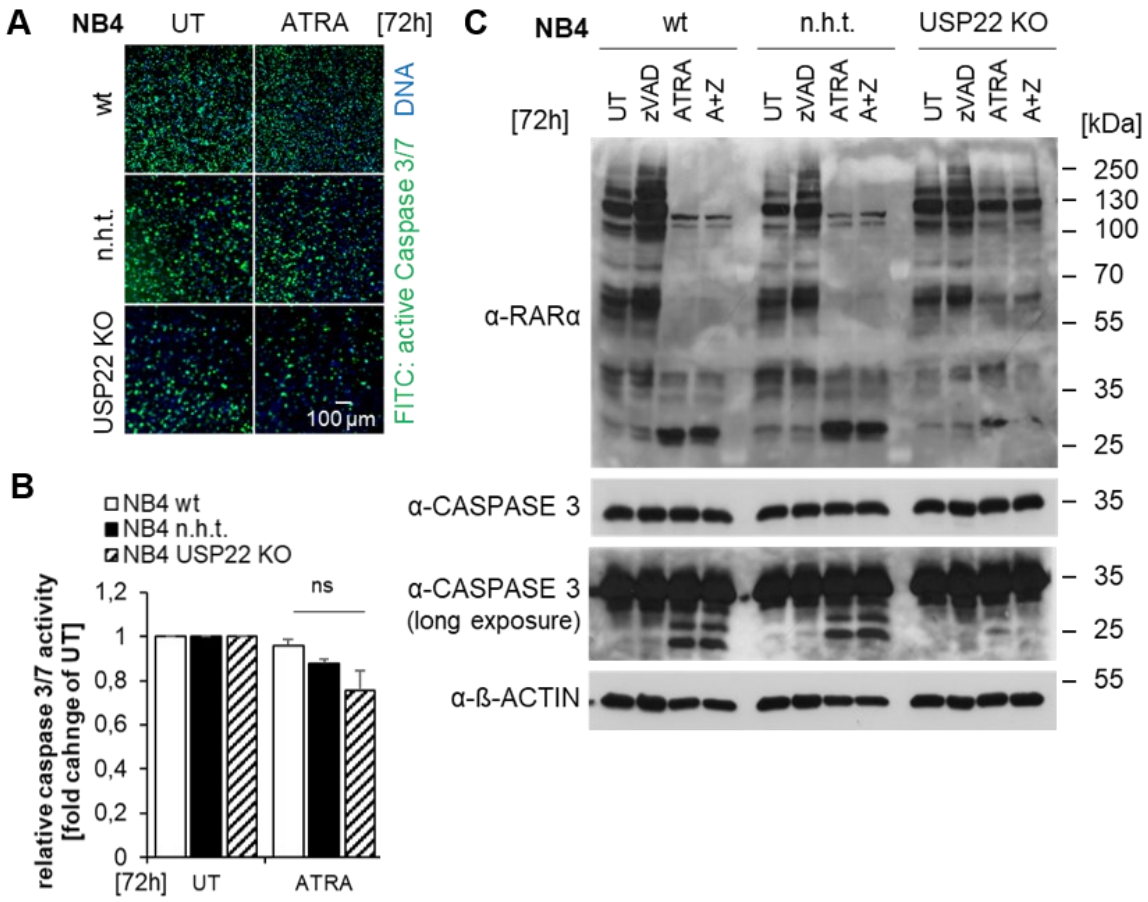

Figure 21: USP22 regulates ATRA-mediated caspase cleavage of PML-RARα. A: Immunofluorescence imaging of wt, n.h.t. and USP22 KO NB4 cells, untreated (UT) or incubated with 100 nM ATRA for 72h in the presence of 1 µM Caspase 3/7-detection reagent (FITC, green) and 1 µg/mL Hoechst-dye for nuclear DNA counter staining (DAPI, blue). Magnification 4X, scalebar 100 µm. B: Quantification of FITC-positive nuclei shown in Figure A as fraction of total nuclei, normalized to untreated cells. C: Western blot analysis of total PML-RARα and caspase-3 protein levels in wt, n.h.t. and USP22 KO NB4 cells incubated with 100 nM ATRA (A), 20 µM pan-caspase inhibitor zVAD.fmk (zVAD, Z) or both for 72h. ß-ACTIN served as loading control.

Interestingly, the pan-caspase inhibitor zVAD.fmk rescued PML-RARα protein levels in the absence of ATRA, despite undetectable levels of activated caspase-3 (Figure 21C). This is in line with the involvement of caspases-1, -6 and -7 but not caspase-3 in the basal turnover of PML-RARα [188]. This zVAD.fmk-induced rescue of steady-state PML-RARα levels was more pronounced in NB4 control cells compared to cells lacking USP22, suggesting a partial interference of USP22 KO-mediated PML-RARα stabilization with caspase-mediated PML-RARα proteolysis. This suggests that applied concentrations of zVAD.fmk were not sufficient to compensate the ATRA-induced degradation of PML-RARα which is reported to occur at a rate of 50% in the presence of 5-fold higher zVAD concentrations [187]. In summary, we identified a link between ATRA-induced caspase-3 activation, PML-RARα degradation and USP22 expression in APL cells.

5.2.4 USP22-regulated stability of PML-RARα interferes with ATRA-induced PML nuclear body re-formation

To investigate the role of USP22 in regulating NB morphology and functional effects downstream of altered PML-RARα stabilization, ATRA treatments were extended to 5 days with re-application of appropriate concentrations after 72 hours due to reported instability of ATRA in cell culture medium [204, 205]. Western blot analysis revealed that these conditions induced the degradation of full-length PML-RARα proteins, with the appearance of a lower running PML-RARα cleavage product in wild-type and n.h.t. NB4 cells (Figure 22A), similar to what we observed after 72 and 96 hours (Figure 20). As expected, lack of USP22 induced a delayed response to ATRA-mediated PML-RARα degradation and stabilized PML-RARα even at day 5 of ATRA treatment (Figure 22A). In addition, ATRA-induced upregulation of PML-RARα mRNA levels was enhanced in the absence of USP22 (Figure 22B), in contrast to basal PML-RARα mRNA levels that were not affected by USP22 deficiency. The observed ATRA-mediated upregulation of PML-RARα mRNA levels by approximately 2-fold over untreated conditions in wild-type and n.h.t. NB4 cells is consistent with the reported ATRA-dependent stimulation of PU.1 and IRF1 expression – two transcription factors that target the PML promoter region [105, 177]. Additional increase in PML-RARα mRNA levels upon USP22 deficiency suggests a role for USP22 in regulating PML-RARα gene expression which also determines PML-RARα protein levels under ATRA treatment.

In line with increased PML-RARα mRNA and protein levels in USP22 KO NB4 cells, an alteration of PML-RARα nuclear distribution was expected under 5-day ATRA incubation in these cells, which we analyzed with immunofluorescence imaging with RARα- and PML-specific antibodies (Figure 22 C and D, respectively). The appearance of the fusion protein, visualized by RARα staining, was spread throughout the nucleus in diffuse clusters, presumably reflecting the binding of PML-RARα multimers to DNA. As described in literature, PML NBs are disrupted in APL cells due to hetero-dimerization of PML with PML-RARα [122, 147, 148]. Upon ATRA-induced degradation of PML-RARα, PML monomers become released and homo-oligomerize to NBs, that can be detected by PML staining in ATRA-treated NB4 cells [148]. Consistently, we observed a decrease in the number of RARα-positive micro-speckles, along with an increase in PML-positive spherical clusters in response to ATRA (Figure 22C-F). In wild-type and n.h.t. NB4 cells, diffuse RARα-positive nuclear clusters re-organized from 15 speckles per cell in the untreated condition to 6 – 8 sphere-like punctae per cell under 1 µM ATRA treatment (Figure 22D). At the same time, PML-positive nuclear punctae increased from an average of 4 to the number of 7 – 8 under ATRA treatment (Figure 22F).

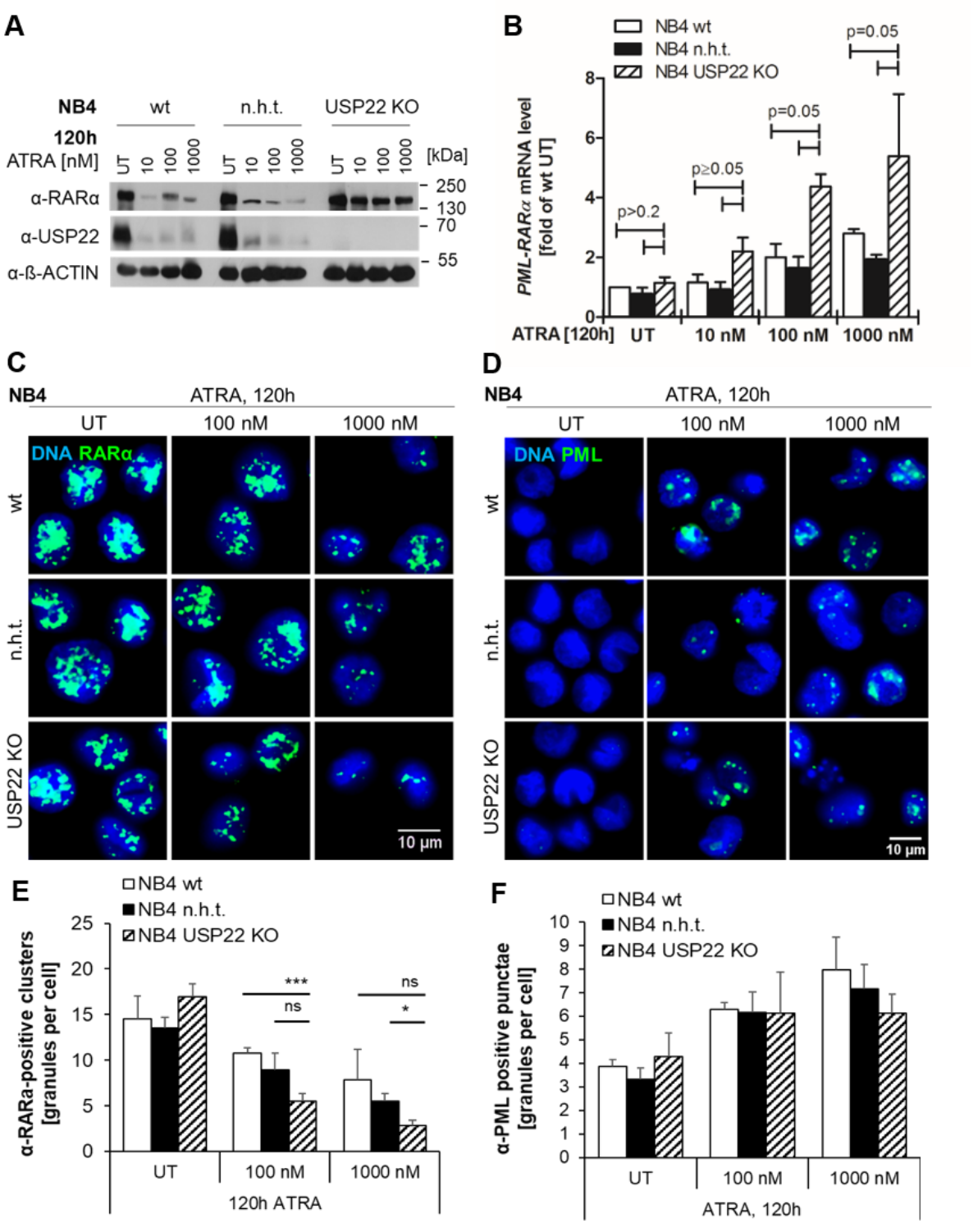

Figure 22: USP22-regulated stability of PML-RARα interferes with ATRA-induced PML nuclear body re-formation. A: Western blot analysis of PML-RARα protein levels in wt, n.h.t. and USP22 KO NB4 cells, untreated (UT) or incubated with increasing concentrations of ATRA for 120h. ß-ACTIN served as loading control. B: qRT-PCR analysis of PML-RARα transcript levels in cells prepared as in Figure A, normalized to UT condition of wt NB4 cells. 28s transcript levels served as internal reference. *p*-values are summarized for wt and n.h.t. in comparison to USP22 KO. C+D: Immunofluorescence imaging of the PML-RARα fusion protein (Cy3, green in C) and PML NBs (Cy3, green in D) in wt, n.h.t. and USP22 KO NB4 cells pre-incubated with indicated concentrations of ATRA for 5 days. DAPI served as nuclear DNA counter-staining (blue). Magnification 60X, scalebar 10 µm. Representative images of one of three biological replicates are shown. E+F: Quantification of absolute number of granules (Cy3) per nucleus of cells shown in Figure C and D. Minimum of 20 sites per condition was analyzed.

This is consistent with previous observations, that ATRA-induced PML NB re-formation co-localizes residual PML-RARα, resulting in an overlap of RARα- and PML-positive nuclear staining in NB4 cells treated with 1 µM ATRA [148]. Here, we assume that detection of PML-RARα associated with PML NBs under 1 µM ATRA in NB4 control cells might reflect the persistence of the PML-RARα cleavage product observed in immunoblots. In contrast to the stabilized protein levels in USP22 KO cells however, we were not able to observe a maintained micro-speckled nuclear appearance of PML-RARα in NB4 USP22 KO cells under ATRA treatment (Figure 22C). Instead, we observed an even stronger reduction in nuclear RARα-positive clusters from initially 17 clusters per cell to 3 clusters per cell upon high ATRA treatment (Figure 22E). This apparent disagreement might be explained by an USP22 KO-dependent shift of nuclear PML-RARα to the cytoplasmic compartment. Several reports indeed propose a predominant localization of the transformed receptor in the cytoplasm [147, 148]. According to this model, PML-monomer retention to cytosolic PML-RARα multimers would cause an impaired NB re-formation. Consistently, we observed a slightly reduced reassembly of NBs in USP22 KO cells from approximately 4 faint structures to 6 NBs per cell in response to ATRA (Figure 22F).

In summary, these findings show ATRA-dependent alterations of sub-nuclear PML-RARα-containing structures that differ in response to USP22 deficiency, accompanied by increased PML-RARα mRNA and protein levels in USP22 KO NB4 cells. Therefore, we anticipate a functional consequence of USP22-dependent PML-RARα modulations in ATRA-mediated terminal differentiation of APL cells.

5.2.5 USP22 controls ATRA-induced granulocytic differentiation of APL cells

In APL therapy, administration of ATRA causes the release of the PML-RARα-mediated transcriptional repression and thereby induces the expression of gene clusters that are determinant for terminal granulocyte differentiation, such as transcription factors, cell cycle regulatory proteins and differentiation markers [172, 225]. While immature promyelocytic APL cells are specifically characterized by low surface marker presentation of CD11a, b and c, CD15, CD45RO and CD54 in combination with high display of CD45RA and CD58 [167], treatment with ATRA specifically leads to upregulation of CD11b and -c, CD15 and CD65 but not CD11a, in contrast to ATRA-stimulated AML cells with high CD11a surface expression [167]. Here, ATRA-induced differentiation of wild-type, n.h.t. and USP22 KO NB4 cells was assessed as increase of the CD11b-positive ($CD11b^+$) cell population in response to increasing ATRA concentration (Figure 23). Incubation with 100 nM ATRA over 5 days resulted in a gradual increase of the mean fluorescence intensity (MFI) of CD11b surface expression on pro-myelocytic cells (Figure 23A).

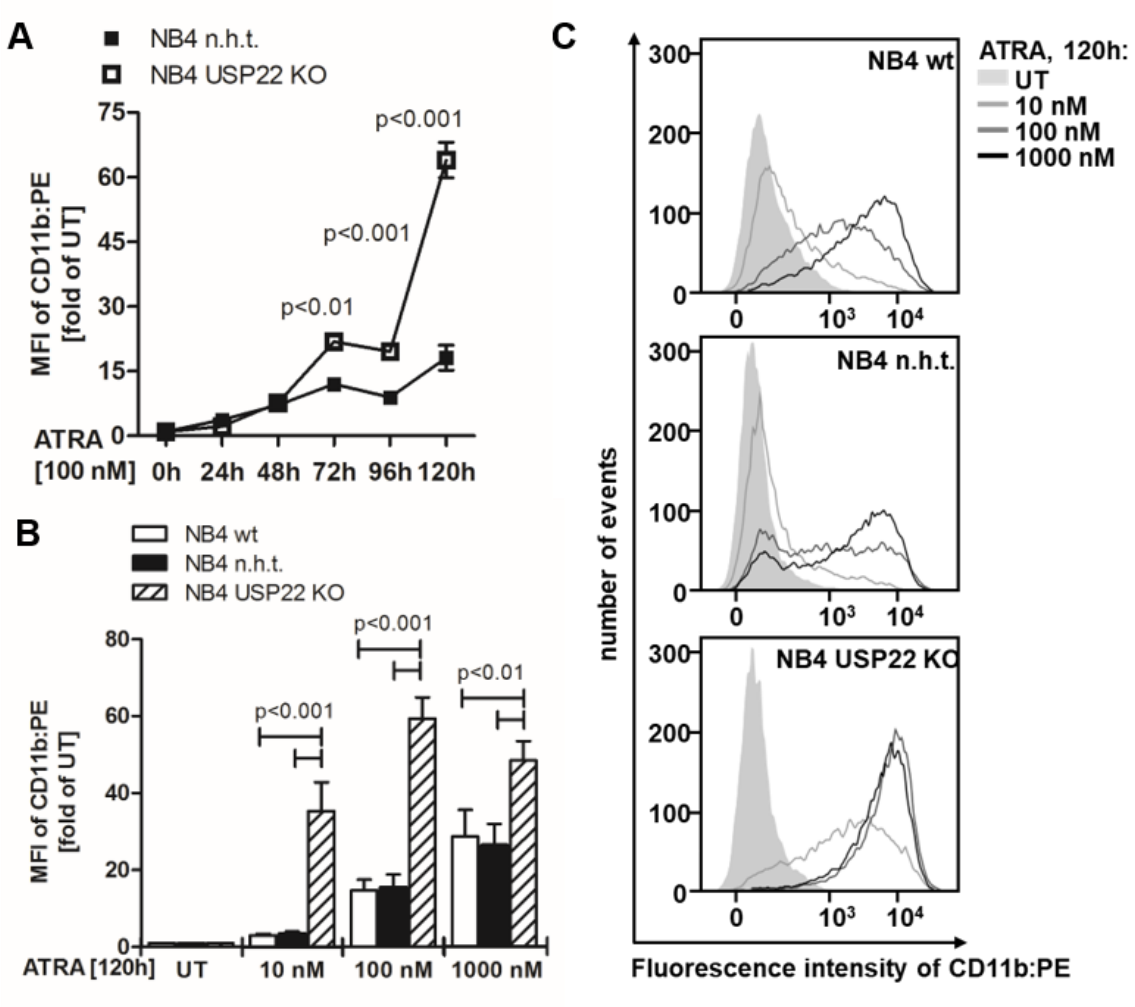

Figure 23: USP22 regulates ATRA-induced granulocytic differentiation of APL cells. A: Incubation of n.h.t. and USP22 KO NB4 cells with 100 nM ATRA for indicated periods of time. Mean fluorescence intensity (MFI) analysis of CD11b surface expression (PE) in treated relative to untreated cells. B: Incubation of wt, n.h.t. and USP22 KO NB4 cells with increasing concentrations of ATRA for 120h. MFI analysis as described in Figure A. Statistical analysis was performed on four independent biological replicates. *p*-values are summarized for wt and n.h.t. in comparison to USP22 KO NB4 cells. C: Representative histograms of CD11b-expressing populations of cells shown in Figure B, presented as number of cells per fluorescence intensity. 10000 events were recorded per condition. Grey area represents untreated population (UT), grey lines represent increasing ATRA concentrations at 120h.

The $CD11b^+$ population of n.h.t. NB4 cells increased from 7-fold elevated MFI after 48 hours ATRA incubation towards 18-fold MFI after 120 hours ATRA compared to untreated cells, which is consistent with the reported onset of pronounced CD11b surface expression after 48 hours ATRA and a maximum of differentiated cells after 96 – 120 hours of ATRA in APL cells [224]. Surprisingly, USP22 deficiency caused a significant increase in MFI of CD11b-presenting NB4 cells to 20-fold over untreated cells after 3 days ATRA treatment and 64-fold after 5 days of ATRA (Figure 23A). Titration of the ATRA concentration at that timepoint revealed a highly significant increase in $CD11b^+$ differentiated USP22 KO NB4 cells at physiological (10 – 100 nM) and clinical doses of ATRA (1000 nM) compared to wild-type and n.h.t. NB4 cells (Figure 23B).

In detail, treatment of wild-type cells with increasing ATRA concentrations for 5 days, caused a concentration-dependent induction of 10- to 30-fold surface expression of CD11b (Figure 23B), while USP22-deficient NB4 cells showed a 40- to 60-fold increase in CD11b surface expression upon ATRA treatment. Strikingly, subclinical concentrations of 10 nM ATRA already led to a 3-fold higher CD11b surface expression in USP22 KO cells compared to wild-type and n.h.t. NB4 cells. Moreover, analysis of the homogeneity of CD11b-presenting cells revealed a complete shift of the USP22 KO NB4 cell population from CD11b-negative towards CD11b-positive cells at 100 nM and 1000 nM ATRA, reflecting a saturation of terminally differentiated cells upon subclinical application of ATRA (Figure 23C). In contrast, the same concentrations were not sufficient to induce a complete shift of the NB4 control cell populations towards CD11b-presenting cells but resulted in a mixed population of CD11b-negative and CD11b-positive cells (Figure 23C upper panels). These results clearly indicate a significant influence of USP22 on the sensitivity of NB4 cells towards ATRA treatment.

According to the reported transcriptional activation in response to ATRA, the observed induction of CD11b surface expression positively correlated with *CD11b* gene expression (Figure 24A). A 5-day incubation of wild-type and n.h.t. NB4 cells with 100 and 1000 nM ATRA revealed an approximate increase of 10- and 30-fold CD11b mRNA levels compared to untreated samples (Figure 24A), while the same concentrations led to an upregulation of CD11b mRNA levels of approximately 100- and 150-fold over untreated conditions in USP22 KO NB4 cells. In addition, we were also able to observe a 2- to 6-fold upregulation of IRF1 mRNA in wild-type and n.h.t. cells with increasing ATRA concentrations (Figure 24B), which is a determinant transcription factor of genes associated with granulocytic differentiation and growth inhibition of APL cells [176, 226]. In line with elevated CD11b mRNA and surface expression levels, deficiency of USP22 led to a 2-fold enhancement of IFR1 mRNA levels compared to the levels of control cells under 1 µM ATRA treatment (Figure 24B), suggesting a global regulation of APL cell differentiation by USP22.

Of note, in addition to enhanced transcriptional activation in response to ATRA treatment, we observed a 5-fold upregulation of CD11b mRNA already in untreated USP22 KO but not in wild-type and n.ht. NB4 cells (Figure 24A), suggesting transcriptional regulation of the differentiation gene network by USP22 independent of ATRA stimulation. Consistently, we were able to observe a 3-fold increase in the damage-regulated autophagy modulator-1 (DRAM-1) mRNA levels in unstimulated USP22 KO cells (Figure 24C), an ATRA-dependent, PU.1-regulated modulator of NB4 cell differentiation [227].

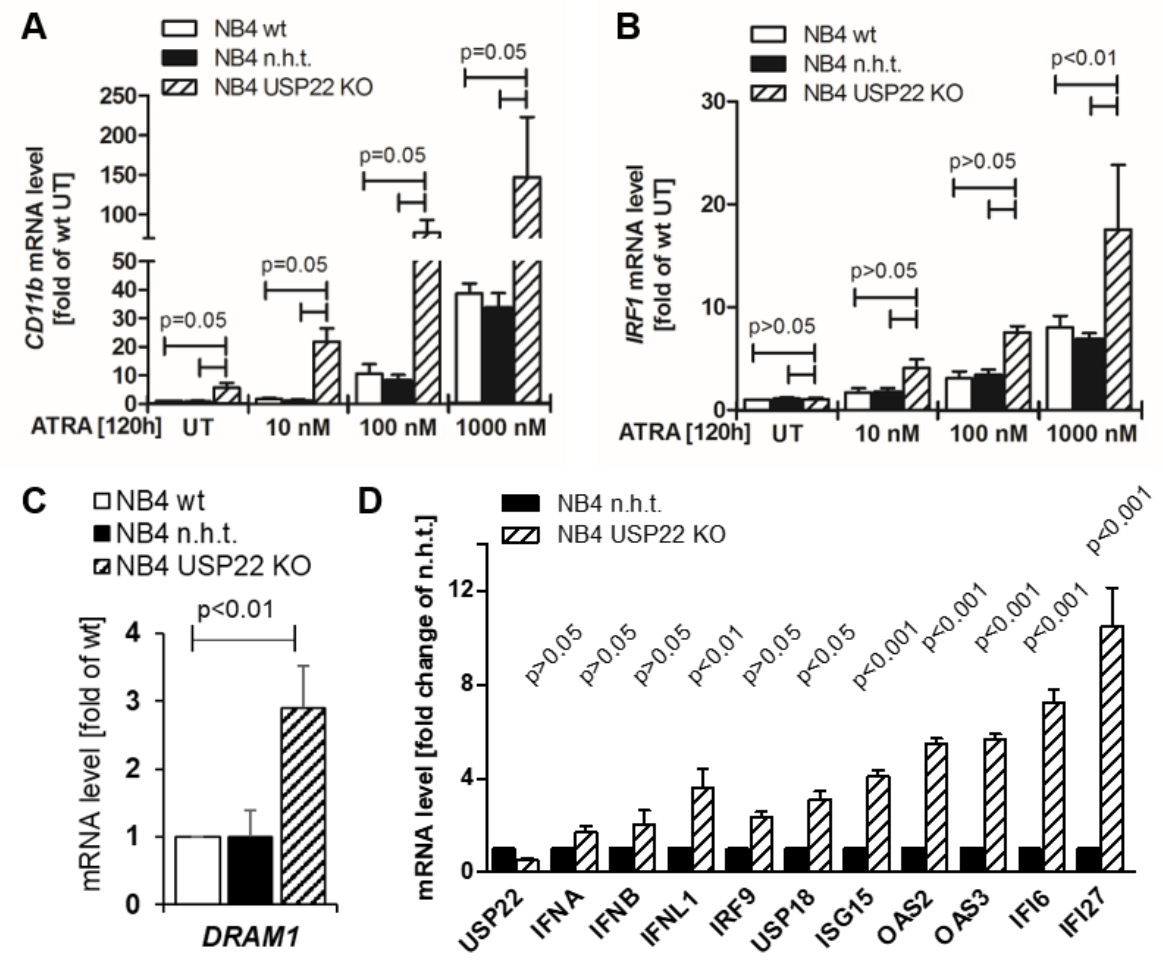

Figure 24: USP22 regulates transcription of genes involved in APL cell differentiation. A+B: Incubation of wt, n.h.t. and USP22 KO NB4 cells with increasing concentrations of ATRA for 120h. qRT-PCR analysis of CD11b (A) and IRF1 (B) transcript levels in these cells, normalized to UT condition of wt NB4 cells. 28s transcript levels served as internal reference. *p*-values are summarized for wt and n.h.t. in comparison to USP22 KO. C+D: qRT-PCR analysis of transcript levels of various differentiation-associated genes in unstimulated USP22 KO NB4 cells relative to wt or n.h.t. NB4 cells. Statistical analysis was performed on three individual biological replicates. Figure D was performed by Sonja Smith.

In line with the assumption of pre-regulated differentiation genes upon USP22 deficiency, a recent pre-print-published study suggests a correlation of USP22 deficiency and lineage determination of hematopoietic stem and progenitor cells towards $CD11b^+$ myeloid cells [66]. The authors delineated a global increase of the interferon response as underlying genetic event, resulting from increased histone H2B mono-ubiquitylation in USP22 KO cells [66]. A similar interferon-regulatory effect by USP22 deficiency was found by our group in the context of colon carcinoma cells (Figure 8A + [62]). In agreement with these findings, several regulators and effectors of interferon response pathways were found to be upregulated in USP22-deficient NB4 cells under homeostatic conditions (Figure 24D). In line with the impact of IFR1-controlled IFN-signaling on $CD11b^+$ commitment and constitutive upregulation of differentiation determining factor DRAM-1, we suggest that USP22-deficiency presumably confers a genetic priming of NB4 cells, sensitizing them for ATRA treatment.

Collectively, our results confirm an important role for USP22 in transcriptional and post-translational regulation of APL progenitor cells under steady-state and ATRA-treated conditions. Targeting USP22 expression in homeostatic situations results in transcriptional predisposition towards terminal myelocyte differentiation, caused by upregulated IFN responses. On the post-translational level, USP22 deficiency induces stabilization of PML-RARα through inhibition of basal and caspase-mediated proteolysis, with USP22-regulated residue K394 playing an essential role in protein stability. Taken together, genetic priming of master regulatory differentiation genes and potentially enhanced ligand-induced transactivation activity of the stabilized PML-RARα fusion receptor reveal highly relevant new functions of USP22 in sensitizing APL cells towards ATRA treatment.

6 Discussion

Targeted cancer therapy requires the knowledge and understanding of cancer-driving oncoproteins and the corresponding signaling networks. One such example is the deubiquitylase USP22, which is associated with malignant cancer progression and poor prognosis for pancreas, prostate, liver, lung and colon cancer [67, 71, 73]. Increased USP22 expression in these tumors is linked to aberrant cell cycle regulation, inhibition of apoptosis, tumor cell stemness and increased invasiveness into peripheral organs [68, 69, 75, 76]. Intriguingly, the majority of these processes is counter-regulated by the tumor suppressor protein PML, which is found to be downregulated in a broad range of progressive tumors [103, 137, 138, 142, 228]. Here, we delineate a novel regulatory function of USP22 in destabilizing PML via its degradation-associated residue K394 in colorectal cancer cells. Similarly, we describe a destabilizing role of this residue in the PML-derived fusion protein PML-RARα in acute promyelocytic leukemia cells. In addition, we demonstrate that USP22 deficiency in APL cells not only causes stabilization of PML-RARα but that it also increases differentiation-associated gene expression and interferon signaling. Together, this dual mechanistic role of USP22 ablation defines an enhanced response of APL cells to the differentiating agent all-*trans* retinoic acid (ATRA), implying a new role for USP22 in APL progenitor cell maintenance.

6.1 Indirect function of USP22 in destabilizing PML and PML-RARα

The tumorigenicity of several tumor entities involves the catalytic DUB activity of USP22 that deubiquitylates and stabilizes direct pro-proliferative targets. In breast cancer, deubiquitylation of transcription factor FBP1 by USP22 reduces the transcriptional activation of p21 and results in increased cancer cell proliferation [46]. In colon cancer, USP22 deubiquitylates and stabilizes the G1-phase regulator cyclin-D1 that mediates cell cycle progression and tumor cell proliferation [56]. In addition, pro-proliferative genes like *BMI-I* or c-*Myc* are activated in cancer cells through histone H2B deubiquitylation by USP22 as member of the transcriptional regulatory SAGA complex [45, 54, 76, 77]. Interestingly, in our study we did not identify USP22 to deubiquitylate and stabilize PML but to inversely regulate PML stability. We observed increased PML protein abundance and slightly decreased PML ubiquitylation in the absence of USP22 which suggests an indirect control of PML stability by USP22. This finding is in line with the recently emerged interaction of USP22 with the interferon-associated cytosolic DNA-sensor protein STING [49]. Direct interaction of USP22 with STING does not lead to USP22-mediated deubiquitylation and stabilization of STING but to suppression of STING-dependent interferon signaling. This indirect function of USP22 is

found to depend on non-catalytical recruitment of USP13 by the UCH-domain of USP22 which results in the removal of signaling-activating K27-linked poly-ubiquitin chains of STING [49, 229]. Consistently, we did not observe PML degradation-related poly-ubiquitin chain signals in the absence of USP22 but rather noted differences in mono-ubiquitylated PML levels. Intriguingly, such an inverse effect on substrate mono-ubiquitylation patterns in the absence of USP22 is described by Atanassov et al., who demonstrate decreased levels of mono-ubiquitylated H2B (H2B-ub1) upon USP22 deficiency [55]. Reason for this inverse regulation are the DUBs USP27X and USP51, that compete with USP22 for H2B-ub1 binding under physiological conditions and that exert potentiated DUB activities towards H2B in the absence of USP22 [55]. Therefore, we suggest an indirect regulation of PML stability either by interaction of USP22 with other ubiquitin-modulating enzymes or by a compensatory action of another PML-associated DUB.

6.2 Regulation of PML stability by the ubiquitin-conjugation system

In human glioma and glioblastoma cells, the DUB USP11 regulates PML stability by physically interacting with PML via its C-terminal USP domain [202]. USP11 deubiquitylates and stabilizes PML under basal and ATO-treated conditions and thereby opposes as well basal PML poly-ubiquitylation conjugated by KLHL20 as RNF4-dependent poly-ubiquitylation in response to ATO-mediated PML SUMOylation [202, 230]. Consistently, in USP22-deficient HT-29 cells we observed a reduction in PML ubiquitylation under basal conditions and a reduction in the SUMO-dependent ubiquitylation pattern of ATO-treated PML, suggesting a compensatory regulation of PML by USP11 in the absence of USP22. However, while the known USP22-compensating DUBs USP27X and USP51 share more than 50% sequence similarity of their catalytic domain with USP22 [231], the domain composition of USP11 and USP22 differs with regard to two additional ubiquitin-like motifs and one extra DUSP in USP11 [24].

Another DUB associated with PML regulation is the herpesvirus associated USP (HAUSP)/ USP7 which directly binds to endogenous PML of nasopharyngeal carcinoma cells and colocalizes particularly with PML I and IV in PML NBs [232]. Similar to what we observed for the regulation of PML isoforms I and IV by USP22, USP7 expression induces PML destabilization, while USP7 knockdown results in PML stabilization and a reduction in poly-ubiquitylated PML levels under basal conditions [232]. Of note, treatment with arsenic trioxide still induces RNF4-mediated PML degradation, independent of the USP7 knockdown-mediated PML stabilization [232]. Similarly, overall ATO-induced degradation of PML and NB disintegration was not majorly affected in the absence of USP22. In addition, USP7 is described to exert deubiquitylating function on histone H2B-ub1 upon Epstein-Barr virus

infection and to regulate cancer stemness similar to USP22 [233, 234], suggesting potentially overlapping functions of USP7 and USP22. As described for the non-catalytical interaction of USP22 and STING, the ubiquitin-specific protease function of USP7 was found to be dispensable for the regulation of PML stability [232]. Furthermore, upon viral infection with HSV-1, USP7 forms a complex with the herpesvirus E3 ubiquitin ligase ICP0 on PML NBs, leading to PML NB disintegration and PML degradation [235]. Similarly, we hypothesize that USP22 might recruit or stabilize an E3 ubiquitin ligase in charge for PML degradation.

In late stage and metastatic colorectal cancer, PML is constitutively degraded by the PML-specific E3-ligase KLHL20, while USP22 is highly expressed in these entities [76, 140]. However, interactome analysis of USP22-overexpressing HT-29 cells performed by Dr. Jens Rödig in our group, failed to identify KLHL20 as potential interactor of USP22 or its catalytically dead mutant. Hence, either recruitment or stabilization of KLHL20 by USP22 might be ruled out in the regulation of PML stability in colon cancer HT-29 cells. Another potential regulatory pathway linking USP22 and KLHL20 might be established via CDK2, which is upregulated by USP22 and likewise is involved in PML phosphorylation as prerequisite for KLHL20 ubiquitylation activity [134, 236]. Analysis of the phosphorylation status of PML in the presence and absence of USP22 is needed to gain more insights in a potential involvement of KLHL20 in USP22-mediated destabilization of PML in colon cancer.

In addition to KLHL20, the E3 ubiquitin ligases SIAH-1 and -2 (SIAH-1/2) regulate PML stability and induce PML and PML-RARα proteasomal degradation [199-201]. In detail, Fanelli et al. show that co-expression of SIAH-2 and PML results in a slower migrating PML signal in Western blot detection, which significantly increases upon proteasomal inhibition [199], suggesting the conjugation of mono-ubiquitin moieties to PML by SIAH-2. Similarly, SIAH-1/2 are involved in target mono-ubiquitylation and proteasomal degradation of α-synuclein in Parkinson's disease or AML1-ETO in acute myelocytic leukemia [200, 237, 238]. In accordance with this observation, we were able to detect slower migrating PML species at a putative size of mono-ubiquitylated PML, that decreased when total PML levels were stabilized in the absence of USP22. This indicates that SIAH-2 might be involved in USP22-dependent regulation of PML. Of note, in neuroblastoma cells, SIAH-1/2 induced mono-ubiquitylation of α-synuclein is counter-regulated by USP9X [239], a DUB that physically interacts with the histone deacetylase HDAC6, which appears in complex with PML [240], suggesting a colocalization of USP9X at PML NBs. In addition, USP9X is described to stabilize its targets as well in the nucleus as in the cytosol [241], possibly explaining the persistence of cytoplasmatic PML isoform I that we observed under PML-degrading conditions. In line with that, previous proteome analyses by Dr. Jens Rödig in our group indicate a potential interaction of USP22 with USP9X in an inverse manner. Taken together, USP22-dependent PML

destabilization in the presence of mono-ubiquitylated PML might result from conjugation of mono-ubiquitin moieties to PML by SIAH-2 in USP22 proficient cells, while in the absence of USP22, SIAH-2 activity might be counter-regulated by USP9X, resulting in PML deubiquitylation and stability prolongation. Still, the mechanism of USP22 to suppress USP9X activity remains to be elucidated.

Collectively, late-stage colon cancer is associated with high USP22 and low PML expression, favoring tumor progression and invasion. With our study we provide evidence for a USP22-dependent regulation of PML protein turnover by indirect modulation of PML post-translational modifications. Potential intermediate regulators of PML destabilization that might be positively regulated by USP22 expression are the PML-specific DUB USP7 as well as the E3 ubiquitin ligases KLHL20 and SIAH-1/2 that exert overlapping effects on PML ubiquitylation pattern as observed for USP22 expression. Vice versa, USP22 deficiency indirectly induces PML stabilization which suggests a counter-regulation of E3-ligases by the DUBs USP9X and USP11. Detailed analysis of the regulators of the ubiquitin-conjugation system will provide further insight to this intricate regulation of the tumor-suppressor PML by USP22 in colon cancer.

6.3 The role of K394 in PML degradation

Complete understanding of PML ubiquitylation requires the delineation of DUB- and E3 ligase-corresponding PML sidechains as in the case of RNF4-targeted PML K401 [124]. Our USP22-dependent profile of ubiquitylated proteins in HT-29 cells, revealed a 2-fold increase in ubiquitylated PML K394 in the absence of USP22. In addition, we demonstrate that substitution of this residue confers a significant increase in PML stability under basal conditions, supporting the involvement of K394 in PML protein turnover. In line with our results, multiple high throughput mass spectrometric ubiquitylome analyses revealed potential direct ubiquitylation sites at 17 of the 30 lysines of full-length PML, of which K380, K394, K400, K401, K476 and K623 appeared most redundantly, as listed in the PhosphoSitePlus® database (v6.6.0.4) [215-218, 242, 243]. Those analyses were conducted under several conditions, including histone deacetylase (HDAC) inhibition, proteasome block or untreated conditions and in various cell lines of different blood cancer types and solid tumors [216-218, 242]. Irrespective of the employed cell line, ubiquitylated PML residue K394 was consistently detected under the condition of proteasomal inhibition with an average increase of 2-fold over untreated samples, implying involvement of K394 ubiquitylation in basal PML turnover [216-218]. The addition of PML degrading agent ATO even results in a 5-fold elevation of ubiquitylated K394 over untreated samples, suggesting a particular role in PML degradation [219].

Noteworthy, particular PML lysine residues are not only described to be ubiquitylated in global proteasome-blocked screens, but also to be conjugated to SUMO remnants in global as well as PML-targeted SUMOylome analyses [92, 93, 219, 244]. For the PML-specific investigation, the group of Pierre Thibault performed sequential peptide purification by primary incubation with an anti-K-(GG) antibody for ubiquitylated remnant enrichment and subsequent incubation with an anti-K-(NQTGG) antibody for SUMOylated remnant enrichment, which resulted in the detection of PML K394 to be SUMOylated as well as ubiquitylated upon ATO treatment [219]. In addition to these findings, we detected decreased levels of SUMOylated PML upon substitution of K394 under basal conditions, suggesting the involvement of PML K394 SUMOylation as well under basal as under ATO-treated conditions. While functional implications of this dual modification of PML K394 remain elusive, detailed studies on the USP22 substrate histone H2B reveal that H2B K120 mono-ubiquitylation decreases in a time-dependent manner under proteasomal inhibition, while H2B-SUMOylation of K120 inversely increases [245]. More such competing PTM conjugations with divergent functional outcome are for example described for K164 of DNA polymerase cofactor Proliferating Cell nuclear antigen (PCNA) and K21 of IκBα [94, 246]. These examples indicate a complex interplay of post translational modifications that need to be investigated with great care in a context-dependent manner.

6.4 PML-RARα degradation in APL cells is controlled by USP22

In the 2nd part of the study, we focused on implications for PML stability regulation in other tumor entities, such as APL. This leukemia subtype originates from an aberrant PML expression in that it is partially fused to the nuclear receptor RARα resulting in severe impairment of transcriptional regulation. For more than 30 years, treatment of APL with the physiological RARα ligand ATRA results in resolution of the PML-RARα-related phenotype and to complete cure of the disease, when combined with cell-death inducing agents [247]. Hallmarks of ATRA induced APL cure are cell cycle arrest, oncogenic fusion receptor degradation and transactivation of lineage committing gene clusters [151, 195, 224, 248]. With the present study, we were able to uncover a novel tumorigenic role of the tumor-associated DUB USP22 in favoring the APL phenotype. We demonstrate, that downregulation of USP22 exerts synergistic effects on APL cells by enhancing ATRA-induced terminal differentiation. Our data provide evidence for a dual role of USP22 in transcriptional as well as post-translational regulation of APL, including suppression of interferon signaling and interference with PML-RARα degradation, respectively.

In the absence of ATRA, USP22-deficiency results in significant stabilization of PML-RARα protein levels in APL cells. Similarly, PML-RARα protein levels were stabilized to a comparable extent upon substitution of the USP22-controlled PML residue K394, suggesting a role for this residue in USP22-regulated degradation of PML-RARα in APL cells. In addition, we detected a significant increase in PML-RARα protein levels in USP22-deficient APL cells that were incubated with ATRA for up to 5 days. In correlation, we observed an altered cleavage pattern of PML-RARα in combination with reduced caspase-3 activity in these cells. Consistently, ATRA-mediated degradation of PML-RARα involves mechanisms of phosphorylation, proteasome engagement and caspase-3-induced proteolysis, which accounts for approximately 50% of degraded PML-RARα protein [187-189]. In line with increased APL cell differentiation upon caspase-3 inhibition in the presence of ATRA [187], we observed dramatically increased APL cell differentiation in caspase-3-impaired USP22-ablated cells. Of note, USP22 ablation is correlated with increased p21 expression in different tumor cells [46]. p21 is able to inhibit caspase-3 activity and to initiate terminal differentiation of hematopoietic cells [249, 250]. Accordingly, USP22-deficient APL cells not only comprise reduced caspase-3 activity but also respond to ATRA with a dramatically increased population of differentiated CD11b^{high}-expressing myelocytes. However, involvement of p21 and a general regulation of caspase-3 activity by USP22 demand further investigation due to diverse regulation of pro-caspase-3 in distinct USP22-deficient tumors. In line with our study, USP22 ablation in glioblastoma cells results in diminished pro-caspase-3 expression levels [236], while results from hepatocellular and renal cell carcinoma suggest an increase in caspase-3 activation [251, 252], emphasizing the need for further investigations.

6.5 USP22 regulates APL cell differentiation upon ATRA

Besides the new role of USP22 in degradation of PML-RARα in basal and ATRA-treated APL cells, we describe a prominent new function of USP22 in sensitizing APL cells for ATRA-induced myelocytic differentiation. Beginning after 72 hours ATRA incubation we observe a dramatic increase in CD11b-presenting myelocytes in USP22-deficient cells compared to control cells. Accordingly, terminally differentiated myelocytes accumulate after 48 – 72 hours ATRA administration in APL cell lines and after 72 hours in APL patients [224, 253]. Terminal myelocytic differentiation is accompanied by cell cycle arrest that depends on cyclin B1 downregulation and CDK2 degradation and occurs after 48 – 72 hours of ATRA incubation [172, 224]. Interestingly, cyclin B1 and -D1 levels and CDK1 and -2 activation are directly regulated by USP22 and become degraded and inhibited upon USP22 ablation, leading to G0/G1-arrest and favoring progenitor cell differentiation [45, 56, 236]. In line with this regulatory impact of USP22 depletion on cell cycle arrest and terminal differentiation, we

were able to observe an ATRA-dependent downregulation of USP22 protein levels commencing after 48 – 72 hours ATRA incubation and reaching a maximum of USP22 suppression after 120 hours. This observation coincides with the increase in CD11b-expressing cells after 72 hours of ATRA treatment and suggests a synergistic effect of conditional USP22 depletion and ATRA administration in USP22 KO APL cells.

This synergistic effect might results from ATRA-induced p21 upregulation which causes Sp1 expression, a repressive element of the USP22 promoter region [254]. Another ATRA-induced *USP22*-inhibitor is the p38/mitogen-activated protein kinase (MAPK), which is essential for ligand-induced transactivation of RARα target genes during myelocytic differentiation [255, 256]. Indeed, we were able to observe overlapping patterns of differentiation-regulating genes that are generally induced by ATRA administration and that were upregulated in response to USP22 ablation in APL cells. Among those, ATRA as well as USP22 deficiency upregulate interferon signaling, including IRF1, STAT1, 2'-5'-oligoadenylate synthetase (OAS) and ISGylation-regulators which are all important for terminal granulocytic differentiation [172, 175, 226, 257]. In previous studies we and others could show, that knockout of USP22, leads to upregulation of the cellular interferon response in in several cancer cell lines [49, 62, 66]. Here, we additionally detect that USP22 depletion in APL cells moderately induces expression levels of IFNs type I-III, IRF9 and OAS and even more pronounced increases the downstream IFN modulators like ISG15, IFI27 and IFI6. This boost in ISG production might result from the stabilization of PML and PML-RARα in the absence of USP22. PML is able to stabilize activated phosphorylated (p)-STAT1, that forms the ISGF3 complex together with p-STAT2 and IRF9 and further activates ISG production [258, 259]. In a feedforward loop, ISRE and GAS elements in the PML and PML-RARα promoter regions respond to IFN and STAT binding and activate PML and PML-RARα expression [104, 260].

Strikingly, pioneer studies on APL treatment already deciphered a synergistic effect of IFN- and ATRA-induced signaling towards terminal differentiation of NB4 cells, yet revealing isolated IFN treatment not to be sufficient to induce differentiation [260-263]. Single administration of IFNα for example moderately pre-induces differentiation-regulatory components like OAS [263, 264], while combined incubation of IFNα and ATRA dramatically increases OAS expression to a maximum after 3 days [264], coinciding with the reported peak of myelocyte differentiation [224, 253]. Consistently, we found OAS2 and OAS3 to be constitutively upregulated by USP22 ablation and we observed the onset of enhanced differentiation of USP22 KO NB4 cells upon 3 days of ATRA treatment. These results suggest a genetic priming in USP22 KO cells by interferon-related signaling that is able to boost the differentiating effect of ATRA.

Indeed, novel investigations on USP22 KO in hematopoietic stem and progenitor cells (HSPCs) revealed an increase in mono-ubiquitylated histone H2B on ISG promoter regions, causing a predisposition of USP22-deficient HSPCs towards the myelocytic but not lymphocytic lineage upon differentiating stimuli [66]. The authors were able to exclude secreted IFNs to take part in the differentiative priming which is consistent with our observations of only subtle increases in IFNα and ß-levels in NB4 USP22 KO cells and the reported lack of secreted type I interferons in USP22-deficient colon cancer cells [62]. The impact of histone regulation on APL cell priming seems to be extended to non-interferon regulated genes, since we see intrinsic upregulation of two crucial differentiation-associated genes *CD11b* and *DRAM-1* in NB4 USP22 KO cells, consistent with the report that *CD11b* is not induced by type I interferon signaling [261]. Together, our results strongly suggest, that the induction of interferon signaling in response to USP22 deficiency genetically prepares APL cells for ATRA-induced expression of a differentiation gene network, implying a synergism of USP22 ablation and ATRA response in the treatment of APL. To which extend the stabilization of PML and PML-RARα further potentiate this synergism remains to be clarified. Indeed, downregulation of PML in myeloid precursor cells is reported to impair ATRA-mediated terminal differentiation [143], supporting a potentiating impact of USP22 KO-dependent stabilization of PML on the above delineated synergism with ATRA treatment.

6.6 Limitations and Outlook

We identified a novel role of the DUB USP22 in the regulation of the basal protein stability of the tumor-suppressor PML by involvement of the ubiquitin-conjugation system. While PML-interacting E3 ubiquitin ligases or DUBs that are controlled by USP22 need to be identified, we collected indications of an involvement of the E2 ubiquitin-conjugating enzyme UBE2L6 in USP22-dependent signaling. In colon carcinoma cells, we observed the upregulation of UBE2L6 mRNA and protein levels in the absence of USP22. UBE2L6 is considered as E2 ubiquitin hub that interacts with approximately 20 distinct E3 ligases [265], among those also several PML-specific E3s such as UBE3A and SIAH1/2 [200, 266, 267]. Moreover, UBE2L6 serves as ISG15-specific E2-conjugase during ISGylation and can be induced by interferon signaling [88]. Consistently, IFNs as well as ISG15, UBE2L6 and the ISG15-specific de-ISGylase USP18 are upregulated in USP22-deficient colon carcinoma and APL cells. Additionally, ISGylation is involved in ATRA-induced granulocyte differentiation and PML-RARα turnover [196, 197, 257]. Therefore, it is of great interest to investigate the USP22-dependent regulation of ISGylation, to unravel its contribution to USP22-mediated turnover of PML and PML-RARα.

To further investigate the regulation of PML stability by a USP22-dependent enrollment of the ubiquitin-conjugation system, the signaling pathway of the PML-specific E3 ubiquitin ligase KLHL20 might be of great interest. KLHL20 is increased expressed in progressive USP22-expressing colorectal cancer and regulates the degradation of PML in concert with the PML-specific kinase CDK2 [76, 140]. To delineate a USP22-dependent impact on KLHL20 signaling, the CDK2-mediated phosphorylation of PML at S518 needs to be addressed by mutant S518A enrollment in cycloheximide-chase experiments in the presence and absence of USP22.

Similar to USP22-regulated stability of PML, we were able to delineate a novel role for USP22 in controlling degradation of the APL-associated fusion protein PML-RARα under basal conditions and in the presence of ATRA. Related to PML degradation, the involvement of degradation-associated phosphorylation of PML-RARα should be analyzed in dependency on USP22 expression. In the presence of ATRA, residue S873 of PML-RARα becomes phosphorylated by the cAMP-induced kinase PKA, leading to PML-RARα degradation [180]. In the absence of USP22, we observed a resistance of PML-RARα degradation under ATRA treatment, suggesting an USP22-dependent alteration of PML-RARα-specific PKA signaling. Indeed, murine APL cells expressing mutant PML-RARα with S873A substitution reveal a resistance towards ATRA-induced PML-RARα degradation. Furthermore, mutant PML-RARα S873A-expressing mice show less differentiative potential and comprise a 10% increased population of leukemia-initiating cells (LICs) [180]. In contrast, USP22-deficient APL cells are characterized by a dramatically increased differentiative potential, questioning the accumulation of LICs under these conditions. To address this feature, ATRA-treated cells could be immunophenotyped for the expression of LIC-surface markers CD11b, c-Kit and Gr-1 [268]. In addition, secondary transplantation experiments of ATRA-treated APL cells in the presence or absence of USP22 expression would allow further assumptions on the persistence of a LIC population.

In general, LIC maintenance and constitutive PML-RARα expression are hallmarks of ATRA treatment resistance that causes a relapse of APL patients [269]. In addition, most ATRA-resistant APL relapse cases acquire additional leukemogenic mutations associated with apoptosis resistance and clonogenicity of leukemic blasts [270, 271]. To which extend USP22 controls the leukemic progenitor cell pool in APL remains matter of investigation. In the case of AML, the contribution of USP22 deficiency to progenitor cell maintenance indeed depends on additionally acquired cancer-driving mutations. In a FLT3-internal tandem duplication (ITD) background, USP22 stabilizes SIRT1 and thereby enhances the oncogenic potential of the LIC compartment [272], while in mutant KRAS-driven AML cases, USP22 is involved in PU.1

stabilization resulting in increased differentiating potential of USP22 proficient cells [48]. In APL, FLT3-ITD mutations are associated with high-risk white blood cell counts, accumulation of PML-RARα, resistance to ATRA-mediated receptor degradation and decomposition of PML NBs [273]. In addition to PML-RARα persistence in USP22-deficient APL cells, we were also able to observe dysregulation of ATRA-dependent re-formation of PML NBs in these cells. Whether this USP22-dependent phenotype coincides with APL mutational burden and whether USP22 expression correlates with the incidence of APL relapse demands detailed investigation.

As a progressive tumor marker, USP22 is an attractive target for late-stage malignant cancer treatment. In both tumor entities analyzed in the present study, USP22 is highly expressed and correlates with significantly decreased survival rates of colon cancer and AML patients compared to cohorts with USP22-low expressing tumors [67, 73, 74]. Among established anti-cancer drugs, two compounds were found to target USP22 and to induce cancer cell apoptosis in vitro. Repression of USP22 is described for the chemotherapeutic drug cisplatin that suppresses USP22 via p38/MAPK signaling [256] and for the HDAC inhibitor trichostatin A (TSA) that directly acts on the USP22 promoter and results in cancer cell apoptosis via p21 upregulation [274]. According to our results on a differentiative synergism of USP22 deficiency and ATRA treatment, combined targeting of USP22 in APL might favor low-dose response to ATRA. Since the differentiation efficacy of ATRA treatment strongly correlates with its bioavailability in APL patients, requirements for low-dose ATRA response are appreciated [253]. Interestingly, both USP22-targeting compounds have already been described in the context of APL. In vitro cisplatin administration in APL cell lines resulted in increased oxidative stress, upregulation of p21 and induction of intrinsic apoptosis leading to cell death of promyelocytes [275]. Likewise, TSA and other HDAC inhibitors induce APL cell apoptosis along with p21 and death receptor upregulation [276, 277]. As single agents, both compounds are not able to induce APL cell differentiation. Whether cisplatin- or TSA-treatment of APL cells is sufficient to mimic USP22 ablation and consequently prime leukemic blasts for ATRA-responsive terminal differentiation remains to be addressed by co-treatment along with respective interferon pathway analysis. Promisingly, novel macrocyclic peptides are recently described to specifically inhibit USP22 activity on enzyme-level, causing an accumulation of histone H2B mono-ubiquitylation in an experimental cell line in vitro [278]. In accordance with increased H2B-ub1 levels in HSPCs upon USP22 silencing that indeed favors interferon signaling and differentiation-directed gene expression [66], those cyclic peptides might represent an effective combination with ATRA and ATO to treat APL, preventing ATRA-resistant relapse cases evolving from incomplete responsiveness to low-dose ATRA.

7 References

1. Walsh, C.T., S. Garneau-Tsodikova, and G.J. Gatto, Jr., *Protein posttranslational modifications: the chemistry of proteome diversifications.* Angew Chem Int Ed Engl, 2005. **44**(45): p. 7342-72.
2. Venne, A.S., L. Kollipara, and R.P. Zahedi, *The next level of complexity: crosstalk of posttranslational modifications.* Proteomics, 2014. **14**(4-5): p. 513-24.
3. Vijay-Kumar, S., C.E. Bugg, and W.J. Cook, *Structure of ubiquitin refined at 1.8 A resolution.* J Mol Biol, 1987. **194**(3): p. 531-44.
4. Dye, B.T. and B.A. Schulman, *Structural mechanisms underlying posttranslational modification by ubiquitin-like proteins.* Annu Rev Biophys Biomol Struct, 2007. **36**: p. 131-50.
5. Buetow, L. and D.T. Huang, *Structural insights into the catalysis and regulation of E3 ubiquitin ligases.* Nature Reviews Molecular Cell Biology, 2016. **17**(10): p. 626-642.
6. Liao, Y., I. Sumara, and E. Pangou, *Non-proteolytic ubiquitylation in cellular signaling and human disease.* Commun Biol, 2022. **5**(1): p. 114.
7. Kulathu, Y. and D. Komander, *Atypical ubiquitylation - the unexplored world of polyubiquitin beyond Lys48 and Lys63 linkages.* Nat Rev Mol Cell Biol, 2012. **13**(8): p. 508-23.
8. West, M.H. and W.M. Bonner, *Histone 2B can be modified by the attachment of ubiquitin.* Nucleic Acids Res, 1980. **8**(20): p. 4671-80.
9. Komander, D. and M. Rape, *The ubiquitin code.* Annu Rev Biochem, 2012. **81**: p. 203-29.
10. Chau, V., et al., *A multiubiquitin chain is confined to specific lysine in a targeted short-lived protein.* Science, 1989. **243**(4898): p. 1576-83.
11. Ciechanover, A., D. Finley, and A. Varshavsky, *The ubiquitin-mediated proteolytic pathway and mechanisms of energy-dependent intracellular protein degradation.* J Cell Biochem, 1984. **24**(1): p. 27-53.
12. Hershko, A. and A. Ciechanover, *The ubiquitin system.* Annu Rev Biochem, 1998. **67**: p. 425-79.
13. Petroski, M.D. and R.J. Deshaies, *Mechanism of lysine 48-linked ubiquitin-chain synthesis by the cullin-RING ubiquitin-ligase complex SCF-Cdc34.* Cell, 2005. **123**(6): p. 1107-20.
14. Kim, H.C. and J.M. Huibregtse, *Polyubiquitination by HECT E3s and the determinants of chain type specificity.* Mol Cell Biol, 2009. **29**(12): p. 3307-18.
15. Haglund, K. and I. Dikic, *Ubiquitylation and cell signaling.* EMBO J, 2005. **24**(19): p. 3353-9.
16. Eddins, M.J., et al., *Mms2-Ubc13 covalently bound to ubiquitin reveals the structural basis of linkage-specific polyubiquitin chain formation.* Nat Struct Mol Biol, 2006. **13**(10): p. 915-20.
17. Iwai, K. and F. Tokunaga, *Linear polyubiquitination: a new regulator of NF-kappaB activation.* EMBO Rep, 2009. **10**(7): p. 706-13.

18. Haas, T.L., et al., *Recruitment of the linear ubiquitin chain assembly complex stabilizes the TNF-R1 signaling complex and is required for TNF-mediated gene induction.* Mol Cell, 2009. **36**(5): p. 831-44.

19. Bremm, A. and D. Komander, *Emerging roles for Lys11-linked polyubiquitin in cellular regulation.* Trends in biochemical sciences, 2011. **36**(7): p. 355-363.

20. Yuan, W.C., et al., *K33-Linked Polyubiquitination of Coronin 7 by Cul3-KLHL20 Ubiquitin E3 Ligase Regulates Protein Trafficking.* Mol Cell, 2014. **54**(4): p. 586-600.

21. Ordureau, A., et al., *Quantitative proteomics reveal a feedforward mechanism for mitochondrial PARKIN translocation and ubiquitin chain synthesis.* Mol Cell, 2014. **56**(3): p. 360-375.

22. Zucchelli, S., et al., *TRAF6 promotes atypical ubiquitination of mutant DJ-1 and alpha-synuclein and is localized to Lewy bodies in sporadic Parkinson's disease brains.* Hum Mol Genet, 2010. **19**(19): p. 3759-70.

23. Zucchelli, S., et al., *Tumor necrosis factor receptor-associated factor 6 (TRAF6) associates with huntingtin protein and promotes its atypical ubiquitination to enhance aggregate formation.* J Biol Chem, 2011. **286**(28): p. 25108-17.

24. Komander, D., M.J. Clague, and S. Urbe, *Breaking the chains: structure and function of the deubiquitinases.* Nat Rev Mol Cell Biol, 2009. **10**(8): p. 550-63.

25. Mevissen, T.E.T. and D. Komander, *Mechanisms of Deubiquitinase Specificity and Regulation.* Annu Rev Biochem, 2017. **86**: p. 159-192.

26. Haahr, P., et al., *ZUFSP Deubiquitylates K63-Linked Polyubiquitin Chains to Promote Genome Stability.* Mol Cell, 2018. **70**(1): p. 165-174 e6.

27. Dikic, I., S. Wakatsuki, and K.J. Walters, *Ubiquitin-binding domains - from structures to functions.* Nat Rev Mol Cell Biol, 2009. **10**(10): p. 659-71.

28. Rehman, S.A.A., et al., *MINDY-1 Is a Member of an Evolutionarily Conserved and Structurally Distinct New Family of Deubiquitinating Enzymes.* Mol Cell, 2016. **63**(1): p. 146-55.

29. Keusekotten, K., et al., *OTULIN antagonizes LUBAC signaling by specifically hydrolyzing Met1-linked polyubiquitin.* Cell, 2013. **153**(6): p. 1312-26.

30. Sato, Y., et al., *Structural basis for specific cleavage of Lys 63-linked polyubiquitin chains.* Nature, 2008. **455**(7211): p. 358-62.

31. Ye, Y., et al., *Dissection of USP catalytic domains reveals five common insertion points.* Mol Biosyst, 2009. **5**(12): p. 1797-808.

32. McCullough, J., et al., *Activation of the endosome-associated ubiquitin isopeptidase AMSH by STAM, a component of the multivesicular body-sorting machinery.* Curr Biol, 2006. **16**(2): p. 160-5.

33. Yan, K., et al., *The deubiquitinating enzyme complex BRISC is required for proper mitotic spindle assembly in mammalian cells.* J Cell Biol, 2015. **210**(2): p. 209-24.

34. Kyrieleis, O.J.P., et al., *Three-Dimensional Architecture of the Human BRCA1-A Histone Deubiquitinase Core Complex.* Cell Rep, 2016. **17**(12): p. 3099-3106.

35. Henry, K.W., et al., *Transcriptional activation via sequential histone H2B ubiquitylation and deubiquitylation, mediated by SAGA-associated Ubp8.* Genes Dev, 2003. **17**(21): p. 2648-63.

36. Lee, B.H., et al., *USP14 deubiquitinates proteasome-bound substrates that are ubiquitinated at multiple sites.* Nature, 2016. **532**(7599): p. 398-401.

37. Verma, R., et al., *Role of Rpn11 metalloprotease in deubiquitination and degradation by the 26S proteasome.* Science, 2002. **298**(5593): p. 611-5.

38. Yao, T., et al., *Proteasome recruitment and activation of the Uch37 deubiquitinating enzyme by Adrm1.* Nat Cell Biol, 2006. **8**(9): p. 994-1002.

39. Kerscher, O., R. Felberbaum, and M. Hochstrasser, *Modification of proteins by ubiquitin and ubiquitin-like proteins.* Annu Rev Cell Dev Biol, 2006. **22**: p. 159-80.

40. Cope, G.A., et al., *Role of predicted metalloprotease motif of Jab1/Csn5 in cleavage of Nedd8 from Cul1.* Science, 2002. **298**(5593): p. 608-11.

41. Malakhov, M.P., et al., *UBP43 (USP18) specifically removes ISG15 from conjugated proteins.* J Biol Chem, 2002. **277**(12): p. 9976-81.

42. Schulz, S., et al., *Ubiquitin-specific protease-like 1 (USPL1) is a SUMO isopeptidase with essential, non-catalytic functions.* EMBO Rep, 2012. **13**(10): p. 930-8.

43. Xiong, J., et al., *Identification of a functional nuclear localization signal within the human USP22 protein.* Biochem Biophys Res Commun, 2014. **449**(1): p. 14-8.

44. Bonnet, J., et al., *Zinc-finger UBPs: regulators of deubiquitylation.* Trends Biochem Sci, 2008. **33**(8): p. 369-75.

45. Zhang, X.Y., et al., *The putative cancer stem cell marker USP22 is a subunit of the human SAGA complex required for activated transcription and cell-cycle progression.* Mol Cell, 2008. **29**(1): p. 102-11.

46. Atanassov, B.S. and S.Y. Dent, *USP22 regulates cell proliferation by deubiquitinating the transcriptional regulator FBP1.* EMBO Rep, 2011. **12**(9): p. 924-30.

47. Atanassov, B.S., et al., *Gcn5 and SAGA regulate shelterin protein turnover and telomere maintenance.* Mol Cell, 2009. **35**(3): p. 352-64.

48. Melo-Cardenas, J., et al., *USP22 deficiency leads to myeloid leukemia upon oncogenic Kras activation through a PU.1-dependent mechanism.* Blood, 2018. **132**(4): p. 423-434.

49. Liu, Q., et al., *Broad and diverse mechanisms used by deubiquitinase family members in regulating the type I interferon signaling pathway during antiviral responses.* Sci Adv, 2018. **4**(5): p. eaar2824.

50. Xiong, J., et al., *PKA/CREB regulates the constitutive promoter activity of the USP22 gene.* Oncol Rep, 2015. **33**(3): p. 1505-11.

51. Lin, Z., et al., *Ubiquitin-specific protease 22 is a deubiquitinase of CCNB1.* Cell Discov, 2015. **1**.

52. Choudhary, C., et al., *Lysine acetylation targets protein complexes and co-regulates major cellular functions.* Science, 2009. **325**(5942): p. 834-40.

53. Armour, S.M., et al., *A high-confidence interaction map identifies SIRT1 as a mediator of acetylation of USP22 and the SAGA coactivator complex.* Mol Cell Biol, 2013. **33**(8): p. 1487-502.

54. Jeusset, L.M. and K.J. McManus, *Ubiquitin Specific Peptidase 22 Regulates Histone H2B Mono-Ubiquitination and Exhibits Both Oncogenic and Tumor Suppressor Roles in Cancer.* Cancers (Basel), 2017. **9**(12).

55. Atanassov, B.S., et al., *ATXN7L3 and ENY2 Coordinate Activity of Multiple H2B Deubiquitinases Important for Cellular Proliferation and Tumor Growth.* Mol Cell, 2016. **62**(4): p. 558-71.

56. Gennaro, V.J., et al., *Control of CCND1 ubiquitylation by the catalytic SAGA subunit USP22 is essential for cell cycle progression through G1 in cancer cells.* Proc Natl Acad Sci U S A, 2018. **115**(40): p. E9298-E9307.

57. Lin, Z., et al., *USP22 antagonizes p53 transcriptional activation by deubiquitinating Sirt1 to suppress cell apoptosis and is required for mouse embryonic development.* Mol Cell, 2012. **46**(4): p. 484-94.

58. Koutelou, E., et al., *USP22 controls multiple signaling pathways that are essential for vasculature formation in the mouse placenta.* Development, 2019. **146**(4).

59. Lee, H.J., et al., *The expression patterns of deubiquitinating enzymes, USP22 and Usp22.* Gene Expr Patterns, 2006. **6**(3): p. 277-84.

60. Sussman, R.T., et al., *The epigenetic modifier ubiquitin-specific protease 22 (USP22) regulates embryonic stem cell differentiation via transcriptional repression of sex-determining region Y-box 2 (SOX2).* J Biol Chem, 2013. **288**(33): p. 24234-46.

61. Kobayashi, T., et al., *Deubiquitinating enzymes regulate Hes1 stability and neuronal differentiation.* FEBS J, 2015. **282**(13): p. 2411-23.

62. Karlowitz, R., et al., *USP22 controls type III interferon signaling and SARS-CoV-2 infection through activation of STING.* Cell Death Dis, 2022. **13**(8): p. 684.

63. Cai, Z., et al., *USP22 promotes IRF3 nuclear translocation and antiviral responses by deubiquitinating the importin protein KPNA2.* J Exp Med, 2020. **217**(5).

64. Li, D. and M. Wu, *Pattern recognition receptors in health and diseases.* Signal Transduct Target Ther, 2021. **6**(1): p. 291.

65. Hu, H. and S.C. Sun, *Ubiquitin signaling in immune responses.* Cell Res, 2016. **26**(4): p. 457-83.

66. Dietlein, N., et al., *Loss of Usp22 enhances histone H2B monoubiquitination and stimulates intracellular and systemic interferon immunity.* bioRxiv, 2021: p. 2021.04.09.439190.

67. Glinsky, G.V., O. Berezovska, and A.B. Glinskii, *Microarray analysis identifies a death-from-cancer signature predicting therapy failure in patients with multiple types of cancer.* J Clin Invest, 2005. **115**(6): p. 1503-21.

68. Schrecengost, R.S., et al., *USP22 regulates oncogenic signaling pathways to drive lethal cancer progression.* Cancer Res, 2014. **74**(1): p. 272-86.

69. Ning, Z., et al., *USP22 promotes the G1/S phase transition by upregulating FoxM1 expression via beta-catenin nuclear localization and is associated with poor prognosis in stage II pancreatic ductal adenocarcinoma.* Int J Oncol, 2014. **45**(4): p. 1594-608.

70. Piao, S., et al., *USP22 is useful as a novel molecular marker for predicting disease progression and patient prognosis of oral squamous cell carcinoma.* PLoS One, 2012. **7**(8): p. e42540.

71. Tang, B., et al., *High USP22 expression indicates poor prognosis in hepatocellular carcinoma.* Oncotarget, 2015. **6**(14): p. 12654-67.

72. Yang, M., et al., *Ubiquitin-specific protease 22: a novel molecular biomarker in cervical cancer prognosis and therapeutics.* Tumour Biol, 2014. **35**(2): p. 929-34.

73. Liu, Y.L., et al., *Increased expression of ubiquitin-specific protease 22 can promote cancer progression and predict therapy failure in human colorectal cancer.* J Gastroenterol Hepatol, 2010. **25**(11): p. 1800-5.

74. Wang, Z., et al., *Decreased H2B monoubiquitination and overexpression of ubiquitin-specific protease enzyme 22 in malignant colon carcinoma.* Hum Pathol, 2015. **46**(7): p. 1006-14.

75. Liu, Y.L., et al., *Aberrant expression of USP22 is associated with liver metastasis and poor prognosis of colorectal cancer.* J Surg Oncol, 2011. **103**(3): p. 283-9.

76. Yuan, X., et al., *Ubiquitin-specific peptidase 22 promotes proliferation and metastasis in human colon cancer.* Oncol Lett, 2019. **18**(5): p. 5567-5576.

77. Liu, Y.L., et al., *USP22 acts as an oncogene by the activation of BMI-1-mediated INK4a/ARF pathway and Akt pathway.* Cell Biochem Biophys, 2012. **62**(1): p. 229-35.

78. Berezovska, O.P., et al., *Essential role for activation of the Polycomb group (PcG) protein chromatin silencing pathway in metastatic prostate cancer.* Cell Cycle, 2006. **5**(16): p. 1886-901.

79. Wang, A., et al., *Overexpression of cyclin B1 in human colorectal cancers.* J Cancer Res Clin Oncol, 1997. **123**(2): p. 124-7.

80. Kosinsky, R.L., et al., *USP22 exerts tumor-suppressive functions in colorectal cancer by decreasing mTOR activity.* Cell Death Differ, 2020. **27**(4): p. 1328-1340.

81. Wang, X.W. and Y.J. Zhang, *Targeting mTOR network in colorectal cancer therapy.* World J Gastroenterol, 2014. **20**(15): p. 4178-88.

82. Wang, Y., et al., *The deubiquitinase USP22 regulates PD-L1 degradation in human cancer cells.* Cell Commun Signal, 2020. **18**(1): p. 112.

83. Sharma, P. and J.P. Allison, *Immune checkpoint targeting in cancer therapy: toward combination strategies with curative potential.* Cell, 2015. **161**(2): p. 205-14.

84. Roedig, J., et al., *USP22 controls necroptosis by regulating receptor-interacting protein kinase 3 ubiquitination.* EMBO Rep, 2021. **22**(2): p. e50163.

85. Fulda, S., *Promises and Challenges of Smac Mimetics as Cancer Therapeutics.* Clin Cancer Res, 2015. **21**(22): p. 5030-6.

86. Swatek, K.N. and D. Komander, *Ubiquitin modifications.* Cell Res, 2016. **26**(4): p. 399-422.

87. Burroughs, A.M., L.M. Iyer, and L. Aravind, *Structure and evolution of ubiquitin and ubiquitin-related domains.* Methods Mol Biol, 2012. **832**: p. 15-63.

88. Mirzalieva, O., et al., *ISG15 and ISGylation in Human Diseases.* Cells, 2022. **11**(3).

89. Aichem, A., et al., *The structure of the ubiquitin-like modifier FAT10 reveals an alternative targeting mechanism for proteasomal degradation.* Nat Commun, 2018. **9**(1): p. 3321.

90. Soucy, T.A., et al., *The NEDD8 Conjugation Pathway and Its Relevance in Cancer Biology and Therapy.* Genes Cancer, 2010. **1**(7): p. 708-16.

91. Kim, W., et al., *Systematic and quantitative assessment of the ubiquitin-modified proteome.* Mol Cell, 2011. **44**(2): p. 325-40.

92. Lumpkin, R.J., et al., *Site-specific identification and quantitation of endogenous SUMO modifications under native conditions.* Nat Commun, 2017. **8**(1): p. 1171.

93. Hendriks, I.A., et al., *Uncovering global SUMOylation signaling networks in a site-specific manner.* Nat Struct Mol Biol, 2014. **21**(10): p. 927-36.

94. Desterro, J.M., M.S. Rodriguez, and R.T. Hay, *SUMO-1 modification of IkappaBalpha inhibits NF-kappaB activation.* Mol Cell, 1998. **2**(2): p. 233-9.

95. Sahin, U., H. de The, and V. Lallemand-Breitenbach, *Sumoylation in Physiology, Pathology and Therapy.* Cells, 2022. **11**(5).

96. Schmidt, D. and S. Muller, *Members of the PIAS family act as SUMO ligases for c-Jun and p53 and repress p53 activity.* Proc Natl Acad Sci U S A, 2002. **99**(5): p. 2872-7.

97. Pichler, A., et al., *The nucleoporin RanBP2 has SUMO1 E3 ligase activity.* Cell, 2002. **108**(1): p. 109-20.

98. Guervilly, J.H., et al., *The SLX4 complex is a SUMO E3 ligase that impacts on replication stress outcome and genome stability.* Mol Cell, 2015. **57**(1): p. 123-37.

99. Kunz, K., T. Piller, and S. Muller, *SUMO-specific proteases and isopeptidases of the SENP family at a glance.* J Cell Sci, 2018. **131**(6).

100. van Wijk, S.J., S. Muller, and I. Dikic, *Shared and unique properties of ubiquitin and SUMO interaction networks in DNA repair.* Genes Dev, 2011. **25**(17): p. 1763-9.

101. Flotho, A. and F. Melchior, *Sumoylation: a regulatory protein modification in health and disease.* Annu Rev Biochem, 2013. **82**: p. 357-85.

102. Tatham, M.H., et al., *RNF4 is a poly-SUMO-specific E3 ubiquitin ligase required for arsenic-induced PML degradation.* Nat Cell Biol, 2008. **10**(5): p. 538-46.

103. Gambacorta, M., et al., *Heterogeneous nuclear expression of the promyelocytic leukemia (PML) protein in normal and neoplastic human tissues.* Am J Pathol, 1996. **149**(6): p. 2023-35.

104. Stadler, M., et al., *Transcriptional induction of the PML growth suppressor gene by interferons is mediated through an ISRE and a GAS element.* Oncogene, 1995. **11**(12): p. 2565-73.

105. Dror, N., et al., *Interferon regulatory factor-8 is indispensable for the expression of promyelocytic leukemia and the formation of nuclear bodies in myeloid cells.* J Biol Chem, 2007. **282**(8): p. 5633-40.

106. Goddard, A.D., et al., *Characterization of a zinc finger gene disrupted by the t(15;17) in acute promyelocytic leukemia.* Science, 1991. **254**(5036): p. 1371-4.

107. Jensen, K., C. Shiels, and P.S. Freemont, *PML protein isoforms and the RBCC/TRIM motif.* Oncogene, 2001. **20**(49): p. 7223-33.

108. Quimby, B.B., et al., *The promyelocytic leukemia protein stimulates SUMO conjugation in yeast.* Oncogene, 2006. **25**(21): p. 2999-3005.

109. Weisshaar, S.R., et al., *Arsenic trioxide stimulates SUMO-2/3 modification leading to RNF4-dependent proteolytic targeting of PML.* FEBS Lett, 2008. **582**(21-22): p. 3174-8.

110. Chu, Y. and X. Yang, *SUMO E3 ligase activity of TRIM proteins.* Oncogene, 2011. **30**(9): p. 1108-16.

111. Duprez, E., et al., *SUMO-1 modification of the acute promyelocytic leukaemia protein PML: implications for nuclear localisation.* J Cell Sci, 1999. **112 (Pt 3)**: p. 381-93.

112. Jeanne, M., et al., *PML/RARA oxidation and arsenic binding initiate the antileukemia response of As2O3.* Cancer Cell, 2010. **18**(1): p. 88-98.

113. Condemine, W., et al., *Characterization of Endogenous Human Promyelocytic Leukemia Isoforms.* Cancer Research, 2006. **66**(12): p. 6192-6198.

114. Sahin, U., et al., *Oxidative stress-induced assembly of PML nuclear bodies controls sumoylation of partner proteins.* J Cell Biol, 2014. **204**(6): p. 931-45.

115. Fogal, V., et al., *Regulation of p53 activity in nuclear bodies by a specific PML isoform.* EMBO J, 2000. **19**(22): p. 6185-95.

116. Krieghoff-Henning, E. and T.G. Hofmann, *Role of nuclear bodies in apoptosis signalling.* Biochim Biophys Acta, 2008. **1783**(11): p. 2185-94.

117. Dvorkina, M., et al., *A Promyelocytic Leukemia Protein-Thrombospondin-2 Axis and the Risk of Relapse in Neuroblastoma.* Clin Cancer Res, 2016. **22**(13): p. 3398-409.

118. Lang, M., et al., *Three-dimensional organization of promyelocytic leukemia nuclear bodies.* J Cell Sci, 2010. **123**(Pt 3): p. 392-400.

119. Li, C., et al., *C-terminal motifs in promyelocytic leukemia protein isoforms critically regulate PML nuclear body formation.* J Cell Sci, 2017. **130**(20): p. 3496-3506.

120. Hands, K.J., et al., *PML isoforms in response to arsenic: high-resolution analysis of PML body structure and degradation.* J Cell Sci, 2014. **127**(Pt 2): p. 365-75.

121. Van Damme, E., et al., *A manually curated network of the PML nuclear body interactome reveals an important role for PML-NBs in SUMOylation dynamics.* Int J Biol Sci, 2010. **6**(1): p. 51-67.

122. Dyck, J.A., et al., *A novel macromolecular structure is a target of the promyelocyte-retinoic acid receptor oncoprotein.* Cell, 1994. **76**(2): p. 333-43.

123. Dellaire, G., et al., *Mitotic accumulations of PML protein contribute to the re-establishment of PML nuclear bodies in G1.* J Cell Sci, 2006. **119**(Pt 6): p. 1034-42.

124. Lallemand-Breitenbach, V., et al., *Arsenic degrades PML or PML-RARalpha through a SUMO-triggered RNF4/ubiquitin-mediated pathway.* Nat Cell Biol, 2008. **10**(5): p. 547-55.

125. Hsu, K.S. and H.Y. Kao, *PML: Regulation and multifaceted function beyond tumor suppression.* Cell Biosci, 2018. **8**: p. 5.

126. Ashley, C.L., et al., *Nuclear domain 10 components upregulated via interferon during human cytomegalovirus infection potently regulate viral infection.* J Gen Virol, 2017. **98**(7): p. 1795-1805.

127. Langley, E., et al., *Human SIR2 deacetylates p53 and antagonizes PML/p53-induced cellular senescence.* EMBO J, 2002. **21**(10): p. 2383-96.

128. Bernardi, R., et al., *PML regulates p53 stability by sequestering Mdm2 to the nucleolus.* Nat Cell Biol, 2004. **6**(7): p. 665-72.

129. Scaglioni, P.P., et al., *A CK2-dependent mechanism for degradation of the PML tumor suppressor.* Cell, 2006. **126**(2): p. 269-83.

130. Rabellino, A. and P.P. Scaglioni, *PML Degradation: Multiple Ways to Eliminate PML.* Front Oncol, 2013. **3**: p. 60.

131. Stehmeier, P. and S. Muller, *Phospho-regulated SUMO interaction modules connect the SUMO system to CK2 signaling.* Mol Cell, 2009. **33**(3): p. 400-9.

132. Kamitani, T., et al., *Identification of three major sentrinization sites in PML.* J Biol Chem, 1998. **273**(41): p. 26675-82.

133. Lallemand-Breitenbach, V., et al., *Role of promyelocytic leukemia (PML) sumolation in nuclear body formation, 11S proteasome recruitment, and As2O3-induced PML or PML/retinoic acid receptor alpha degradation.* J Exp Med, 2001. **193**(12): p. 1361-71.

134. Yuan, W.C., et al., *A Cullin3-KLHL20 Ubiquitin ligase-dependent pathway targets PML to potentiate HIF-1 signaling and prostate cancer progression.* Cancer Cell, 2011. **20**(2): p. 214-28.

135. Guan, D., et al., *The epigenetic regulator UHRF1 promotes ubiquitination-mediated degradation of the tumor-suppressor protein promyelocytic leukemia protein.* Oncogene, 2013. **32**(33): p. 3819-28.

136. Louria-Hayon, I., et al., *E6AP promotes the degradation of the PML tumor suppressor.* Cell Death Differ, 2009. **16**(8): p. 1156-66.

137. Gurrieri, C., et al., *Loss of the tumor suppressor PML in human cancers of multiple histologic origins.* J Natl Cancer Inst, 2004. **96**(4): p. 269-79.

138. Koken, M.H., et al., *The PML growth-suppressor has an altered expression in human oncogenesis.* Oncogene, 1995. **10**(7): p. 1315-24.

139. Wolyniec, K., et al., *E6AP ubiquitin ligase regulates PML-induced senescence in Myc-driven lymphomagenesis.* Blood, 2012. **120**(4): p. 822-32.

140. Chen, H.Y., et al., *KLHL39 suppresses colon cancer metastasis by blocking KLHL20-mediated PML and DAPK ubiquitination.* Oncogene, 2015. **34**(40): p. 5141-51.

141. Sasagawa, K., et al., *Identification of Nd1, a novel murine kelch family protein, involved in stabilization of actin filaments.* J Biol Chem, 2002. **277**(46): p. 44140-6.

142. Trotman, L.C., et al., *Identification of a tumour suppressor network opposing nuclear Akt function.* Nature, 2006. **441**(7092): p. 523-7.

143. Wang, Z.G., et al., *Role of PML in cell growth and the retinoic acid pathway.* Science, 1998. **279**(5356): p. 1547-51.

144. Grignani, F., et al., *The acute promyelocytic leukemia-specific PML-RAR alpha fusion protein inhibits differentiation and promotes survival of myeloid precursor cells.* Cell, 1993. **74**(3): p. 423-31.

145. de The, H., et al., *The PML-RAR alpha fusion mRNA generated by the t(15;17) translocation in acute promyelocytic leukemia encodes a functionally altered RAR.* Cell, 1991. **66**(4): p. 675-84.

146. Kastner, P., et al., *Structure, localization and transcriptional properties of two classes of retinoic acid receptor alpha fusion proteins in acute promyelocytic leukemia (APL): structural similarities with a new family of oncoproteins.* EMBO J, 1992. **11**(2): p. 629-42.

147. Daniel, M.T., et al., *PML protein expression in hematopoietic and acute promyelocytic leukemia cells.* Blood, 1993. **82**(6): p. 1858-67.

148. Koken, M.H., et al., *The t(15;17) translocation alters a nuclear body in a retinoic acid-reversible fashion.* EMBO J, 1994. **13**(5): p. 1073-83.

149. Pandolfi, P.P., et al., *Genomic variability and alternative splicing generate multiple PML/RAR alpha transcripts that encode aberrant PML proteins and PML/RAR alpha isoforms in acute promyelocytic leukaemia.* EMBO J, 1992. **11**(4): p. 1397-407.

150. Zelent, A., et al., *Translocations of the RARalpha gene in acute promyelocytic leukemia.* Oncogene, 2001. **20**(49): p. 7186-203.

151. de The, H. and Z. Chen, *Acute promyelocytic leukaemia: novel insights into the mechanisms of cure.* Nat Rev Cancer, 2010. **10**(11): p. 775-83.

152. Grignani, F., et al., *Formation of PML/RAR alpha high molecular weight nuclear complexes through the PML coiled-coil region is essential for the PML/RAR alpha-mediated retinoic acid response.* Oncogene, 1999. **18**(46): p. 6313-21.

153. Piskacek, M., et al., *Nuclear hormone receptors: Ancient 9aaTAD and evolutionally gained NCoA activation pathways.* J Steroid Biochem Mol Biol, 2019. **187**: p. 118-123.

154. Lin, R.J. and R.M. Evans, *Acquisition of oncogenic potential by RAR chimeras in acute promyelocytic leukemia through formation of homodimers.* Mol Cell, 2000. **5**(5): p. 821-30.

155. Glass, C.K. and M.G. Rosenfeld, *The coregulator exchange in transcriptional functions of nuclear receptors.* Genes Dev, 2000. **14**(2): p. 121-41.

156. Zhou, J., et al., *Dimerization-induced corepressor binding and relaxed DNA-binding specificity are critical for PML/RARA-induced immortalization.* Proc Natl Acad Sci U S A, 2006. **103**(24): p. 9238-43.

157. Kamashev, D., D. Vitoux, and H. De The, *PML-RARA-RXR oligomers mediate retinoid and rexinoid/cAMP cross-talk in acute promyelocytic leukemia cell differentiation.* J Exp Med, 2004. **199**(8): p. 1163-74.

158. Sanz, M.A., et al., *Management of acute promyelocytic leukemia: recommendations from an expert panel on behalf of the European LeukemiaNet.* Blood, 2009. **113**(9): p. 1875-91.

159. Merghoub, T., et al., *Modeling acute promyelocytic leukemia in the mouse: new insights in the pathogenesis of human leukemias.* Blood Cells Mol Dis, 2001. **27**(1): p. 231-48.

160. Walter, M.J., et al., *Reduced PU.1 expression causes myeloid progenitor expansion and increased leukemia penetrance in mice expressing PML-RARalpha.* Proc Natl Acad Sci U S A, 2005. **102**(35): p. 12513-8.

161. Sanz, M.A. and P. Montesinos, *Advances in the management of coagulopathy in acute promyelocytic leukemia.* Thromb Res, 2020. **191 Suppl 1**: p. S63-S67.

162. Falanga, A., L. Russo, and C.J. Tartari, *Pathogenesis and treatment of thrombohemorrhagic diathesis in acute promyelocytic leukemia.* Mediterr J Hematol Infect Dis, 2011. **3**(1): p. e2011068.

163. Lo-Coco, F., et al., *Retinoic acid and arsenic trioxide for acute promyelocytic leukemia.* N Engl J Med, 2013. **369**(2): p. 111-21.

164. Ai, Z. and I.A. Udalova, *Transcriptional regulation of neutrophil differentiation and function during inflammation.* J Leukoc Biol, 2020. **107**(3): p. 419-430.

165. Paietta, E., *Expression of cell-surface antigens in acute promyelocytic leukaemia.* Best Pract Res Clin Haematol, 2003. **16**(3): p. 369-85.

166. McKenna, E., et al., *Neutrophils: Need for Standardized Nomenclature.* Front Immunol, 2021. **12**: p. 602963.

167. Di Noto, R., et al., *All-trans retinoic acid (ATRA) and the regulation of adhesion molecules in acute myeloid leukemia.* Leuk Lymphoma, 1996. **21**(3-4): p. 201-9.

168. Duprez, E., et al., *C/EBPbeta: a major PML-RARA-responsive gene in retinoic acid-induced differentiation of APL cells.* EMBO J, 2003. **22**(21): p. 5806-16.

169. Park, D.J., et al., *CCAAT/enhancer binding protein epsilon is a potential retinoid target gene in acute promyelocytic leukemia treatment.* J Clin Invest, 1999. **103**(10): p. 1399-408.

170. Wang, K., et al., *PML/RARalpha targets promoter regions containing PU.1 consensus and RARE half sites in acute promyelocytic leukemia.* Cancer Cell, 2010. **17**(2): p. 186-97.

171. Rahmé, R., C. Esnault, and H. de Thé, *Molecular Targets of Treatment in APL*, in *Acute Promyelocytic Leukemia : A Clinical Guide*, O. Abla, F. Lo Coco, and M.A. Sanz, Editors. 2018, Springer International Publishing: Cham. p. 17-27.

172. Liu, T.X., et al., *Gene expression networks underlying retinoic acid-induced differentiation of acute promyelocytic leukemia cells.* Blood, 2000. **96**(4): p. 1496-504.

173. Mueller, B.U., et al., *ATRA resolves the differentiation block in t(15;17) acute myeloid leukemia by restoring PU.1 expression.* Blood, 2006. **107**(8): p. 3330-8.

174. Mueller, B.U., et al., *Heterozygous PU.1 mutations are associated with acute myeloid leukemia.* Blood, 2002. **100**(3): p. 998-1007.

175. Gianni, M., et al., *Stat1 is induced and activated by all-trans retinoic acid in acute promyelocytic leukemia cells.* Blood, 1997. **89**(3): p. 1001-12.

176. Matikainen, S., et al., *Regulation of IRF and STAT gene expression by retinoic acid.* Leuk Lymphoma, 1998. **30**(1-2): p. 63-71.

177. Chelbi-Alix, M.K., et al., *Induction of the PML protein by interferons in normal and APL cells.* Leukemia, 1995. **9**(12): p. 2027-33.

178. Ablain, J., et al., *Uncoupling RARA transcriptional activation and degradation clarifies the bases for APL response to therapies.* J Exp Med, 2013. **210**(4): p. 647-53.

179. Gianni, M., et al., *Combined arsenic and retinoic acid treatment enhances differentiation and apoptosis in arsenic-resistant NB4 cells.* Blood, 1998. **91**(11): p. 4300-10.

180. Nasr, R., et al., *Eradication of acute promyelocytic leukemia-initiating cells through PML-RARA degradation.* Nat Med, 2008. **14**(12): p. 1333-42.

181. Muindi, J., et al., *Continuous treatment with all-trans retinoic acid causes a progressive reduction in plasma drug concentrations: implications for relapse and retinoid "resistance" in patients with acute promyelocytic leukemia.* Blood, 1992. **79**(2): p. 299-303.

182. Chen, G.Q., et al., *Use of arsenic trioxide (As2O3) in the treatment of acute promyelocytic leukemia (APL): I. As2O3 exerts dose-dependent dual effects on APL cells.* Blood, 1997. **89**(9): p. 3345-53.

183. Soignet, S.L., et al., *Complete remission after treatment of acute promyelocytic leukemia with arsenic trioxide.* N Engl J Med, 1998. **339**(19): p. 1341-8.

184. Zhu, J., et al., *Arsenic-induced PML targeting onto nuclear bodies: implications for the treatment of acute promyelocytic leukemia.* Proc Natl Acad Sci U S A, 1997. **94**(8): p. 3978-83.

185. Ablain, J., et al., *Activation of a promyelocytic leukemia-tumor protein 53 axis underlies acute promyelocytic leukemia cure.* Nat Med, 2014. **20**(2): p. 167-74.

186. Yoshida, H., et al., *Accelerated degradation of PML-retinoic acid receptor alpha (PML-RARA) oncoprotein by all-trans-retinoic acid in acute promyelocytic leukemia: possible role of the proteasome pathway.* Cancer Res, 1996. **56**(13): p. 2945-8.

187. Nervi, C., et al., *Caspases mediate retinoic acid-induced degradation of the acute promyelocytic leukemia PML/RARalpha fusion protein.* Blood, 1998. **92**(7): p. 2244-51.

188. Zhu, J., et al., *Retinoic acid induces proteasome-dependent degradation of retinoic acid receptor alpha (RARalpha) and oncogenic RARalpha fusion proteins.* Proc Natl Acad Sci U S A, 1999. **96**(26): p. 14807-12.

189. Kopf, E., et al., *Dimerization with retinoid X receptors and phosphorylation modulate the retinoic acid-induced degradation of retinoic acid receptors alpha and gamma through the ubiquitin-proteasome pathway.* J Biol Chem, 2000. **275**(43): p. 33280-8.

190. vom Baur, E., et al., *Differential ligand-dependent interactions between the AF-2 activating domain of nuclear receptors and the putative transcriptional intermediary factors mSUG1 and TIF1.* EMBO J, 1996. **15**(1): p. 110-24.

191. Gaillard, E., et al., *Phosphorylation by PKA potentiates retinoic acid receptor alpha activity by means of increasing interaction with and phosphorylation by cyclin H/cdk7.* Proc Natl Acad Sci U S A, 2006. **103**(25): p. 9548-53.

192. Guillemin, M.C., et al., *In vivo activation of cAMP signaling induces growth arrest and differentiation in acute promyelocytic leukemia.* J Exp Med, 2002. **196**(10): p. 1373-80.

193. Slack, J.L. and M. Yu, *Constitutive expression of the promyelocytic leukemia-associated oncogene PML-RARalpha in TF1 cells: isoform-specific and retinoic acid-dependent effects on growth, bcl-2 expression, and apoptosis.* Blood, 1998. **91**(9): p. 3347-56.

194. Jing, Y., et al., *The cleavage product deltaPML-RARalpha contributes to all-trans retinoic acid-mediated differentiation in acute promyelocytic leukemia cells.* Oncogene, 2003. **22**(26): p. 4083-91.

195. Zhu, J., V. Lallemand-Breitenbach, and H. de The, *Pathways of retinoic acid- or arsenic trioxide-induced PML/RARalpha catabolism, role of oncogene degradation in disease remission.* Oncogene, 2001. **20**(49): p. 7257-65.

196. Kitareewan, S., et al., *UBE1L is a retinoid target that triggers PML/RARalpha degradation and apoptosis in acute promyelocytic leukemia.* Proc Natl Acad Sci U S A, 2002. **99**(6): p. 3806-11.

197. Shah, S.J., et al., *UBE1L represses PML/RAR{alpha} by targeting the PML domain for ISG15ylation.* Mol Cancer Ther, 2008. **7**(4): p. 905-14.

198. Guo, Y., et al., *Blockade of the ubiquitin protease UBP43 destabilizes transcription factor PML/RARalpha and inhibits the growth of acute promyelocytic leukemia.* Cancer Res, 2010. **70**(23): p. 9875-85.

199. Fanelli, M., et al., *The coiled-coil domain is the structural determinant for mammalian homologues of Drosophila Sina-mediated degradation of promyelocytic leukemia protein and other tripartite motif proteins by the proteasome.* J Biol Chem, 2004. **279**(7): p. 5374-9.

200. Kramer, O.H., et al., *Mechanism for ubiquitylation of the leukemia fusion proteins AML1-ETO and PML-RARalpha.* FASEB J, 2008. **22**(5): p. 1369-79.

201. Pietschmann, K., et al., *Differential regulation of PML-RARalpha stability by the ubiquitin ligases SIAH1/SIAH2 and TRIAD1.* Int J Biochem Cell Biol, 2012. **44**(1): p. 132-8.

202. Wu, H.C., et al., *USP11 regulates PML stability to control Notch-induced malignancy in brain tumours.* Nat Commun, 2014. **5**: p. 3214.

203. Kowarz, E., D. Loscher, and R. Marschalek, *Optimized Sleeping Beauty transposons rapidly generate stable transgenic cell lines.* Biotechnol J, 2015. **10**(4): p. 647-53.

204. Tsukada, M., et al., *High albumin levels restrict the kinetics of 13-cis retinoic acid uptake and intracellular isomerization to all-trans retinoic acid and inhibit its anti-proliferative effect on SZ95 sebocytes.* J Invest Dermatol, 2002. **119**(1): p. 182-5.

205. Huynh, T.T., et al., *Retinoic acid and arsenic trioxide induce lasting differentiation and demethylation of target genes in APL cells.* Sci Rep, 2019. **9**(1): p. 9414.

206. O'Doherty, U., W.J. Swiggard, and M.H. Malim, *Human immunodeficiency virus type 1 spinoculation enhances infection through virus binding.* J Virol, 2000. **74**(21): p. 10074-80.

207. Livak, K.J. and T.D. Schmittgen, *Analysis of relative gene expression data using real-time quantitative PCR and the 2(-Delta Delta C(T)) Method.* Methods, 2001. **25**(4): p. 402-8.

208. Hjerpe, R., et al., *Efficient protection and isolation of ubiquitylated proteins using tandem ubiquitin-binding entities.* EMBO Rep, 2009. **10**(11): p. 1250-8.

209. Cox, J. and M. Mann, *MaxQuant enables high peptide identification rates, individualized p.p.b.-range mass accuracies and proteome-wide protein quantification.* Nat Biotechnol, 2008. **26**(12): p. 1367-72.

210. Wang, Z.G., et al., *PML is essential for multiple apoptotic pathways.* Nat Genet, 1998. **20**(3): p. 266-72.

211. McCann, J.J., et al., *USP22 Functions as an Oncogenic Driver in Prostate Cancer by Regulating Cell Proliferation and DNA Repair.* Cancer Res, 2020. **80**(3): p. 430-443.

212. Shalem, O., et al., *Genome-scale CRISPR-Cas9 knockout screening in human cells.* Science, 2014. **343**(6166): p. 84-87.

213. Hsu, K.S., et al., *Dual regulation of Stat1 and Stat3 by the tumor suppressor protein PML contributes to interferon alpha-mediated inhibition of angiogenesis.* J Biol Chem, 2017. **292**(24): p. 10048-10060.

214. Ennis, H.L. and M. Lubin, *Cycloheximide: Aspects of Inhibition of Protein Synthesis in Mammalian Cells.* Science, 1964. **146**(3650): p. 1474-6.

215. Wagner, S.A., et al., *A proteome-wide, quantitative survey of in vivo ubiquitylation sites reveals widespread regulatory roles.* Mol Cell Proteomics, 2011. **10**(10): p. M111 013284.

216. Udeshi, N.D., et al., *Refined preparation and use of anti-diglycine remnant (K-epsilon-GG) antibody enables routine quantification of 10,000s of ubiquitination sites in single proteomics experiments.* Mol Cell Proteomics, 2013. **12**(3): p. 825-31.

217. Mertins, P., et al., *Integrated proteomic analysis of post-translational modifications by serial enrichment.* Nat Methods, 2013. **10**(7): p. 634-7.

218. Akimov, V., et al., *UbiSite approach for comprehensive mapping of lysine and N-terminal ubiquitination sites.* Nat Struct Mol Biol, 2018. **25**(7): p. 631-640.

219. Rinfret Robert, C., et al., *Interplay of Ubiquitin-Like Modifiers Following Arsenic Trioxide Treatment.* J Proteome Res, 2020. **19**(5): p. 1999-2010.

220. Fanelli, M., et al., *Constitutive degradation of PML/RARalpha through the proteasome pathway mediates retinoic acid resistance.* Blood, 1999. **93**(5): p. 1477-81.

221. Wei, S., et al., *Active Pin1 is a key target of all-trans retinoic acid in acute promyelocytic leukemia and breast cancer.* Nat Med, 2015. **21**(5): p. 457-66.

222. Zhu, J., et al., *A sumoylation site in PML/RARA is essential for leukemic transformation.* Cancer Cell, 2005. **7**(2): p. 143-53.

223. Gianni, M., et al., *Inhibition of the peptidyl-prolyl-isomerase Pin1 enhances the responses of acute myeloid leukemia cells to retinoic acid via stabilization of RARalpha and PML-RARalpha.* Cancer Res, 2009. **69**(3): p. 1016-26.

224. Fang, Y., et al., *The ubiquitin-proteasome pathway plays essential roles in ATRA-induced leukemia cells G0/G1 phase arrest and transition into granulocytic differentiation.* Cancer Biol Ther, 2010. **10**(11): p. 1157-67.

225. Meani, N., et al., *Molecular signature of retinoic acid treatment in acute promyelocytic leukemia.* Oncogene, 2005. **24**(20): p. 3358-68.

226. Jin, W., et al., *IRF1 Is Crucial for ATRA-Induced Differentiation By Regulating Its Multiple Functional Targets.* Blood, 2014. **124**(21): p. 2220-2220.

227. Humbert, M., et al., *Inhibition of damage-regulated autophagy modulator-1 (DRAM-1) impairs neutrophil differentiation of NB4 APL cells.* Leuk Res, 2012. **36**(12): p. 1552-6.

228. Pearson, M., et al., *PML regulates p53 acetylation and premature senescence induced by oncogenic Ras.* Nature, 2000. **406**(6792): p. 207-10.

229. Sun, H., et al., *USP13 negatively regulates antiviral responses by deubiquitinating STING.* Nat Commun, 2017. **8**: p. 15534.

230. Hendriks, I.A., et al., *Ubiquitin-specific Protease 11 (USP11) Deubiquitinates Hybrid Small Ubiquitin-like Modifier (SUMO)-Ubiquitin Chains to Counteract RING Finger Protein 4 (RNF4).* J Biol Chem, 2015. **290**(25): p. 15526-15537.

231. Clague, M.J., S. Urbe, and D. Komander, *Breaking the chains: deubiquitylating enzyme specificity begets function.* Nat Rev Mol Cell Biol, 2019. **20**(6): p. 338-352.

232. Sarkari, F., et al., *The herpesvirus associated ubiquitin specific protease, USP7, is a negative regulator of PML proteins and PML nuclear bodies.* PLoS One, 2011. **6**(1): p. e16598.

233. Sarkari, F., et al., *EBNA1-mediated recruitment of a histone H2B deubiquitylating complex to the Epstein-Barr virus latent origin of DNA replication.* PLoS Pathog, 2009. **5**(10): p. e1000624.

234. Suresh, B., et al., *Regulation of pluripotency and differentiation by deubiquitinating enzymes.* Cell Death Differ, 2016. **23**(8): p. 1257-64.

235. Everett, R.D., et al., *A novel ubiquitin-specific protease is dynamically associated with the PML nuclear domain and binds to a herpesvirus regulatory protein.* EMBO J, 1997. **16**(7): p. 1519-30.

236. Li, Z.H., et al., *RNA interference-mediated USP22 gene silencing promotes human brain glioma apoptosis and induces cell cycle arrest.* Oncol Lett, 2013. **5**(4): p. 1290-1294.

237. Liani, E., et al., *Ubiquitylation of synphilin-1 and alpha-synuclein by SIAH and its presence in cellular inclusions and Lewy bodies imply a role in Parkinson's disease.* Proc Natl Acad Sci U S A, 2004. **101**(15): p. 5500-5.

238. Rott, R., et al., *Monoubiquitylation of alpha-synuclein by seven in absentia homolog (SIAH) promotes its aggregation in dopaminergic cells.* J Biol Chem, 2008. **283**(6): p. 3316-3328.

239. Rott, R., et al., *alpha-Synuclein fate is determined by USP9X-regulated monoubiquitination.* Proc Natl Acad Sci U S A, 2011. **108**(46): p. 18666-71.

240. Joshi, P., et al., *The functional interactome landscape of the human histone deacetylase family.* Mol Syst Biol, 2013. **9**: p. 672.

241. Nathan, J.A., et al., *The ubiquitin E3 ligase MARCH7 is differentially regulated by the deubiquitylating enzymes USP7 and USP9X.* Traffic, 2008. **9**(7): p. 1130-45.

242. Wu, Q., et al., *Suberoylanilide hydroxamic acid treatment reveals crosstalks among proteome, ubiquitylome and acetylome in non-small cell lung cancer A549 cell line.* Sci Rep, 2015. **5**: p. 9520.

243. Hornbeck, P.V., et al., *PhosphoSitePlus, 2014: mutations, PTMs and recalibrations.* Nucleic Acids Res, 2015. **43**(Database issue): p. D512-20.

244. Galisson, F., et al., *A novel proteomics approach to identify SUMOylated proteins and their modification sites in human cells.* Mol Cell Proteomics, 2011. **10**(2): p. M110 004796.

245. Lamoliatte, F., et al., *Uncovering the SUMOylation and ubiquitylation crosstalk in human cells using sequential peptide immunopurification.* Nat Commun, 2017. **8**: p. 14109.

246. Moldovan, G.L., B. Pfander, and S. Jentsch, *PCNA, the maestro of the replication fork.* Cell, 2007. **129**(4): p. 665-79.

247. Thomas, X., *Acute Promyelocytic Leukemia: A History over 60 Years-From the Most Malignant to the most Curable Form of Acute Leukemia.* Oncol Ther, 2019. **7**(1): p. 33-65.

248. Ablain, J. and H. de The, *Retinoic acid signaling in cancer: The parable of acute promyelocytic leukemia.* Int J Cancer, 2014. **135**(10): p. 2262-72.

249. Asada, M., et al., *Apoptosis inhibitory activity of cytoplasmic p21(Cip1/WAF1) in monocytic differentiation.* EMBO J, 1999. **18**(5): p. 1223-34.

250. Viale, A., et al., *Cell-cycle restriction limits DNA damage and maintains self-renewal of leukaemia stem cells.* Nature, 2009. **457**(7225): p. 51-6.

251. Lin, Y., et al., *USP22 promotes proliferation in renal cell carcinoma by stabilizing survivin.* Oncol Lett, 2020. **20**(5): p. 246.

252. Zhang, J., et al., *USP22 knockdown enhanced chemosensitivity of hepatocellular carcinoma cells to 5-Fu by up-regulation of Smad4 and suppression of Akt.* Oncotarget, 2017. **8**(15): p. 24728-24740.

253. Agadir, A., et al., *All-trans retinoic acid pharmacokinetics and bioavailability in acute promyelocytic leukemia: intracellular concentrations and biologic response relationship.* J Clin Oncol, 1995. **13**(10): p. 2517-23.

254. Xiong, J., et al., *Cloning and characterization of the human USP22 gene promoter.* PLoS One, 2012. **7**(12): p. e52716.

255. Bruck, N., et al., *A coordinated phosphorylation cascade initiated by p38MAPK/MSK1 directs RARalpha to target promoters.* EMBO J, 2009. **28**(1): p. 34-47.

256. Xiong, J., et al., *p38 mitogen-activated protein kinase inhibits USP22 transcription in HeLa cells.* Biomed Rep, 2015. **3**(4): p. 461-467.

257. Wu, S.F., et al., *RIG-I regulates myeloid differentiation by promoting TRIM25-mediated ISGylation.* Proc Natl Acad Sci U S A, 2020. **117**(25): p. 14395-14404.

258. Kim, Y.E. and J.H. Ahn, *Positive role of promyelocytic leukemia protein in type I interferon response and its regulation by human cytomegalovirus.* PLoS Pathog, 2015. **11**(3): p. e1004785.

259. Patra, U. and S. Muller, *A Tale of Usurpation and Subversion: SUMO-Dependent Integrity of Promyelocytic Leukemia Nuclear Bodies at the Crossroad of Infection and Immunity.* Front Cell Dev Biol, 2021. **9**: p. 696234.

260. Nason-Burchenal, K., et al., *Interferon augments PML and PML/RAR alpha expression in normal myeloid and acute promyelocytic cells and cooperates with all-trans retinoic acid to induce maturation of a retinoid-resistant promyelocytic cell line.* Blood, 1996. **88**(10): p. 3926-36.

261. Gianni, M., et al., *Interferons induce normal and aberrant retinoic-acid receptors type alpha in acute promyelocytic leukemia cells: potentiation of the induction of retinoid-dependent differentiation markers.* Int J Cancer, 1996. **68**(1): p. 75-83.

262. Chelbi-Alix, M.K. and L. Pelicano, *Retinoic acid and interferon signaling cross talk in normal and RA-resistant APL cells.* Leukemia, 1999. **13**(8): p. 1167-74.

263. Kumar, R. and L. Korutla, *Growth inhibition of human acute promyelocytic leukemia NB-4 cells by interferons and all-trans retinoic acid: trans-modulation of inducible gene expression pathways.* Anticancer Res, 1995. **15**(2): p. 353-60.

264. Pelicano, L., et al., *Retinoic acid enhances the expression of interferon-induced proteins: evidence for multiple mechanisms of action.* Oncogene, 1997. **15**(19): p. 2349-59.

265. Zhao, C., et al., *Human ISG15 conjugation targets both IFN-induced and constitutively expressed proteins functioning in diverse cellular pathways.* Proc Natl Acad Sci U S A, 2005. **102**(29): p. 10200-5.

266. Eletr, Z.M. and B. Kuhlman, *Sequence determinants of E2-E6AP binding affinity and specificity.* J Mol Biol, 2007. **369**(2): p. 419-28.

267. Kumar, S., W.H. Kao, and P.M. Howley, *Physical interaction between specific E2 and Hect E3 enzymes determines functional cooperativity.* J Biol Chem, 1997. **272**(21): p. 13548-54.

268. Wojiski, S., et al., *PML-RARalpha initiates leukemia by conferring properties of self-renewal to committed promyelocytic progenitors.* Leukemia, 2009. **23**(8): p. 1462-71.

269. Albano, F., et al., *Absolute quantification of the pretreatment PML-RARA transcript defines the relapse risk in acute promyelocytic leukemia.* Oncotarget, 2015. **6**(15): p. 13269-77.

270. Madan, V., et al., *Comprehensive mutational analysis of primary and relapse acute promyelocytic leukemia.* Leukemia, 2016. **30**(8): p. 1672-81.

271. Noguera, N.I., et al., *Acute Promyelocytic Leukemia: Update on the Mechanisms of Leukemogenesis, Resistance and on Innovative Treatment Strategies.* Cancers (Basel), 2019. **11**(10).

272. Li, L., et al., *SIRT1 activation by a c-MYC oncogenic network promotes the maintenance and drug resistance of human FLT3-ITD acute myeloid leukemia stem cells.* Cell Stem Cell, 2014. **15**(4): p. 431-446.

273. Esnault, C., et al., *FLT3-ITD impedes retinoic acid, but not arsenic, responses in murine acute promyelocytic leukemias.* Blood, 2019. **133**(13): p. 1495-1506.

274. Xiong, J., et al., *USP22 transcriptional activity is negatively regulated by the histone deacetylase inhibitor trichostatin A.* Mol Med Rep, 2014. **10**(6): p. 3343-7.

275. Kumar, S. and P.B. Tchounwou, *Molecular mechanisms of cisplatin cytotoxicity in acute promyelocytic leukemia cells.* Oncotarget, 2015. **6**(38): p. 40734-46.

276. Nebbioso, A., et al., *Tumor-selective action of HDAC inhibitors involves TRAIL induction in acute myeloid leukemia cells.* Nat Med, 2005. **11**(1): p. 77-84.

277. Insinga, A., et al., *Inhibitors of histone deacetylases induce tumor-selective apoptosis through activation of the death receptor pathway.* Nat Med, 2005. **11**(1): p. 71-6.

278. Morgan, M., et al., *Potent macrocycle inhibitors of the human SAGA deubiquitinating module.* Cell Chem Biol, 2022. **29**(4): p. 544-554 e4.